SPATIOTEMPORAL IMPACT OF PHAGE EXPOSURE ON BIOFILM SYSTEMS

A Dissertation
Presented to
The Academic Faculty

By

Hemaa Selvakumar

In Partial Fulfillment
of the Requirements for the Degree
Doctor of Philosophy in the
School of Physics

Georgia Institute of Technology

December 2021

SPATIOTEMPORAL IMPACT OF PHAGE EXPOSURE ON BIOFILM SYSTEMS

Approved by:

Dr. Jennifer E. Curtis, Advisor
School of Physics
Georgia Institute of Technology

Dr. Joshua S. Weitz
School of Biological Sciences and
School of Physics
Georgia Institute of Technology

Dr. James C. Gumbart
School of Physics
Georgia Institute of Technology

Dr. Stephen P. Diggle
School of Biological Sciences
Georgia Institute of Technology

Dr. Peter Yunker
School of Physics
Georgia Institute of Technology

Date Approved: December 17, 2021

Science is organized knowledge. Wisdom is organized life.

Immanuel Kant

For my dear parents, Visalakshmi and Selvakumar,

little sister Sahitya,

and my late grandfather Padmasekaran,

for their unconditional love and unwavering support for all my pursuits.

ACKNOWLEDGEMENTS

First and foremost, I would like to express my deepest gratitude to Dr. Jennifer Curtis, for being a great advisor and a thoughtful mentor. It has been a wonderful experience to work with her and I have learnt so much during this journey with her guidance, both academically and personally. I cannot thank her enough for being a pillar of support through the toughest of times these past few years.

In some sense, this journey began when I was in tenth grade (high school). It was then that I had acquired the knowledge about the existence of phages and their mechanism of action. I still distinctly remember being mind-blown when I learnt that there were creatures smaller than a bacterium, and not just smaller, but smarter. These nano-sized viruses that prey on bacteria are the most abundant organisms on earth (10^{31}), approximately ten times the number of bacteria. The next time I heard about phage was during a Physics of Living Systems (PoLS) talk at Georgia Tech and expressed my interest in the research area to Dr. Curtis. To my delight, she was interested in the topic as well and encouraged me to pursue my doctoral degree researching phage. I was glad to have the opportunity to make a contribution towards improving the understanding of phage-bacteria dynamics so that phage therapy could be a viable option for patients who dont respond to treatment with antibiotics. This led to a multidisciplinary collaboration between Curtis lab, Weitz group, and Diggle lab.

Next, I would like to thank the immunophage team for their collaborative spirit and stimulating discussions without which this project would not have been possible. It was my pleasure to work with Dr. Joshua Weitz and Dr. Stephen Diggle; they brought in their unique perspectives and expertise to the project which helped to broaden my thinking and push my limits. I am grateful for the discussions with Dr. Chung-Yin Leung, Marian Dominguez, Jacob Thomas, Sheyda Azimi, James Gurney, Rogelio Rodriguez, and the members of the Center for Microbial Dynamics and Infection (CMDI).

I am indebted to Dr. Patrick Chang and Dr. Wenbin Wei for welcoming me into the Curtis lab, patiently training me, and helping me get acclimated when I first joined. I would like to thank my labmates Jessica Faubel, Shlomi Cohen, and Rebecca for extending their friendship. It has been a great experience to serve as the graduate mentor for enthusiastic undergraduate students like James Butler, Megan Souza, and Bolatito Fatoki.

Next, I would like to acknowledge my friends and social support system at Georgia Tech and Atlanta without who have lifted my spirits numerous times. I would like to highlight a few fellow physics PhD students - Maryrose Barrios, Bhavesh Khamesra, Shashank Markande, Natalie Brown. I am thankful to Aroua Gharbi,Bahnisikha Dutta, Sudarshan Ghonge, Sanjay Senthikumar, Pooja Rao, Keertana Subramani, Swati Mardia, and Isha Lodhi for all the adventures and philosophical discussions. I am grateful to Partiban uncle, Sumathi aunty, Raja uncle, and Kowsi aunty for their warmth and support in a foreign land.

I would like to recognize my mentors, Dr. Ambarish Ghosh and Dr. Rohini Godbole, at the Indian Institute of Science for providing encouragement at every step of the way during this academic journey. I met some of my best friends at IISc, Namrata Das, Sunandha Srikanth, and Naveen Senthinathan. I am thankful to Sunandha and Naveen for just being a call away, anytime. It feels like I have known Namrata Das forever, she is practically family. She would know the perfect thing to say and show me the light at the end of the tunnel everytime.

Finally I would like to thank my family. They give me the strength to endure the toughest of times despite living on the other side of the planet (during a once-in-a-century pandemic!). I love them and they love me, for which I am ever grateful. Though my grandfather is no longer alive, his teachings and warmth guide me to this day. His penchant for mathematics and travel is something I cherish. My other grandparents bring a smile to my face whenever I think of them. I am forever thankful to my mother for providing valuable ideas and input for illustrations and presentations, in addition to being my moral compass. I would like to thank my dad for pushing me to be better in all aspects of life and

providing the much needed constructive criticism. Finally, I would like to thank my little (though she pretends like she is a thousand years old) sister for being so adorable, she is my source of constant support and shenanigans!

TABLE OF CONTENTS

LIST OF TABLES

LIST OF FIGURES

LIST OF SYMBOLS AND ABBREVIATIONS

P. aeruginosa	*Pseudomonas aeruginosa*
EPS	Extracellular polymeric substance
QS	Quorum sensing
CV	Crystal violet
ODE	Ordinary differential equation
PDE	Partial differential equation
CFU	Colony forming unit
PFU	Plaque forming unit
MOI	Multiplicity of infection
PMN	Polymorphonuclear neutrophils
NET	Neutrophil extracellular trap
PRR	Pathogen recognition receptor
TLR	Toll-like receptor
IL	Interleukin
ROS	Reactive oxygen species

SUMMARY

When single-celled prokaryotic organisms, one of the simplest forms of life, develop the ability to exhibit complex emergent properties such as social cooperation, resource capture, and enhanced survivability, the individual limitations of existence can be overcome which would otherwise be unlikely. Emergent properties of biofilms such as matrix production, quorum sensing, and coordinated lifecycle offers structural and functional advantages which makes them highly successful at evading destruction by antimicrobials and immune defenses. With few, if any, novel antibiotics in the clinical pipeline, there is a resurgence of interest in alternatives such as phage therapy, the practice of bacterial viruses known as bacteriophages that infect and lyse bacteria to treat infections. In this thesis, we explore the understudied impact of phage titer on biofilm dynamics and outcomes. We determined that the biofilm developmental stage at the time of phage addition modulates its response. These responses vary as a function of the phage dose and can be broadly organized into four distinct classes. In each of these classes, we observe that high phage doses restrain the biofilm from transitioning into the next stage of their developmental cycle. A paradoxical aspect of this result is that mature biofilms exposed to high phage titers are enhanced by phage treatment. Despite this apparently unwanted outcome, the inhibition of biofilm dispersion in phage-treated samples could potentially minimize the further spread of infections to other locations. These results comprehensively demonstrate predictable biofilm outcomes versus phage dosage and biofilm age, and will provide guidance in advancing phage-based personalized medicine when generalized treatments fail. Collectively, this dissertation derives insights on the advantages and limitations of phages to inhibit, control, and eliminate biofilms.

CHAPTER 1
INTRODUCTION

Microbes are ubiquitous in the biosphere of planet Earth. Single-celled prokaryotic microbes such as bacteria are present in all natural systems. Their population dynamics are governed via local interactions which in turn are regulated through physical and biological constraints imposed by the environment. One of the survival strategies employed by many microbial strains is to form aggregates and live in communities, thus modulating their interaction with each other in response to changing microenvironments [1].

Such bacterial communities, known as biofilms, are complex three-dimensional structures comprising mainly of live and dead bacteria, and a protective, integrative matrix referred to as the extracellular polymeric substance (EPS) [2]. This multi-component EPS is a mixture of polysaccharides, protein, and extracellular DNA. It provides structural support and helps holds the biofilm structure together while offering functional advantages to protect the bacterial cells, such as reduced susceptibility to antibiotics, immune cells, and other threats. The bacteria in a biofilm use quorum sensing, a process through which they send chemical modulators to communicate with each other [3–7]. Biofilms have also been reported to utilize electrical signals to relay information rapidly [8]. Therefore, when single-celled organisms subscribe to such communal way of living, they unlock a variety of evolutionary advantages that would otherwise not be accessible - making biofilms a dominant form of life that is resilient to extreme environmental stressors.

The National Institute of Health reported that about 80% of chronic infections in vivo, such as infections at the site of burn wounds and surface of medical implants [9], alveoli of cystic fibrosis patients, and dental plaque are biofilms [10]. Secondary bacterial infections with viral respiratory infections such as COVID-19 could endanger life and lower likelihood of survival [11, 12]. Resilience of biofilms, although key to evolution

of life on earth, presents a great challenge to human health. Existence in the biofilm mode offers survival advantages and evolutionary status quo for the bacteria, rendering traditional strategies of combating bacterial infections through the use of antibiotics and antimicrobials ineffective and therefore, demanding the development of alternative measures [13, 14].

A few alternate strategies considered by researchers in the past were to use the bioacoustics effect of ultrasound to increase the efficacy of antimicrobials, design new drugs capable of inhibiting quorum sensing, synthesize enzymes that depolymerize the protective matrix or employ bacteriophages to lyse bacteria, also known as phage therapy [15–21].

The therapeutic application of bacteriophages, also known as phages, was prevalent in the 1920s before the advent of broad-spectrum antibiotics in the 1940s [22]. In the recent times, due to the rise in multi-drug resistant species of bacteria, there is renewed interest in phage therapy as a potential alternative solution. Several animal studies demonstrate up to 100% success rate for phage therapy. A limited number of human trials have been conducted [16], some of which show promising results while some do not show any evidence of improvement in outcomes. In order to understand and improve the clinical outcomes, it is essential to understand precisely how phage therapy works, factors which govern phage-bacteria interactions, and the regulation of interaction mechanisms when bacteria organize themselves into biofilms.

Each phage consists of genetic material compactly packed in a protein capsid. Once a phage infects a host bacterium, it initiates one of two major pathways: lysis or lysogeny. In the lytic cycle, the phages adsorb to the host cell surface, injects and integrates its genetic material with that of the host, hijacks the metabolic machinery of the host to make more copies of itself and eventually lyse the host to release the progenies. In the lysogenic cycle, the phage genetic material is integrated with that of the bacteria but they do not produce progeny phages and hosts are not lysed until induced to follow the lytic pathway. Since the lytic pathway leads to successful elimination of the bacterial host, obligately lytic phages

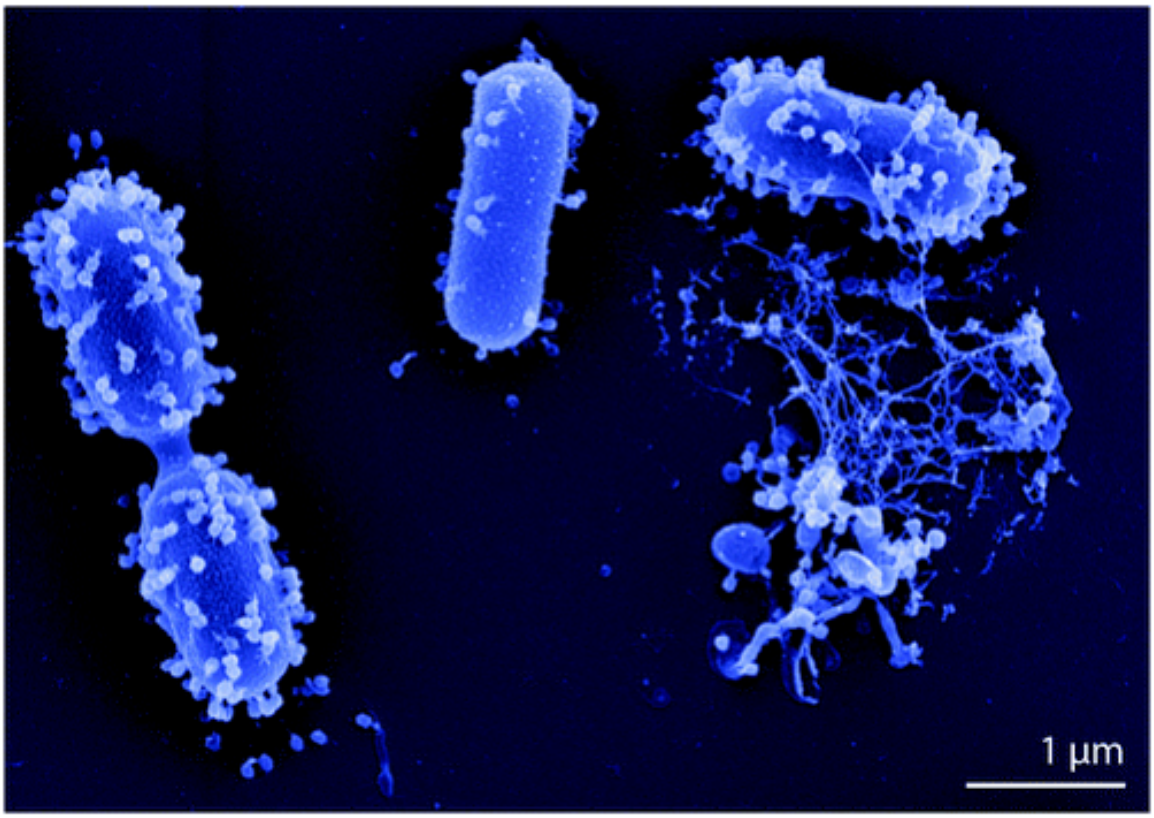

Figure 1.1: **Phage vBAb-M-G7 on host strain Acinetobacter baumannii G7 and after host cell lysis** | Scanning electron micrograph by Manfred Rohde, HZI, Braunschweig, Germany. Origin of phage and host strain: Eliava Institute IBMV, Tbilisi, Georgia. This image was originally published in [23]. Reprinted here under the Attribution-NonCommercial 4.0 International (CC BY-NC 4.0).

are employed in phage therapeutic interventions. Two timescales that characterize the lytic pathway of a phage are the eclipse period and latent period. The eclipse period is the time between phage infection and first formation of intracellular phage particles and the latent period is the time between phage infection and bacterial lysis. The number of progeny phages released upon the lysis of an infected bacteria is called the burst size [24].

It is essential to understand the dynamics of phage-bacteria and phage-biofilm interactions to determine the therapeutic effectiveness of phage therapy. Phage-bacteria dynamics have been successfully modeled by a set of coupled ordinary differential equations (ODEs) which result in Lotka-Volterra type predator-prey oscillating population cycles. The equations are summarized below:

$$\frac{dB}{dt} = rB(1 - \frac{B}{K_c}) - \phi BP - \gamma B \tag{1.1}$$

$$\frac{dP}{dt} = \beta\phi BP - \omega P \tag{1.2}$$

where r is the growth rate, K_c is the carrying capacity, γ is the natural death rate of the bacterial population; ϕ is the phage infection rate of the bacteria, β is the burst size and ω is the natural decay rate of the phage. Such mathematical formulations describe the experimental results of phage-bacteria dynamics in homogeneously mixed continuous culture flasks, such as chemostats. They assume that spatial correlations are quickly eliminated in shaken flasks and often predict mechanisms of coexistence. Such mean-field theories do not capture the dynamics that arise due to interactions specific to niche spatial microenvironments, density-dependent non-linear feedback caused by spatial constraints, nor modulated diffusion of phages through complex terrains in a biofilm.

Physics of phage-biofilm dynamics is relatively a nascent field of study compared to the study of biofilms or phage-bacteria dynamics. The heterogeneous spatial structure of biofilms offer niche microenvironments for certain phage-bacteria interactions. Their

susceptibility to phage is modulated through several factors such as, biofilm size, matrix composition, internal architecture, and cellular metabolic state.

In addition to targeted phages, immune system of the infected host is actively involved in clearing the infection. A recent report of phage therapy in animal models suggests that phages are successful only when the organism is not neutropenic [25]. In other words, phages effectively protected only those mice against *P. aeruginosa* which could produce neutrophils. Such results lead to the question of whether phages and neutrophils work synergistically to eliminate bacteria. Building on the work of Bull and Levin [26], Roach, Leung, Weitz, and Debarbieux recently proposed a non-linear model to examine how phages and innate immune responses together can eliminate the bacterial population, when neither can do so alone [27, 28]. These models are mean-field like and do not consider interactions which arise due to spatial structure of bacterial populations. Whether such synergies would be possible in spatially structured biofilms is a question of great scientific interest and one that motivated this thesis. As we began work to investigate this tripartite system, we recognized the gaps in the literature of the bipartite interactions between phage and biofilms as well as neutrophils and biofilms.

Therefore, in this thesis, we mainly explore the bipartite interactions of phage-biofilm systems which lays the foundation for investigating the tripartite interactions between phage-biofilm-immune cell systems in the future. For this purpose, we chose *P. aeruginosa* as our model bacterium because of its innate antimicrobial resistance, clinical relevance, accessibility, and potential for obtaining genetic variants from our collaborator Dr. Stephen P. Diggle at Georgia Tech. We then chose the Pseudomonas phage PEV2 for its ability to infect and lyse under anaerobic conditions which is often the case in high density biofilms.

In the second chapter, we present a compilation of the protocols for preparation and characterization of bacteria and phage. We elaborate on ways to design high-throughput phage-biofilm experiments and analyze the obtained multidimensional data. Further, we include the laboratory protocols for the extraction and processing of neutrophils for

performing immunophage studies. Some methods listed here were extensively used to obtain the results presented in later chapters whereas the others are yet to be employed widely. We hope that this chapter would serve as an experimental guide for future researchers.

In the third chapter, we discuss the impact of phage exposure on the planktonic fraction of spatially complex bacterial systems . Here, we probe a large parameter space of initial conditions high-throughput microtiter-based methods to gain a broad understanding of the dynamical landscape. Such detailed *in vitro* kinetic analyses offered valuable insights about the outcome of phage action in systems with sub-populations in different physiological states. We found that phages decimate bacterial populations when inoculated simultaneously, whereas when bacterial populations are allowed to form biofilms prior to phage exposure, planktonic population often reduces in a phage-dose dependent way.

In the fourth chapter, we examine the impact of phage addition on biofilms at different stages in their developmental cycle. We monitored the biofilms and phages under static conditions at high spatiotemporal resolution for a large number of initial biofilm conditions and phage titers. Four distinct response classes emerged, corresponding to the different biofilm developmental stages. The response classes exhibit unique functional dependences on the phage dosage, with a paradoxical reversal in the response between early stage biofilms and mature biofilms. Meanwhile, very little impact on biofilm outcome is evident for the dispersion stage even at high phage exposures. Interestingly, for each of the response classes, the highest phage exposure halts the biofilm from transitioning into the next developmental stage of the biofilm lifecycle.

In the final chapter, we present an outlook of the work done in this thesis and the questions we have answered in the process. We further discuss the questions it raises and elaborate on ways to address some of these questions. Lastly, we discuss the broad framework of immunophage synergy and what the future holds for this field.

CHAPTER 2
EXPERIMENTAL METHODS

Broader Context: This chapter is a compilation of the tools and techniques that were employed in this thesis to study the interactions between phage, bacteria, and immune cells. We present the experimental protocols in a numbered list format, a style typically used in JoVE articles. The collection of protocols presented here include basic microbiological methods for handling and characterizing the growth of bacteria and phage as well as practical methods for designing and implementing successful high-throughput experiments to study phage-biofilm dynamics. Further, we include the laboratory protocols for the extraction and advanced processing of neutrophils, a critical step for performing immunophage studies. Some of the methods listed here were extensively used to obtain the results presented in this thesis whereas the others were developed to perform preliminary studies but are yet to be employed widely to get concrete quantitative results.

2.1 Overview

Reliable scientific advancement depends on sound and reproducible laboratory methods. Therefore, in this chapter, we present a comprehensive record of the protocols that were developed and used as a part of this study. Since biofilm processes can be difficult to reproduce, we provide a clear, step-by-step instruction for performing the experiments and include the nuances that were critical for experimental success. Further, we provide detailed procedures for designing confocal microscopy experiments for large scale data acquisition and processing the obtained multidimensional image dataset. Additionally, the neutrophils were a generous gift from the lab of Dr. Rebecca Levit, Emory University. We followed the established protocols from the Levit lab to handle the neutrophils and the details are presented here.

2.2 Bacterial preparation and characterization

The bacteria used in this thesis is the wild-type strain of *Pseudomonas aeruginosa* (PAO1 - University of Nottingham, NPAO1 or University of Washington, PAO1), unless otherwise stated. It should be handled in BSL2 conditions, through aseptic techniques (work station sterilized with 70% ethanol) and proper use of personal protective equipment (lab coat, gloves, and googles).

P. aeruginosa is an opportunistic Gram-negative bacterium that grows readily in LB media. Its growth occurs in four stages lag, exponential, stationary, and death stage. The corresponding growth kinetics follows a sigmoidal curve and can be explained using the logistic model of bacterial growth. The characterization of bacterial growth in homogeneous system is generally performed through measurements of optical density and colony forming units (CFUs). The data obtained is then used to generate a standard growth curve for a given strain of bacterium.

2.2.1 Preparation of Media

A nutritionally rich medium known as Lysogeny broth (LB) is used for the growth of bacteria in this study. It contains tryptone, yeast extract, and salt. Tryptone offers the essential amino acids such as peptides and peptones, yeast extact offers a range of organic compounds that support bacterial growth, and sodium ions in salt aid in transport and maintaining osmotic balance. The broth formulation is used to grow liquid bacterial cultures and the agar formulation is used to create a nutritional surface for the growth of bacterial colonies and lawns.

1. Prepare the LB broth by adding 25 g of LB broth media (Sigma-Aldrich, L3522) to 1L of ultrapure water (ACS Reagent Grade, ASTM Type I and II).

2. Prepare the LB agar by adding 40 g of LB agar media (Sigma-Aldrich, L3147) to 1L of ultrapure water (ACS Reagent Grade, ASTM Type I and II).

3. Sterilize the media with a semi-tightened cap sealed with autoclave tape in an autoclave set to 121^oC for a sterilization time of 20 minutes.

4. After autoclaving, add any antibiotics if required at appropriate concentrations.

5. Place the agar media in a temperature bath set to 50^oC for 30 minutes to cool. Then pour 10-15 mL of agar media into 100 x 15 mm into circular petri dishes. Allow to set at room temperature, after an hour, invert the petri dish (to avoid condensation on agar surface) and let it set further overnight.

6. Tighten the cap and store the LB broth at room temperature. Store the LB agar plates in 4^oC fridge for up to two weeks.

2.2.2 Preparation of bacteria

Bacteria are typically stored in ultra-cold mechanical freezers (-70^oC to -90^oC) to decrease chances of growth (and therefore mutations and variations). Hence, prior to any experimentation, bacteria needs to be brought to appropriate temperature and growth conditions.

1. Streak bacteria from frozen stock on LB agar plates in lines (of decreasing densities) to obtain single bacterial colonies. Incubate the inverted plate in an incubator set to 37^oC for 16-18 hours (overnight).

2. Inoculate a single bacterial colony from the agar plate into 5 mL of LB broth in a 50 mL falcon tube. Let the bacteria grow overnight in a shaking incubator at 200 rpm, 37^oC.

3. Add 100 μL of the overnight culture to 5 mL of fresh LB broth and let grow under similar conditions for 3-4 hours so that the optical density of this sub-culture is approximately 1.

2.2.3 Measurement of colony forming units

Colony forming units (CFUs) are microbiological units for estimating the number of viable cells in a sample. After significant growth, colonies of bacteria become visible. Estimation of bacterial numbers by CFU has the implicit assumption that every colony is founded by a single viable bacterial cell. Therefore, it is important to obtain a plate count in the linear range (30-300 CFU for *P. aeruginosa*). To get a yield CFU in this range, serial ten-fold dilutions are used and several dilutions are plated in replicates.

1. For every measurement, prepare nine 15 mL falcon tubes by adding 9 mL of LB broth in each and label them: -1, -2, -3, -4, -5, -6, -7, -8, and -9 and prepare 27 (nine times three, for triplicate data) agar plates by labelling them with the details of the sample and dilution factors.

2. Add 1 mL of the bacterial culture of interest to the tube labelled -1 and vortex thoroughly.

3. Serially transfer 1 mL from the -1 tube to the other dilution tubes down to the -9 tube, vortexing after each transfer.

4. Dispense 100 μL of the bacterial dilution to the corresponding LB agar plate and spread using a sterile cell spreader. The range can be narrowed down based on previous calibration data.

5. Invert the spread plates and incubate overnight at 37^{o}C.

6. Once colonies grow visibly, count the number of colonies for each dilution plate and record all the measurements. Choose the dilution plate with 30-300 colonies for each replicate and obtain the average value. Next, perform the following calculation to obtain CFU/mL:

$$\text{CFU/mL} = \text{Number of colonies} \times 10^{(\text{-Dilution factor+1})} \tag{2.1}$$

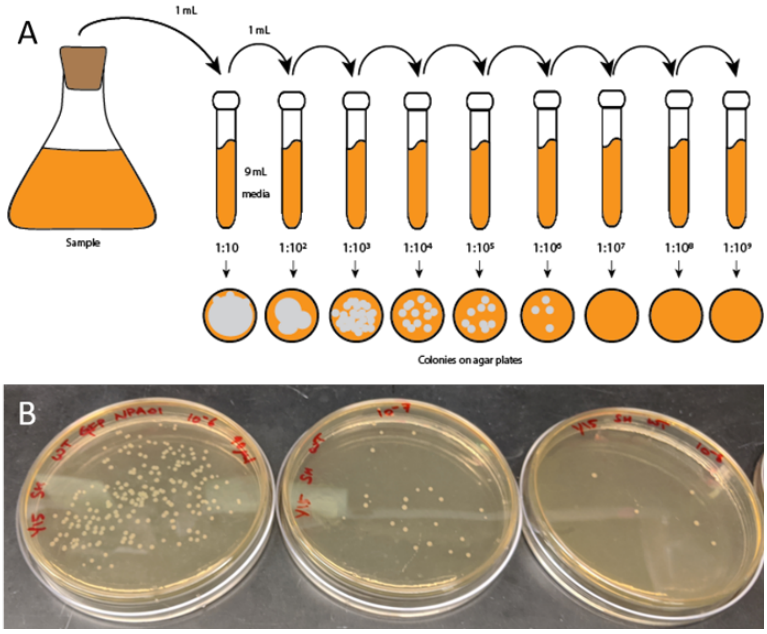

Figure 2.1: ***Pseudomonas aeruginosa* bacterial culture** A) This schematic shows the experimental procedure for determining the viable bacterial density in a particular sample at that point in time; B) Bacterial colonies on agar plated at different dilutions

2.2.4 Measurement of optical density

Optical density (OD) of bacterial cultures is a measure of turbidity and at low bacterial concentrations, it is linearly proportional to the concentration of bacteria present. These measurements are typically obtained using spectrophotometers. For bacterial optical density determination, light of 600 nm wavelength is incident on the sample and resulting absorbance values are recorded. Since these values are obtained using light scattering, it depends sensitively on the optical setup of spectrophotometer. Comparison between ODs from different spectrophotometers should happen after appropriate normalization through correction factors or comparison of calibration curves.

1. Withdraw 1 mL of the bacterial sample of interest into a clean spectrophotometer cuvette.

2. Record the absorbance or optical density reading at 600 nm.

3. In case the measurement is greater than 1, dilute the sample by 10-fold and record the optical density. Multiply the new OD by 10 to get the final OD_{600} measurement.

2.2.5 Generation of growth curve and calibration curve

The proliferation of microbial cells with time can be monitored using closely spaced optical density measurements. The implicit assumption is that of Beer-Lambert law which states that the optical density is proportional to concentration. It is true in the regime where the number of bacteria in the sample is small. The size and shape of bacteria, its index of refraction with respect to media, etc. are factors that go into determining the proportionality constant. The actual relationship between optical density and cell number can be obtained by performing both optical density as well as colony forming unit measurements simultaneously and constructing a calibration curve.

1. Grow the bacteria of interest in a flask at chosen growth conditions (see 2.1.2 for details about PAO1).

2. Choose appropriate timepoint interval depending on the growth characteristics of the bacteria (shorter intervals for fast-growers and longer intervals for slow-growers).

3. At each timepoint, measure the colony forming unit (CFU/mL) and the optical density as outlined in 2.1.3 and 2.1.4 respectively.

4. To obtain the growth curves, plot the OD and CFU/mL measurements against time.

5. To obtain the calibration curve, plot the CFU vs OD for all measurements whose OD was less than 1.0. Fit the curve using linear regression and obtain the equation and the R^2value.

2.3 Phage preparation and characterization

Standardized protocols for phage handling is crucial for the reproducibility of phage-biofilm experiments. In this section, we present the procedures for phage amplification, extract, purification, enumeration, fluorescent tagging, and determination of its life trait parameters.

2.3.1 Amplification, extraction, and purification of phage

Phages proliferate within their target host bacterium like all viruses. Here, we use this natural mechanism of amplification to obtain phages at high titers. This method amplifies phages in liquid bacterial culture. Chloroform treatment lyses infected cells with intracellular phages. It is a common step in isolation and propagation protocols for maximizing phages that are released. In addition, this treatment excludes filamentous phages from being isolated as it inactivates both filamentous and lipid containing phages. Centrifugation is performed to separate the bacterial debris from the phage isolate. The extracted phages are further purified using filtration. It is advisable to use the same phage stock for a set of experiments to ensure consistency.

1. In a 50 mL Falcon tube with 5 mL LB, inoculate 20 μL from an overnight bacterial culture. Incubate at 37^oC (if *P. aeruginosa*), shaking at 200 rpm, for 6 hours.

2. Use a sterile loop to introduce in the tube a single plaque of phage or 10 μl of the phage master stock.

3. Incubate at 37^oC, static, for 24 hours (depending on the phage, it can be useful to gently mix two or three times during incubation).

4. To isolate phages from the culture after he 24-hour incubation period, sample 1 mL of culture with bacteria and phage. Add 110 μL chloroform (safety precautions to be followed according to SDS) that will kill bacteria.

5. Vortex thoroughly then centrifuge at 16000g for 4 minutes. Keep the supernatant with phage.

6. Purify the supernatant with a filter of pore size 200 nm (4612, Acrodisc Syringe Filters with Supor Membrane, Sterile, 0.2 μm, 25 mm) and store the stock at 4^{o}C.

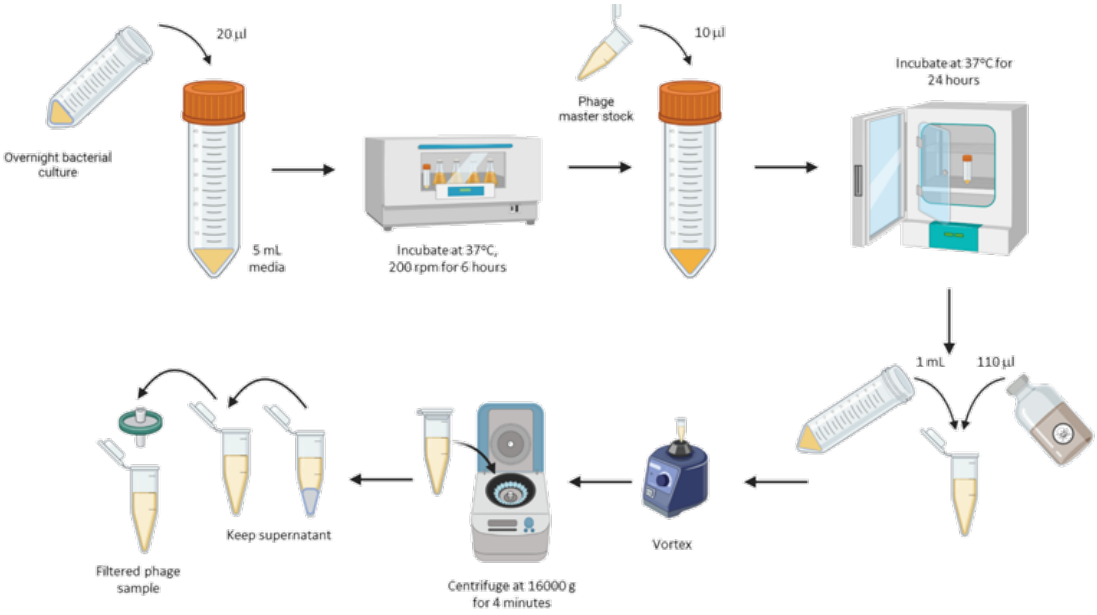

Figure 2.2: **Phage propagation and purification**Schematic illustrating the steps for phage propagation and purification. Created with BioRender.com

2.3.2 Quantification of phage using double agar overlay assay

The double agar overlay assay is a technique used for the enumeration and identification of phages. Many phages including PEV2 form large, well-defined plaques that are easily observed and can be used for enumeration. In fact, the ability of phages to produce plaques in a bacterial lawn led to their discovery in 1915. This technique has been widely since then to isolate, quantify, and characterize phages. The hard agar layer at the bottom functions as an additional nutritional layer. The soft agar layer on top of it allows for the growth of bacterial lawn within it. Similar to the principle of obtaining CFU (bacterial count), after

significant growth, plaques of phages become visible. Estimation of phage numbers by plaques has the implicit assumption that every plaque is founded by a single viable phage. To get a countable yield of plaques, serial ten-fold dilutions are used and several dilutions are dropped onto the plates in replicates.

1. Preparation of soft agar: Soft agar contains 0.75% w/v agar. Prepare by adding 20 g of LB agar media (Sigma-Aldrich, L3147) and 12.5 g of LB broth media (Sigma-Aldrich, L3522) to 1L of ultrapure water (ACS Reagent Grade, ASTM Type I and II).

2. Melt soft agar and let the temperature cool down to about 55^oC (you should be able to touch the tube easily).

3. Add $\sim$10% of bacterial overnight culture (recommended: 1 mL of bacteria in 10 mL of soft agar, if you prepare more you need to be very fast otherwise the soft agar will solidify and will no longer serve the purpose). Vortex the mixture carefully avoiding spills (high temperature and quantity of soft agar has higher probability of spilling in spite of tight closure of the tube).

4. Spread 1-1.5 mL of this mixture onto a typical LB agar Petri dish. Let dry.

5. Separate each Petri dish in 3 or 6 parts and write the dilution on each part at the back of the petri dish. Prepare the phage dilutions in LB broth.

6. Plate 5 μL droplets of each phage dilution. Usually you can do 2 or 3 droplets in each part but be sure you are not too close from the edge of the dish and that they wont merge. Let dry, dishes open (it takes about 30 minutes depending on the temperature and humidity conditions in the lab).

7. Once dry, invert the petri dishes upside down and leave it at room temperature on the bench. You can start counting about 12 hours after plating (you can use a binocular

or count it against the light). If you are in a hurry you can put them at 37^{o}C but check them often.

2.3.3 Quantification of phage using light scattering

NanoSight instruments characterize nanoparticles of size 10-1000 nm using Nanoparticle Tracking Analysis (NTA). It analyses the diffusion properties of each particle using light scattering and Brownian motion. The scattered light can be visualized with a 20x magnification microscope and the camera mounted on it records a video of the Brownian motion of particles at 30 frames per second (fps). The software tracks multiple particles, calculates their hydrodynamic radii using Stokes-Einstein equation and outputs high-resolution results for nanoparticle size distribution and concentration. PEV2 phages are 70 nm in size and can theoretically be characterized using NanoSight.

1. Perform the sample set-up according to recommended protocols of the NanoSight manufacturer (Malvern Panalytical, NS300).

2. Prepare 10 mL of each of these phage dilutions 10^8, 10^7, and 10^6 PFU/mL.

3. Inject 300-400 μL of the 10^8 PFU/mL dilution aseptically into the specimen chamber until it reaches the nozzle tip and is visible.

4. Use the NTA software to adjust parameters prior to video capture.

5. Record the analysis details, particle sizes and their corresponding concentrations. Limitations based on problems encountered Highly sensitive to impurities as it measures all particles including debris (if sample is not ultra-pure), dead and/or nonviable phages. In addition, the suspension media (LB broth) leads to high levels of background noise and makes result interpretation often impossible. (needs clear media but phages cannot be diluted below 106 PFU/mL due to detection limits of the instrument).

2.3.4 Fluorescent labeling of phage

Since traditional culture-based methods are effort-intensive and time-consuming, high-throughput methods like fluorescent labeling of phages to track their dynamics will accelerate the process of understanding phage-biofilm systems. Fluorescently tagging phages for interaction and dynamical studies are less simpler compared to laborious purification procedures and genetic engineering of phages to express fluorescent phages. Fluorescent labelling of phage involves three key steps purification, labelling with dye, and removal of excess dye as detailed below.

1. Purification through PEG precipitation: Add 1 mg of DNaseI to 50 mL of the isolated phage and incubate for 30 minutes. Add NaCl to the lysate such that the final concentration is 0.25 M. Incubate for 1 hour at 4C. Centrifuge the mixture at 4C, 8000g for 10 minutes and collect the supernatant. Filter it with a filter of pore size 200 nm (4612, Acrodisc Syringe Filters with Supor Membrane, Sterile, 0.2 μm, 25 mm). Add PEG8000 such to the filtered phage such that the final PEG concentration is 20% and let the phage precipitate overnight at 4^oC. Next, centrifuge for 15 minutes at 8000g, 4C and suspend the phages in phosphate-buffered saline (PBS).

2. Labelling with dye: Add 0.1 mg of Alexa Fluor 488 to 100 μL of phage mixed with sodium carbonate. Incubate for 1 hour at room temperature.

3. Dialysis to remove excess dye: Transfer the phage sample to a dialysis cassette (3 kDa 50 kDa NWCO cutoff). Dialyze against 1 liter of gelatin-free SM buffer containing 1 M NaCl, (add 52 g NaCl per liter buffer) at 4^oC overnight. Transfer the dialysis cassette to 1 liter of normal gelatin-free SM and dialyze for 2-3 hrs at room temperature. Repeat once more.

2.3.5 One step phage growth parameter determination

The one-step phage growth experiment was developed by Max Delbruck and Emory Ellis is 1939, marking the beginning of modern bacteriophage research [29]. It measures the latent period and burst size of the chosen phage for a given host in planktonic conditions. Latent period is the minimum time taken from phage adsorption to bacterial lysis and release of progeny phages. Burst size is a measure of the average number of phages released per infected bacterium. This can be adapted to test the effects of different environmental factors on the infection process.

1. Mix a culture of the susceptible bacteria and the phage, allow the phage a short interval of time to adsorb.

2. Dilute the mixture by multiple-fold so that the phage released on lysis would not immediately infect other bacterial cells.

3. Determine the phage particles released from bacteria through subsequent double agar overlay assays performed at frequent intervals.

4. Plot the phage number released from host cells versus time. The curve would consist of a latent period followed by a rise period or burst, when bacteria lyse and release new phage.

During the first part of the latent period, infected bacteria do not contain complete virions this period is known as the eclipse period. In order to estimate the eclipse period, bacteria could be lysed prior to performing the plaque count using double agar overlay assay. The number of phage within the host increases at the end of eclipse period and the host bacterium is prepared for lysis.

2.4 Designing and implementing biofilm experiments

To test the susceptibility of biofilms towards phage, microtiter-well-plate based optical methods offer a reproducible and high-throughput platform with reasonable experimental turnaround times. The protocol presented here is inspired from a fast and reliable method for the formation of *P. aeruginosa* biofilms proposed by Musken et al [30]. It has been adapted here for phage susceptibility testing and monitoring of spatiotemporal dynamics. Here, we combine bacterial viability staining and automated spinning disk laser confocal microscopy for the quantitative evaluation of the phage impact on bacterial cells within biofilms. In addition, we employ crystal violet staining for assessing the overall impact on phage on biofilm biomass including the polymeric matrix.

2.4.1 Preparation of biofilm samples

We prepare biofilm samples in 96 well-microtiter-plate systems for high-throughput experimentation. The following protocol is optimized for humidity control and number of samples for probing. The 36 outermost wells in the plate are filled with water to ensure high humidity and moisture. Therefore, we have 60 wells available per plate for biofilm preparation and experimentation. To visualize bacteria within the biofilm, we use Filmtracer LIVE/DEAD Biofilm Viability Kit with SYTO9 and Propidium iodide stains to label live and dead bacterium. We found that this method led to lower photobleaching effects compared with the use of fluorescent protein expressing bacteria. SYTO9 stains both live and dead (with damaged membrane) bacteria in a system when added alone. When added along with propidium iodide, the fluorescence of SYTO9 in damaged bacteria is reduced and these bacteria stain fluorescent red.

1. Prepare bacterial solution as outlined in Section 2.2.2. Dilute this solution to desired seeding densities according to dilution factor obtained using the calibration curve. Add the appropriate dilutions into the microtiter plate wells to seed the well with

bacterium for biofilm growth.

2. Prepare stock solutions for each stain depending on final concentration requirements (e.g. SYTO9, propidium iodide, etc.)

3. Add 10 μL of stock staining solution to each well directly to achieve a final concentration of 1.4 μM of SYTO9 and 8.3 μM of PI in the wells.

4. Place the plate in a static incubator at 37^oC

Use a pipette and add the solution at a 45^o angle toward the centre. With some *P. aeruginosa* strains, the solution sticks to the well wall because of some kind of strain-induced hydrophobicity and does not come in contact with the biofilm. In these cases, solutions (dye and phage) need to be added carefully from the top without touching the wall.

Do not expose the fluorescent dyes to light, as both components are light sensitive. Incubation and microscopy are usually performed in the dark.

2.4.2 Confocal microscopy

Confocal microscopy allows for high-contrast imaging of dense live samples by optical sectioning. It reduces the out-of-focus light from the plane of interest using a spatial pinhole placed in front of the detector and/or laser. Laser scanning confocal microscopes allow for high resolution imaging but take longer to generate the images, which is often not suitable for capturing a dynamical system. We therefore used spinning disk laser confocal microscopy to overcome some of these constraints. This method splits the main laser beam into $\sim$1000 smaller beams which pass through a matching pinhole and are focused on the sample. This disk is rotated to sweep the pattern of laser beams and excite the corresponding fluorescent molecules in the sample, thereby illuminating multiple points in the sample simultaneously and reduces the image acquisition time (Figure 2.4b. This setup

combined with a microscope that has an automated stage and Perfect Focus feature allows for complete automation of time-series data acquisition.

Wear appropriate protective equipment when working with lasers. Avoid exposure to the laser beam as it can cause serious, irreversible eye injuries.

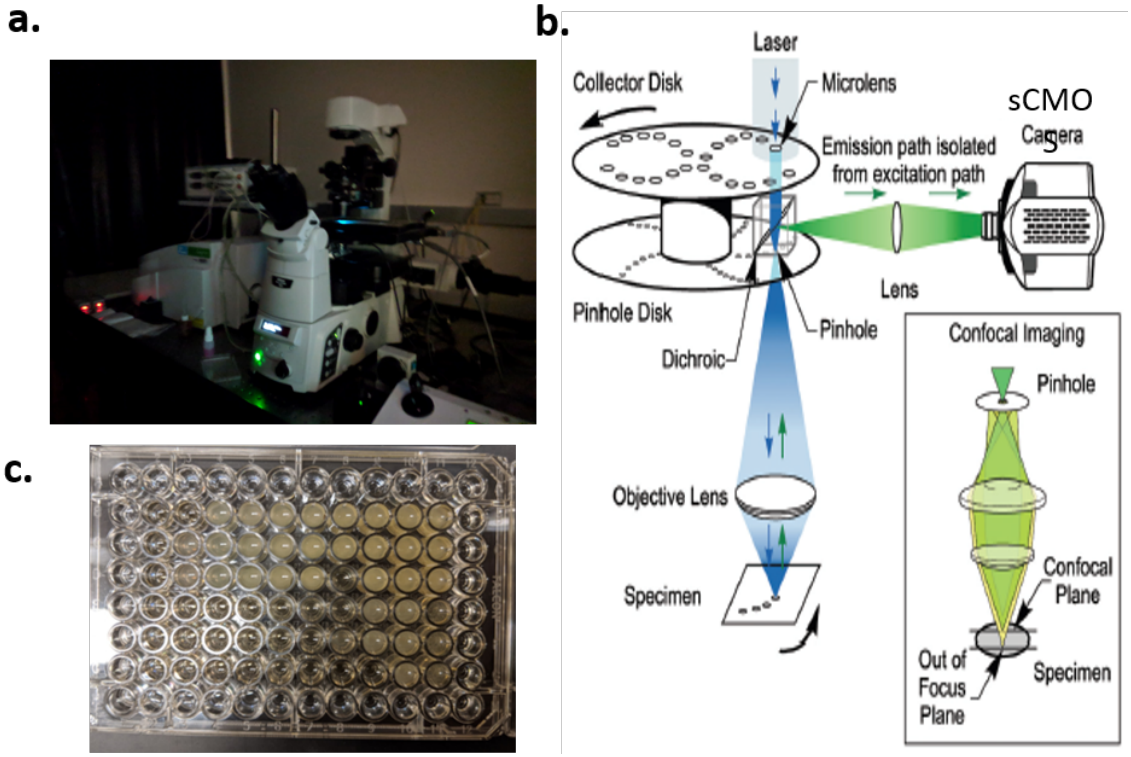

Figure 2.3: **Spinning disk laser confocal microscopy.** a | Photograph of the microscope in action used in this thesis; b | Schematic illustrating the principle of operation. This image was originally published in "An Overview of Spinning Disk Confocal Microscopy", Andor, Oxford Instruments. Reprinted here under the Attribution-NonCommercial 4.0 International (CC BY-NC 4.0).; c | Microtiter plate with wells filled with phage-biofilm samples for imaging

1. Use the automated spinning disk confocal microscope (Perkin Elmer UltraVIEW VoX, Nikon Ti-Eclipse inverted microscope with Perfect Focus 3 and Yokogawa spinning disk confocal unit, using a 60x oil objective with N.A. 1.49 and Hamamatsu FLASH 4 sCMOS version 2 camera) to image the biofilms every 60 minutes for 16 hours.

2. With this optical setup and imaging objective, the magnification was 0.117 μm in the XY plane and 1 μm step size in the z-direction. The shutters were managed for balanced protection and speed.

3. Calibrate the XY stage and create the well overlay using the Make Well Overlay option from the Stage menu of the Volocity software. Save the overlay for future reference. Next, choose points in the wells using Create Points from Well Overlay option from the Stage menu. Select Multiple Tiled Points from the drop-down menu to add a matrix of multiple points at the centre of each well. 4. Specify the required number of Points per well.

4. Determine the maximum height of the z-stacks and acquire the z-stack of the biofilm. Focal planes are acquired starting from few planes below the bottom of the plate with an interplane distance (z-step size) of Y μm (depends on the Nyquist spacing for the objective and the goals of the experiment). Autofocus once per well per timepoint. SYTO9 is excited with a 488-nm laser and detected with a 540/75 nm band-pass emission filter, whereas PI is excited at 561 nm and detected with a 600/40 nm band-pass emission filter. Set the exposure time to 100 ms per image or appropriate values.

5. If a non-automated confocal microscope is used, choose adequate filter settings for SYTO9 and PI. To enhance comparability, biofilm images should be recorded at the center of a well (z-stacks should be acquired at the center of the well because images of peripheral structures are less comparable and are not representative of the broader dynamics.

2.4.3 Image Analysis

The images obtained from the confocal microscope are generally accessible only through the microscopes software. It needs to be exported to formats such as .tiff, .png, etc so that it can be read and processed through other programs. Here, Volocity is a licensed

software of Perkin Elmer used for image acquisition. The data from Volocity is exported as .tiff files for further custom processing with MATLAB. MATLAB is a licensed software and is not readily available everywhere. We use the MATLAB compiler to compile our MATLAB programs as executables. Example pseudocodes are provided below to explain the workflow (Section A.1). The major feature of interest for this study is the volume occupied by live and dead bacteria in the biofilm. The data from different fluorescent dyes are captured through different channels in the microscope each channel has its own set of images. Due to the large amount of image data generated in these experiments, we designed an automated image processing pipeline for analyzing the images in a similar fashion. On extracting the image of interest, we apply the matlab inbuilt function known as adaptthresh for thresholding and binarizing the image. This function has two main parameters, sensitivity and statistic. We keep the two parameters constant for all images acquired with the same imaging properties. We then create a small disk-shaped structuring element to morphologically close appropriate gaps. The close operation is a dilation followed by an erosion, using the same structuring element for both. Next, to remove any noise from being detected as bacteria, we use the bwareaopen function to eliminate any objects with pixels fewer than that mentioned as its parameter. The sum of all the pixels of a binarized image gives the area occupied by the object generating the fluorescent signal. The volume of the relevant objects in the confocal stack can be obtained by summing over the area of all the planes belonging to the particular channel of the stack and multiplying it by the z step size. Further, since SYTO9 stains all bacteria, we obtained the volume of live bacteria by subtracting the volume of propidium iodide from that of SYTO9.

1. Preprocessing: The 3D z-stacks were exported as .tiff files from the Volocity software and processed with Matlab through custom codes (pseudo-codes available in section A.1).

2. Thresholding and binarization: The images were initially binarized using an adaptive thresholding algorithm. The total number of bacteria was determined for all samples

by counting all voxels in the confocal z-stacks that had a signal that was above the noise threshold, indicating bacteria was present.

3. Morphological operations: We performed morphological closing on the grayscale or binary image I using a single structuring element object returned by the strel or offsetstrel functions. The morphological close operation is a dilation followed by an erosion, which uses the same structuring element for both operations.

4. Volume determination: The total volumes of objects in the confocal stack were estimated by counting the non-zero voxels in the binarized image stack for each channel.

5. One imaging location within a well was defined as one replicate. Three locations were imaged per well.

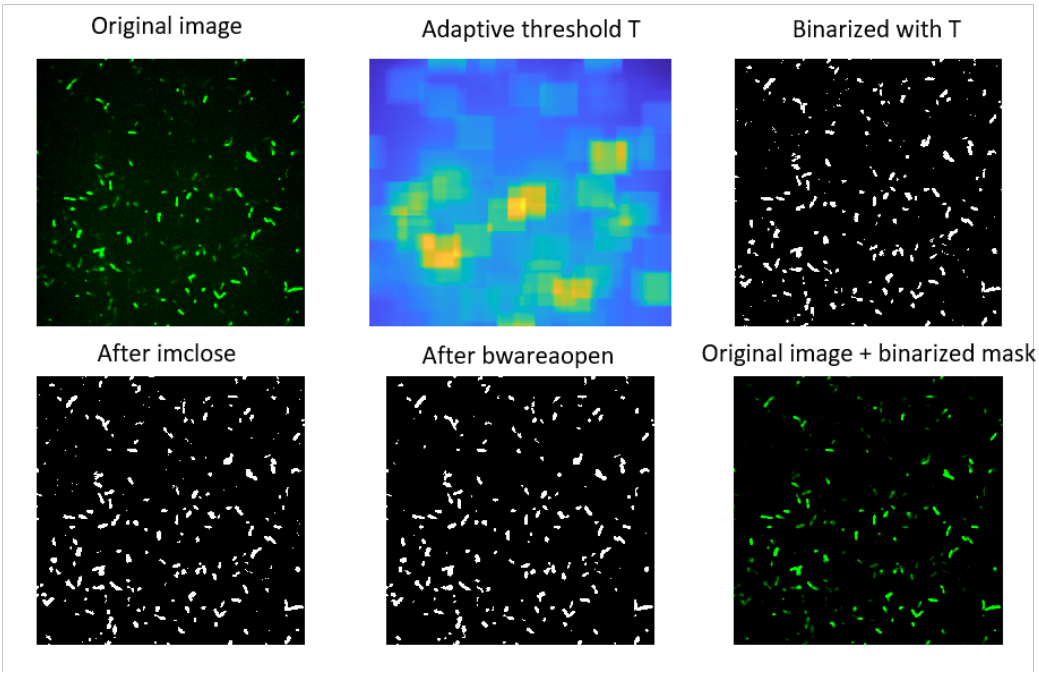

Figure 2.4: **Image processing pipeline** | Representaive image from spinning disk confocal microscopy (1024 x 1024 pixels) and the visualization of intermediate processing steps. The last image (bottom left) shows the image after the application of the binary mask (bottom center).

2.4.4 Crystal violet staining

The following protocol for quantifying the biofilm biomass in a microtiter well using the crystal violet (CV) dye has been adapted from the seminal paper written by George OToole [113].

1. Prepare 3 replicates of the sample of interest for biofilm biomass quantification. It could be biofilms grown for a certain duration or biofilms treated with specific agents in well plates.

2. Discard the cells by inverting the plate and shaking away the liquid component.

3. Submerge the plate in a small container of water. Repeat again to help remove unattached cells and reduce background staining.

4. Add 125 μL of a 0.1% solution of crystal violet in water to each well of the 96-well plate (Note: CV is hydroscopic and stains easily)

5. Submerge the plate in water and rinse 3-4 times and blot vigorously on paper to remove excess cells and dye.

6. Invert the plate and let dry for a few hours or overnight.

7. Then add 125 μL of 30% acetic acid in water to each well of the microtiter plate to solubilize the CV.

8. Incubate the microtiter plate for 10-15 min at room temperature.

9. Transfer 125 μL of the solubilized CV to a new flat bottomed microtiter dish.

10. Measure absorbance at a wavelength between 500-570 nm using 30% acetic acid in water as blank.

2.5 Characterization of immune cells

In collaboration with the Levit Cardiovascular Lab (PI: Dr. Rebecca Levit) at Emory University, peripheral blood from healthy human volunteers was collected. All studies that involve drawing human blood were approved by the Emory University Institutional Review Board and were in accordance with institutional guidelines. All donors gave consent before blood draw.

The cells of interest for testing immunophage synergy are neutrophils. Neutrophils have been identified as an essential component of innate immunity against bacterial infections **??** through *in vivo* studies. Therefore, for the in vitro experimentation in this thesis, we employ neutrophils to probe neutrophil-biofilm interactions and dynamics.

2.5.1 Neutrophil collection and counting

Neutrophils are the most common circulating white blood cell, making up 50% to 75% of these cells. Neutrophils are made in the bone marrow and live for less than a day. The body can make $\sim 10^{11}$ neutrophils a day. Neutrophils are extracted from blood using the following protocol and due to their short life span, these cells should be used immediately after extraction.

1. Collect 10 mL of venous blood from healthy volunteers using a 21-gauge needle in EDTA containing Vacutainer (366643; Becton, Dickinson and Company, Franklin Lakes, NJ) and overlaid on 5 ml lympholyte cell separation media (CL5071; Cedarlane Labs, Burlington, NC).

2. Centrifuge the tubes at 1600 rpm for 35 minutes at 20^{o}C.

3. Collect the neutrophils from interphase and dilute in 10 mL of Hanks balanced salt solution without calcium/magnesium (SH30588.02; GE Health Life Sciences).

4. Spin the cell suspension at 1600 rpm for 10 minutes at 20^oC and remove the supernatant.

5. Wash the pellet, lyse with red blood cell lysis buffer (11814389001; SigmaAldrich, St. Louis, MO), centrifuge at 1200 rpm for 5 minutes at 20^oC, and remove the supernatant.

6. Resuspend the cells in 10 mL Hanks balanced salt solution without calcium/magnesium.

7. Centrifuge the tubes at 1600 rpm for 10 minutes at 20^oC and the resuspend the pellet in RPMI 1640 medium without lglutamine and phenol red (R75091L; SigmaAldrich).

8. Determine the health of the neutrophils by examining them under a low magnification microscope and ascertain the density of viable cells using a hemocytometer.

2.5.2 Neutrophil staining

The components of a neutrophil can be stained with appropriate fluorescent dyes for visualization through microscopy. For example, Hoechst dye is a blue fluorescent stain specific for DNA and can be used for labeling the nuclei of neutrophils. It is a cell-permeable stain that is excited by ultraviolet light and emits blue fluorescence at 460 to 490 nm. SYTOX Green is another nucleic acid stain that is impermeant to live cells, making it a useful indicator of dead cells within a population. In this case, it can be used to identify neutrophils that have disintegrated to form neutrophil extracellular traps (NETs).

1. Seed neutrophils onto 96-well plates at a density of 5 10^4 cells/well in 100 μl RPMI 1640 media.

2. Add Hoescht dye (H3570, ThermoFisher) at 0.2 to 5 μg/mL for 20-30 minutes to label nuclei of intact neutrophils.

3. Add 5 μM SYTOX green dye (S7020; Invitrogen, Carlsbad, CA) to each well and the image using confocal microscopy with filter setting at 485-nm excitation/525-nm emission.

2.6 Conclusion

In this chapter, we presented protocols for preparation and characterization of bacteria and phage, designing high-throughput biofilm experiments and analyzing obtained data, and handling neutrophil samples. Scaling biofilm experiments to high throughput levels requires standardization of each step and detailed documentation. Such biophysical experiments, especially those involving microscopy, could generate large amounts of data. Adequate computing power and algorithmic knowledge would help extract relevant features that are essential for generating scientific insights. We hope that this chapter would serve as a guide to future students interested in performing phage-biofilm-immune cell research.

CHAPTER 3

POPULATION DYNAMICS OF PLANKTONIC BACTERIA ON PHAGE EXPOSURE IN MIXED-STATE SYSTEMS

Adapted from H. Selvakumar, M. Dominguez, S. P. Diggle, J. S. Weitz, and J. E. Curtis., Population dynamics of planktonic bacteria on phage exposure in mixed-state systems, (In preparation).

Broader Context: Bacteria adopts different modes of growth, mainly planktonic and biofilm lifestyles. Planktonic-state bacteria are freely swimming and fast growing whereas biofilm-state bacteria are spatially clustered and slow growing. Due to these structural and physiological differences, we hypothesized that their susceptibility to phage attack and resulting dynamics would differ significantly. In this study, we limit our experiments and discussions to the effect of phage exposure on planktonic fractions of a mixed state system containing both planktonic and biofilm bacteria. Such mixed state systems are often used to determine susceptibility to antimicrobials in a high-throughput fashion. They are therefore important systems to understand which would in turn facilitate better interpretation of results. Our investigations led to the mapping of bacterial dynamics for a wide range of initial conditions in the parameter space. We found interesting features in the dynamics that existing models do not explain. We hope that ongoing work with our collaborators where we use this rich data set to test quantitative models would yield insights into the mechanisms leading to observed outcomes.

3.1 Overview

The population dynamics of homogeneously distributed planktonic or freely swimming bacteria and phage systems at ecological and evolutionary scales has been explored in prior

studies [24, 31, 32]. Yet, little is known about the dynamics that unfolds when planktonic bacteria co-existing with biofilms are exposed to phage. Planktonic-state bacteria are considered to be fast growing and fragile whereas biofilm-state bacteria are often slow growing and resilient [33]. Here, we investigate this mixed-state dynamical system for a wide range of initial conditions using an experimental approach. The central motivation is to understand the differential impact of phage, a therapeutically promising agent, on planktonic and biofilm sub-populations in a system.

In these studies, we use the wild-type Nottingham strain of *Pseudomonas aeruginosa* (PAO1) as the model bacterium to perform our experiments unless otherwise stated. *P.aeruginosa* is an opportunistic, rod-shaped gram-negative bacterium found in nosocomial, acute, and chronic infections [34]. Patients suffering cystic fibrosis, cancer, and severe burns and wounds are at a higher risk of mortality when infected by this pathogen [34, 35]. It is found in natural, industrial, and medical settings [36]. Due to its high innate resistance to antibiotics and ability to readily forms biofilms, *P.aeruginosa* infections result in significant morbidity and mortality rates [37, 38]. Reports have shown that extrinsic antibiotic resistance can be acquired through horizontal gene transfer and mutation-driven resistance [38–40].

Further, we employ the *Pseudomonas* phage PEV2, a podovirus that encapsulates $\sim$75 kb of genome in its protein capsid [41, 42]. It is $\sim$70 nm in size and has a latent period of 25 minutes. PEV2 is known to obligately lyse *Pseudomonas* under aerobic conditions. Under anerobic conditions, its latent period triples, lysis slows down, and burst rate decreases. The burst rate for aerobic infection is $\sim$100-150 phage/cell. LPS, particularly O-specific 2 antigen (B-band) serves as an essential receptor for phage adsorption to PAO1.

The study of this system is motivated by the necessity to understand the therapeutic limits of phage therapy. Phage therapy, the practice of using bacterial viruses to treat infections, is currently considered the last resort strategy for patients who do not respond to other forms of treatment [16, 17, 43, 44]. In such cases, there is a high likelihood of biofilm

formation in these infections and understanding phage-bacteria interactions and phage-biofilm dynamics is essential to determine the efficacy and limitation of this therapeutic approach [45–48]. Most preclinical in vitro studies characterize phage-bacteria dynamics through killing curves and focus on planktonic cultures neglecting the complexities that arise due to spatial structures within biofilms. The effects of bacterial infections amplify when biofilms are present, especially observed in chronic infections [49, 50]. Biofilms offer the perfect environment for the constituent bacteria to become virulent and often obtain antibiotic-resistant properties [2, 49, 51–58]. Therefore, for phages to realize their full potential as a therapeutic agent, a comprehensive understanding of phage-bacteria interactions and dynamics in complex environments is critical.

In this chapter, we present a brief review of phage-bacteria dynamical systems in section 3.2 before diving into the details of our experimental approach and findings in section 3.3. Our investigations led to the characterization of the dynamics of a large set of unique phage-bacteria initial conditions. Here, we limit our discussion to the planktonic-state sub-population of the complex bacterial system while in the next chapter, we address the dynamics of biofilm-state sub-population in the presence of phage. Samples inoculated simultaneously with planktonic-state bacteria and phage are decimated by the PEV2 bacteriophage, except at low viral exposures or high initial bacterial densities. In matured bacterial communities that are allowed to develop a planktonic and biofilm fraction before phage exposure, the planktonic bacteria survive for at least the experimental duration albeit at reduced, often at steady densities. Further, our observations suggest two unique outcomes states in the phage-treated biofilms : reemergent states and pseudo-steady states. Moreover, these experiments uncover novel dynamics while providing a rich data set to facilitate the testing of quantitative models. Together with our collaborators at the Weitz group, we are working on developing mathematical models to provide insights about the underlying processes.

3.2 Background

Bacteriophages were identified as novel bacteriolytic agents by two independent studies a century ago [59–61]. They were used as a therapeutic for common bacterial infections a few decades before antibiotics dominated the forefront. Due to the high specificity of phages with respect to the bacterial strain they infect, they were quickly overshadowed by the inexpensive broad-spectrum antibiotics to treat infections. In the meanwhile, phages continued to be a critical tool for the advancement molecular biology [62, 63]. With the overuse and misuse of antibiotics, the number of multidrug resistant (MDR) strains of bacteria, commonly known as superbugs, has expanded worldwide [17, 64, 65]. This has led to renewed interest in phage from a therapeutic perspective over the last 20 years [43, 59, 66–70].

Phages have been highly regarded for their self-amplifying effect at the target site, ability to infiltrate biofilms, potential to lyse persister cells on reactivation, and their high degree of specificity against the pathogenic microbe, without causing harm to the commensals [71–73]. Despite their apparent potential, systematic studies on phage-bacteria and phage-biofilm dynamics are limited currently. Such studies are the need of the hour in order to evaluate the pros and cons of phage and phage-combination therapies. In this section, we detail some of the approaches employed in the literature to shed light on phage-bacteria interactions and the dynamical outcomes that follow.

3.2.1 Understanding of phage-bacteria systems through experimentation

In vitro experimentation provides a high degree of control over initial conditions and easy access to monitor changes in phage-bacteria systems. This approach helps gain qualitative and quantitative insights to understand phage-bacteria dynamics. Once a phage is well-characterized, the susceptibility of bacteria to the phage under consideration is first determined through a standard plaque assay. During a plaque assay, a soft agar bacterial

lawn is grown over a layer of hard agar, followed by the addition of diluted phage in spots. The clearance of the lawn (known as plaques) is an indicator of bacterial susceptibility to the phage. Enumeration of the plaques under appropriate conditions yields the phage titer.

Following the fundamental characterization of the phage and bacteria of interest, can be broadly divided into two categories: 1) chemostat-based ecological experiments and 2) microtiter-plate based susceptibility experiments. The spatiotemporal scales of these approaches widely vary due to the difference in the types of questions they aim to answer. While chemostat-based experiments provide insight about the dynamical systems from a theoretical ecology perspective, microtiter-plate based studies either focus on the efficacy of phage to clear planktonic bacteria or on the potential of phage to control or remove biofilms.

Chemostat-based experimentation of phage-bacteria systems over long timescales have helped obtain insights into the ecological and evolutionary dynamics of the system [31, 74, 75]. A chemostat is a continuous flow-reactor with a constant volume and a constant input of resources. The constant mixing within chemostats made it possible to main a homogenous distribution of the microbes. Therefore, the non-linear populations dynamics of such systems is well approximated by mean-field models (more in 2.2.2). Quantitative experiments measuring the phage-bacteria populations over time were used by Levin and colleagues originally in 1977 to understand complex dynamics that arise due to interaction between phage, bacteria, and nutrients [76]. Further studies revealed dynamical possibilities such as predator-driven top-down control of bacterial populations, oscillations between the phage-bacteria populations, and evolution of phage-resistant sub-populations over long durations [24].

On the other hand, *in vitro* microtiter-plate based growth kinetics and susceptibility tests [77, 78] are performed over a shorter timescale and are used to inform therapeutic dosing *in vivo*. Such experiments are performed under finite and diminishing resource conditions. In addition, they often involve static conditions with the possibility of emergence of spatially

structured bacterial communities. Most phage microtiter-plate based susceptibility tests are performed by adding a range of phage titers to a fixed initial starting density of bacteria under well-mixed conditions and monitoring the effect under shaking conditions. A central experimental parameter for some of the studies is the ratio of phages to bacteria, known as multiplicity of infection (MOI). It has been widely used in the literature as a therapeutic dosing parameter, yet its relevance has been questioned many times [79–81].

Susceptibility tests utilize both spectrophotometric tools as well as imaging techniques such as confocal microscopy. Spectrophotometric characterization such as measurement of optical densities at high frequencies is employed to construct kinetic curves and tetrazolium-dye based cell viability assays are used to assess the metabolism level of the bacterial system when treated with phage [82]. Confocal microscopy is typically used to assess the ability of the phage to inhibit biofilm formation. Mainly, such studies focus on the relative change in populations that result due to phage action.

In Table 2.1, we list some of the relevant phage-bacteria studies and their findings. One study that comes close to systematically exploring phage-bacteria dynamics in a *E.Coli* based system was performed by Rajnovic et al [83]. They analysed the optical density kinetics of 90 combinations of phage-bacteria concentrations for 3-5 hours. Their focus was on model development for phage enumeration and detection. Almost all other studies perform endpoint analysis, and in the ones that do consider the kinetics, only the first 5 hours or less were recorded. The number of initial conditions probed are often limited or the experimental conditions chosen at random or based on qualitative arguments. Further, the number of explored conditions are typically limited due to reasons such as labor intensive nature of the methodology, barriers to automate the process for high-throughput testing, and computational capabilities to handle the huge amounts of generated data. This leaves a gap in the understanding of phage-bacteria dynamics which we attempt to address through our study.

Table 3.1: Phage-bacteria susceptibility studies and their key results

First author and year	Bacterial strain	Phage type	Experimental results	Reference
Denis Rajnovic 2019	*E.Coli* DSMZ 613	T4 phage	Devleoped a method to detect and quantify bacteriophages based on the analysis of optical density kinetics in bacterial cultures exposed to phage	[84]
Tamta Tkhilaishvili 2018	*E.coli* TG1	T3 phage	Phage inhibited the production of biofilm at lower titers (10^3 PFU/ml)	[85]
Phitchayapak Wintachai 2019	XDR *A.baumannii*	Phage AB1801	Phage inhibited biofilm formation and reduced established biofilms in a dose-dependent manner	[86]
Nikhil D. Thawal 2012	Clinical isolate of *A.baumannii* strain AIIMS 7	Phage AB7-IBB2	Phage could inhibit biofilm formation and disrupt preformed biofilm	[87]
Pei, Ruoting 2014	*P.aeruginosa* PAO1	Engineered T7 phage that encode lactonase enzyme	Effective lysis and expression of quorum-quenching enzymes inhibited biofilm formation	[88]
P. Knezevic 2011	*P.aeruginosa* ATCC 9027	δ, J-1, σ-1 and 001A	Phages δ and 001A inhibited bacterial growth and biofilm formation at all MOIs, but σ-1 significantly inhibited bacterial growth only at very high MOIs and had no effect on biofilm formation	[89]
Yangyijun Guo 2019	*P.aeruginosa* PAO1	vB_PaeM_ SCUT-S1 and S2	Phages inhibited the growth of bacterium at low MOI, good performance on preventing biofilm formation and eradicating preformed biofilms	[90]

3.2.2 Mathematical modelling of phage-bacteria population dynamics

Alan Campbell was the first to develop a virus-host model for microbial hosts by adapting the general models used to study predator-prey interactions [91]. The changes in population densities of the virus and microbial host were modelled by including key mechanisms like reproduction of host cells, infection and lysis of host cells by viruses, time delay between the infection and lysis, and decay of viruses. Such virus-host interaction models have been used to explain chemostat-based ecological population dynamics experimental outcomes. The mean-field dynamics models consisting of coupled differential equations describing changes in populations of virus and host (and nutrient levels in nutrient-explicit models) can be derived from a set of Poisson processes.

The interactions between virus-host populations leads to either ecological steady states or oscillations, as shown in Figure 3.1. The incorporation of model parameters such as the latent period or changing the choice of model structure affects model predictions of various relevant quantities [92].

In well-mixed systems of phage-bacteria, the interactions among them happen at a rate proportional to the product of their concentrations (mass-action kinetics) [24]. Whereas in heterogeneous environments, factors such as spatial correlations, longer latent period, differential nutrient distribution, and emergence of resistant strains can affect the model parameters dynamically and lead to deviations from model predictions [93–96].

Many mean-field models have historically focused on outcomes at ecological and evolutionary timescales [97, 98]. Over the recent years, there has been a surge in interest for developing models focused on the effectiveness of a phage in controlling a bacterial population. Such models and simulations often consider the biofilm-state bacteria and phage dynamics ignoring the history of interaction with a planktonic sub-population prior to the recording of a measurement. Only a few and simple quantitative models of *in vitro* phage-bacteria (planktonic-state) dynamics in the context of phage therapy exist. They argue about the existence of bacterial thresholds above which phage densities increase

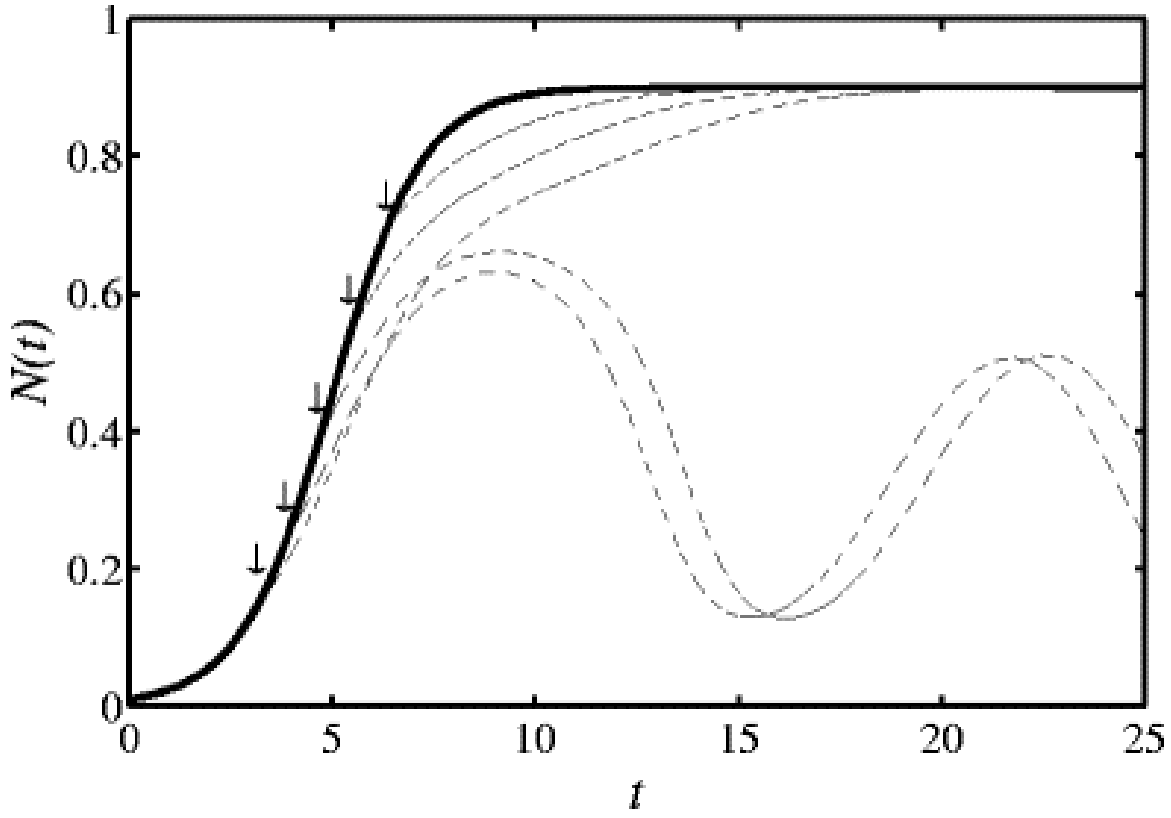

Figure 3.1: **Alternate stable states proposed by mathematicaling model of phage-bacteria systems** | Dynamics of hosts without phages (solid line) and with phages added at different time points of logistic growth (dashed lines). This image was originally published in Weitz, J.S. and Dushoff, J., 2008. Alternative stable states in hostphage dynamics. Theoretical Ecology [92]. Reprinted here under the Attribution-NonCommercial 4.0 International (CC BY-NC 4.0).

and viral thresholds above which bacterial densities decline, termed proliferation and inundation thresholds, respectively [99, 100].

In order to identify and understand the therapeutic efficacy of phage under different settings, it is essential to combine high-throughput quantitative experimentation and mathematical modeling.

3.3 Results

In this section, we present the results of the experiments focused on dynamics of phage-treated planktonic-state bacteria in mixed-state systems. These results offer insight about the efficacy of phages in controlling and eliminating planktonic-state bacteria in the presence underlying biofilms at various stages of development. The systematic exploration of bacterial dynamics under a wide range of initial conditions helps uncover dynamics that was previously missed, while providing a rich data set to facilitate the testing of quantitative models.

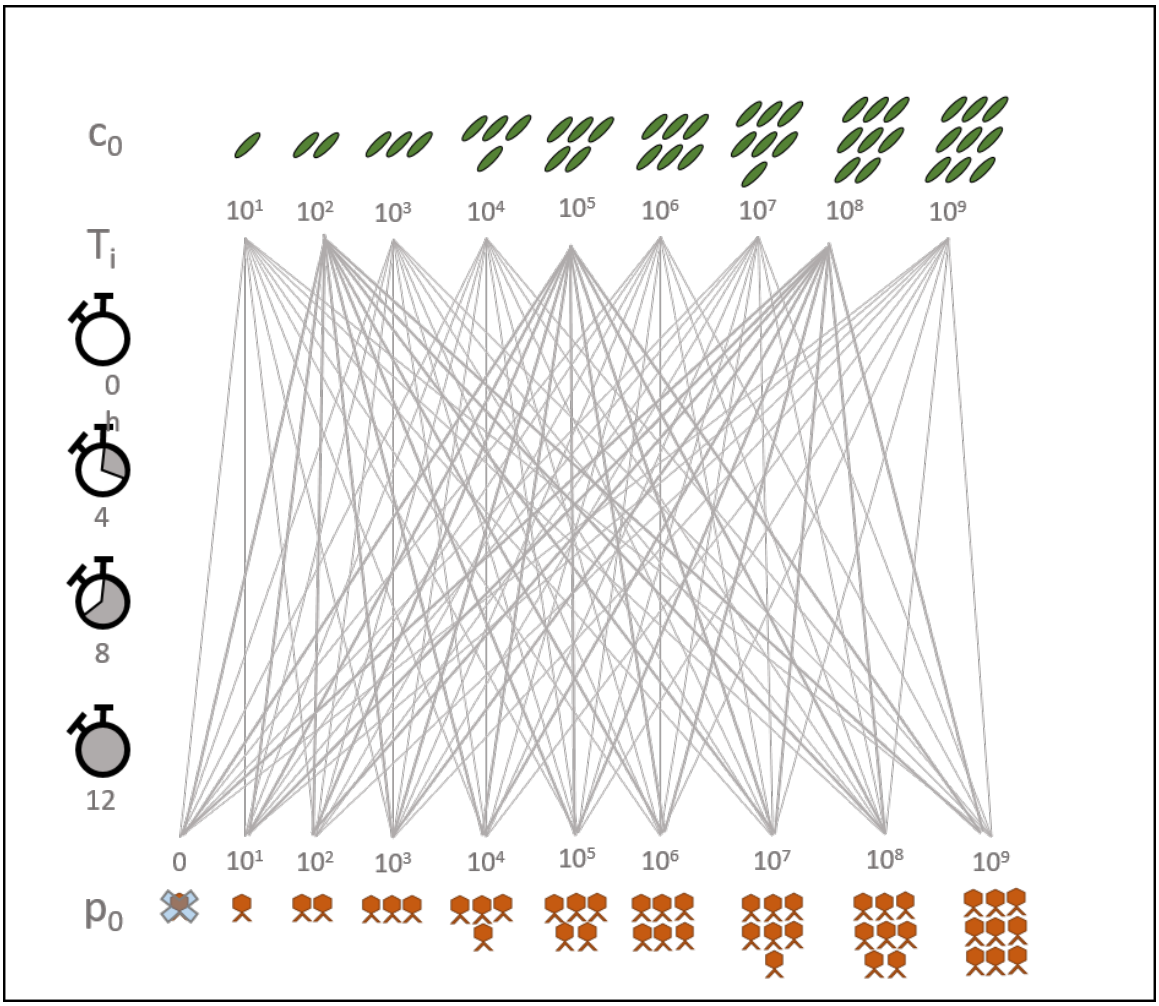

Figure 3.2: **Experimental design** | Schematic illustrating the *in vitro* experimental design employed in this study to discern the effect of initial conditions on the dynamics of planktonic bacteria in mixed-state systems when exposed to phages. Green rods denote *P.aeruginosa* bacteria and orange hexagons with two tails denote PEV2 bacteriophages. Different initial densities of *P.aeruginosa* bacteria ($c_0 = 10^1, 10^2, 10^3, 10^4, 10^5, 10^6, 10^7, 10^8$ and 10^9 CFU/mL) are allowed to form biofilms for various lengths of time (T_i = 0, 4, 8, and 12 h) and exposed to a number of phage titers ((p_0 = 0 (mock-control), $10^1, 10^2, 10^3, 10^4, 10^5, 10^6, 10^7, 10^8$ and 10^9 PFU/mL). Planktonic bacterial density was monitored for 16 h following phage exposure using spectroscopy.

3.3.1 Phage-driven bacterial dynamics in mixed-state systems

In these experiments, the parameters that were varied include the initial bacterial density, c_0, initial phage density, p_0, and the time of phage inoculation, T_i. Bacterial samples were seeded with c_0 in a 96 well microtiter plate with 250 μL LB broth at 37^oC, allowed to grow until T_i (T_i = 0, 4, 8, 12 h), at which time, phage inoculation took place. The initial bacterial densities ranged from c_0 = 10-10^9 CFU/mL in increments given by factors of 10; and each bacterial density was exposed to nine different phage inoculants, p_0 = 10-10^9 PFU/mL in increments given by factors of 10 PFU/mL. Optical density measurements were recorded every 30 minutes for 16 hrs after phage inoculation without nutrient replenishment, such that experiments lasted for a total time of T = T_i+16 hr (T = 16, 20, 24, 28 h). In total, 360 bacterial-phage combinations in triplicates (1140 samples) were analyzed as shown in Figure 2.1.

The resultant data is summarized in Figure 2.3. The black curves represent mock controls of bacterial growth. The color-coded curves range from low phage (yellow, 10 PFU/mL) to high phage densities (red, 10^9 PFU/mL) for a given c_0 and T_i . The rows report data associated with a given inoculation time, T_i , and the columns correspond to a fixed c_0.

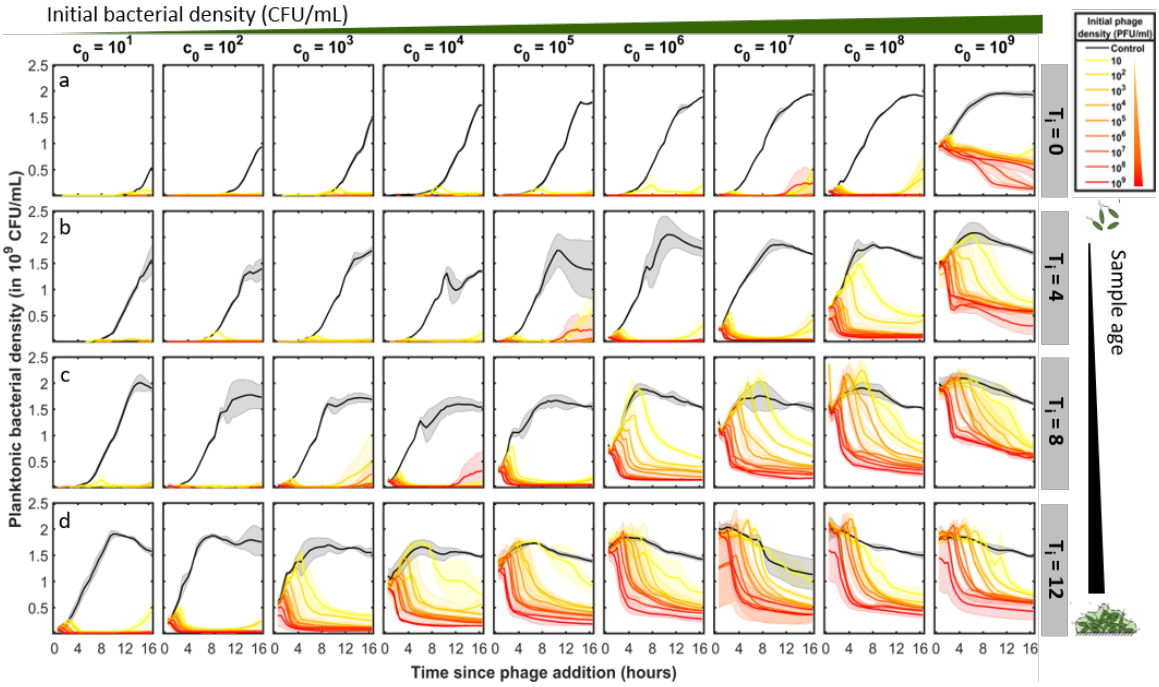

Figure 3.3: **Dynamical plots of planktonic bacteria exposed to phages** | We observe the effect of adding phages to bacteria at different stages of biofilm growth and investigate the dynamics as a function of initial bacterial density, initial phage density, and biofilm age. Each column shows the responses of samples initiated with the same bacterial density to different levels of phage, while the rows indicate increasing biofilm age and growth maturity (a) T_i =0 h: planktonic bacteria and phage at the time of phage addition, (b) T_i =4 h, (c) T_i =8 h, and (d) T_i =12 h respectively. In the well-mixed samples with no time for biofilm formation in the 96 well plates prior to phage addition, phages are quite effective at driving the bacterial densities well below detection thresholds except when initiated at high bacterial densities and a few exceptions where we observe stochastic reemergence. When the time prior to biofilm formation is longer, the bacteria often survives at lower levels determined by the initial phage densities.

3.3.2 *Phage decimate bacteria on simultaneous inoculation*

The unaged T_i=0 h samples with simultaneous phage and bacterial inoculation yielded outcomes similar to previous reports. The lytic PEV2 phage reduced bacterial levels to 10 to 100 times less than the mock control values, for all but the lowest phage levels (10,10^2 PFU/mL) and highest bacterial densities, $c_0 = 10^{8,9}$ CFU/mL. Most outcomes were close to or below the level of detection of the spectrophotometer ($\sim 10^7$ CFU/mL) and are more easily assessed if replotted on a semi-log plot (Figure B.1).

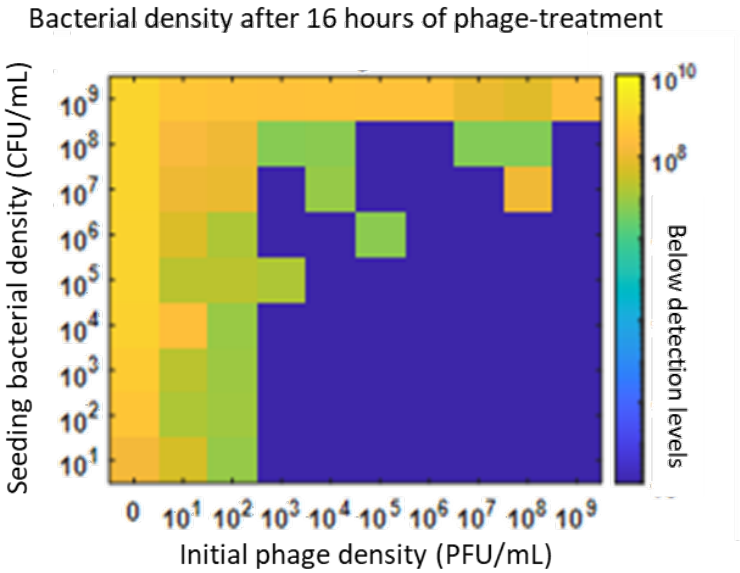

Figure 3.4: **Simultaneous inoculation of phage decimates planktonic bacterial population** | Heatmap depicting the the final bacterial densities (in CFU/mL) on the addition of various phage dosages. Yellow indicates maximal bacterial density and blue indicates levels below detection levels). Phages were added in tandem with the bacteria and allowed to act on the bacterial population for 16 hours. The first column on the left corresponds to the mock-control.

Phage treatment is less successful for initially high $c_0 = 10^9$ CFU/mL, with all but the highest phage values only reducing the final bacterial concentrations from mock control by $\sim 30\%$. Also evident in the $c_0 = 10^{7,8}$ CFU/mL samples is reemergent activity for a subset of phage inoculant values. Reemergence has been previously reported in such experiments,

typically between 8-12 hours [101], consistent with the timescales in this new data set. The reemergence can be either phenotypic or genotypic [102, 103]. Further analysis and discussion of the reemergent conditions is presented in a subsequent section. While data similar to that of T_i=0 h samples has been discussed previously by other studies, the literature lacks a comprehensive report of dynamics specific to T_i=4,8,and 12 h samples. To our knowledge, this is a pioneer study of such magnitude to map the dynamical landscape.

3.3.3 Steady-state plateaus and dosage dependent outcomes

The most striking feature that emerges in the aged planktonic samples are the quasi-steady state plateaus reached by the bacterial communities when exposed to a wide range of phage. Similar plateaus are present at very low bacterial densities for a subset of low phage exposures in the T_i=0 h samples, but they are only visible when plotted on a semi-log plot (Figure B.1). The final values of bacterial density in the plateaus and at the end of experiments scale inversely with the phage dosage.

The onset of the plateaus at times earlier than the mock control reaches its stationary state indicates that nutrient depletion does not play a central role in this outcome. Instead, the dynamics are consistent with predictions from quantitative models of the co-existence of phage with planktonic bacteria

3.3.4 Maximal bacterial density and its time of occurrence scales inversely with the density of exposed phages

Delayed treatment of planktonic bacterial samples with phage at times T_i = 4,8,12 h produces or emphasizes features less evident in the simultaneous inoculation data (T_i=0). Suprisingly, for of p_0 values below a critical density, the bacterial growth at early times follows the mock control curve (black) until a peak concentration of bacteria is reached, at which point the bacterial concentration rapidly decays. The critical threshold p_0 needed to suppress this behavior increases with the initial bacterial concentration upon phage

inoculation, c_i where c_i is determined both by c_0 and T_i. A inverse relationship between p_0 and the maximal bacterial density and the time at which it occurs is displayed in 3.5.

In a subset of the conditions, the phage-treated bacteria grow to densities higher than the mock controls maximum value. This is particularly evident for example in Figure 2.3 at T_i = 8,12 h and $c_0 = 10^{7,8}$ CFU/mL. These unexpected dynamics likely arise from the nutrient release of bacterial contents during lysis, which replenishes the nutrient depleted samples and enables enhanced bacterial growth [24].

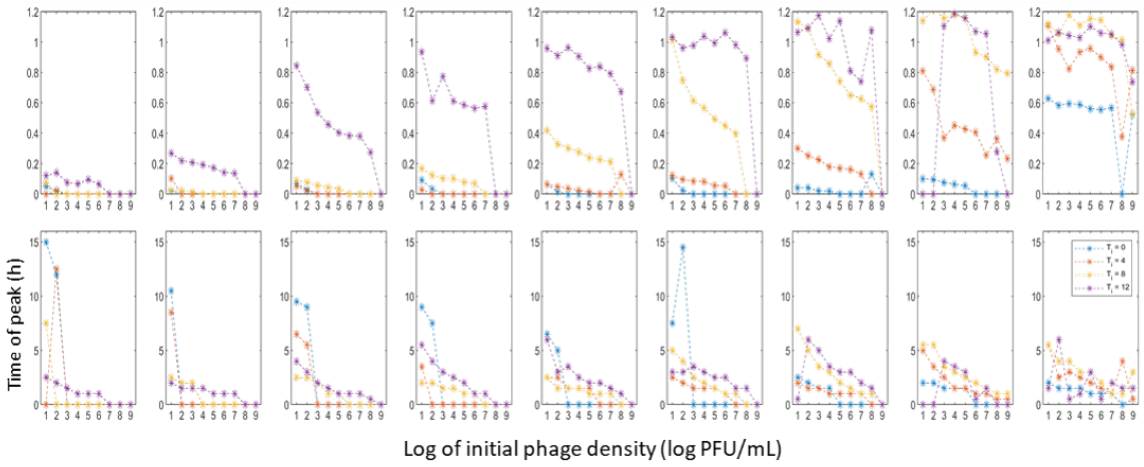

Figure 3.5: **Maximal bacterial density and time of occurrence scales inversely with magnitude of phage exposure** | a. Maximal bacterial density at various levels of phage exposure; b. Time at which planktonic bacteria attain maximal density versus log of initial phage density. The scatter plots shows the inverse relationship.

3.3.5 Probabilistic reemergence of planktonic population

Increasing the initial bacterial density of seeding led to lower bacterial clearance on adding same amount of phage which is in accordance with what one would expect since the number of phage available per bacteria would be lower (for populations not on death phase of logistic growth). However, in some samples that were seeded at low bacterial densities or allowed to grow for shorter time prior to phage addition, when treated with phage showed

signs of bacterial recovery after 8-13 hours since the introduction of phage. Such re-emergence in the observed timescale could be the result of the stochastic emergence of phenotypic or genotypic resistance.

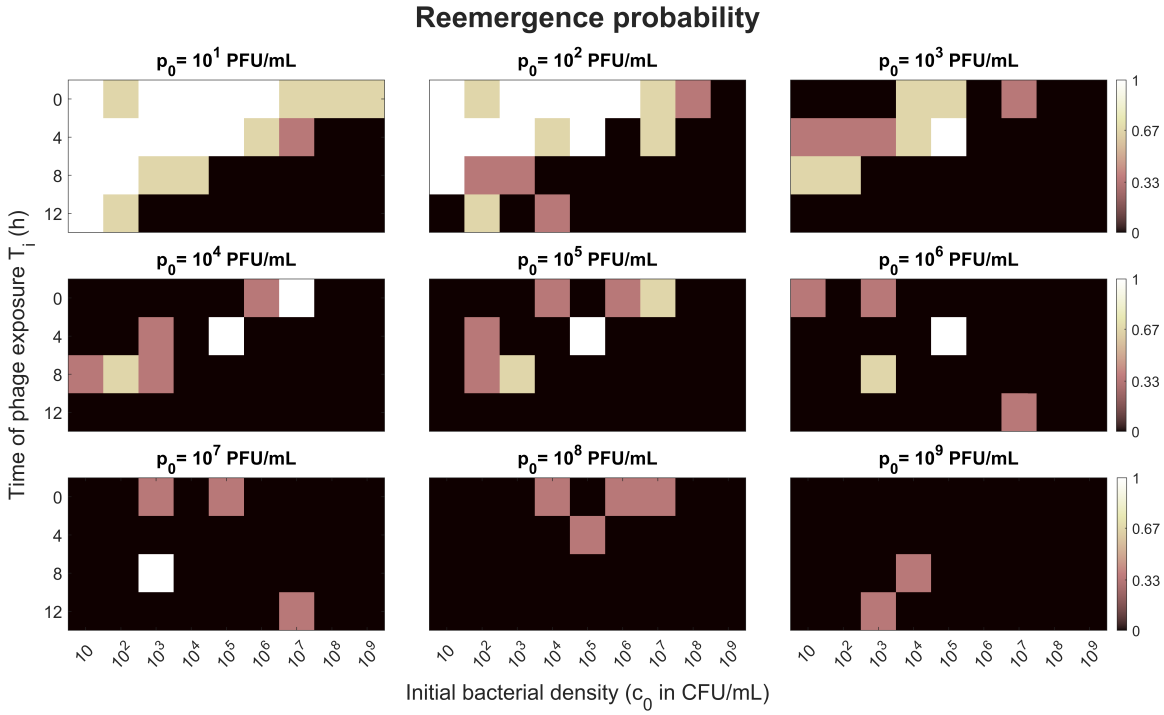

Figure 3.6: **Plot showing the probability of bacterial re-emergence after phage action for 16 hours** | The probabilities were calculated by counting the number of samples with higher optical density at the end of experiment compared to the beginning and dividing it by the total number of samples for that initial condition (n=3). Each box represents a different initial phage density, and within a given box, the rows represent different times of phage addition and the columns indicate the initial seeding bacterial density.

We determine the probability of reemergence by counting the number of samples with higher optical density at the end of experiment compared to the beginning and dividing it by the total number of samples for that initial condition. Since the bacterial population drops below initial values prior to reemergence, our approach for classifying an outcome as reemergent would err on the side of underestimation, and therefore a conservative approach. A heatmap of the reemergence probabilities suggest that the least mature samples (low c_0 and short T_i) when treated with low concentrations of phage have the highest probability

of reemergence in the observed duration. Moreover, the stochastic nature of the process, evident from the heatmap, supports the existence of hypothesis of resistant populations as opposed to oscillations intrinsic to the dynamical system.

3.3.6 Insights from multiplicity of infection (MOI) based analysis

Several trends are immediately evident if one examines the relationship between the multiplicity of infection (MOI) and the final planktonic bacterial density, c_f (Figure 2.6). MOI is the ratio of the inoculation phage density to the bacterial concentration at the time of inoculation, p_0/c_i. Each plot corresponds to a specific inoculation time, T_i, reporting the final bacterial density versus the range of accessible MOI. For a given MOI, a several values of (p_0, c_i) values are possible; the degenerate data is therefore displayed with the highest initial bacterial concentration ci on the left and the lowest on the right. Here, c_i, is the bacterial concentration at the time of phage inoculation, determined from the mock control growth curve.

Consistent with earlier analysis, higher levels of phage (and hence higher MOI) eliminate more bacteria, with the trend evident in all four T_i plots. The results also illustrate that the same value of MOI with different (p_0, c_i) is not useful for predicting bacterial outcomes. Instead, for a given MOI, the sample with the highest initial c_i, has the worst outcome with the smallest reduction in bacteria (unless an emergent event occurs). Hence, phage therapy for acute infections is less effective for larger bacterial loads. Last, major reemergent events stand out and are easily enumerated.

A misleading trend in the MOI data is the apparent dependence on sample age. For a fixed MOI, it appears that older samples resist killing more effectively than younger samples. However, when one directly compares the similar starting conditions (p_0/c_i) for different sample ages, the effect is diminished. In fact, we see that sample age has little impact on the final outcome of the planktonic bacterial population (Figure B.2). This is an important insight, because it indicates that the underlying biofilms formed in the more aged

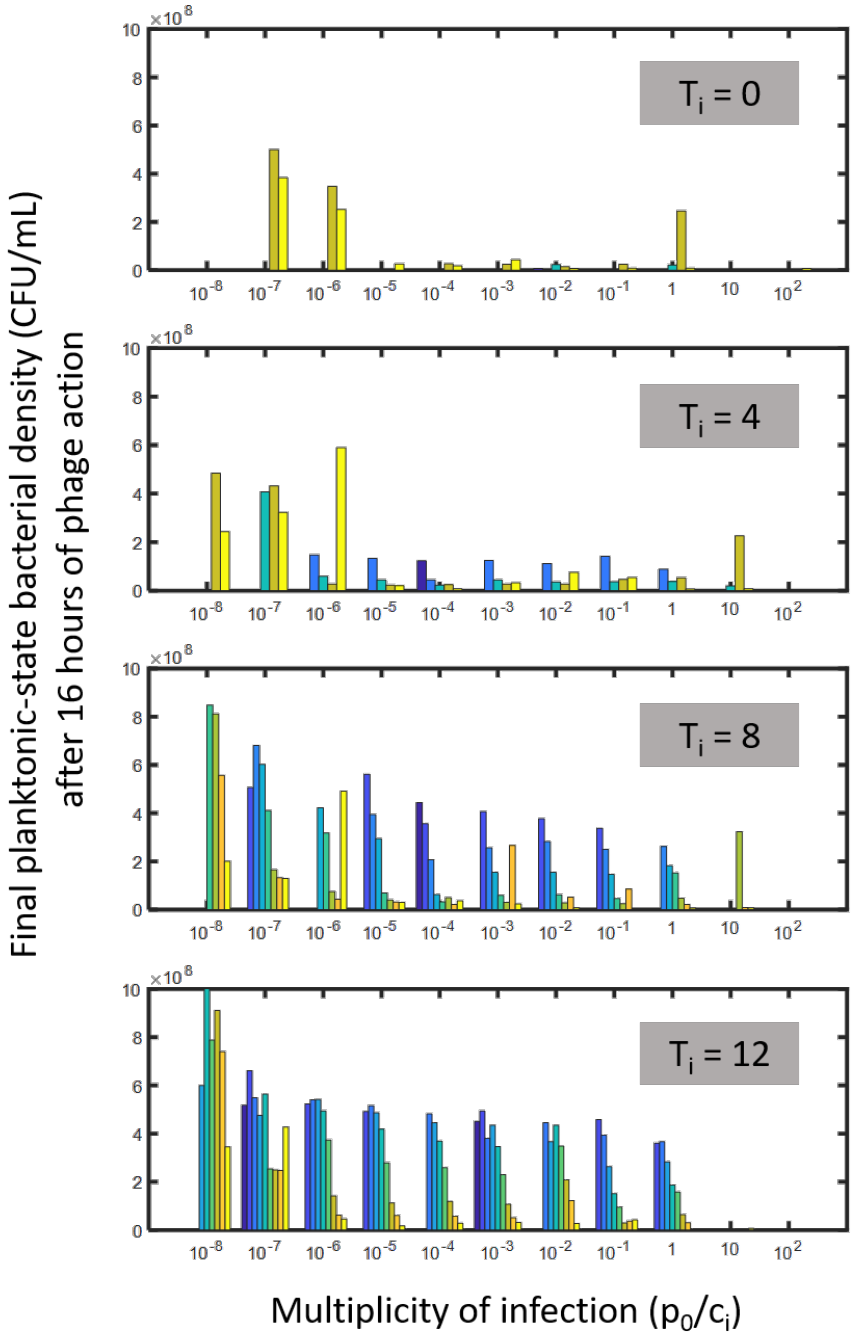

Figure 3.7: **Final planktonic bacterial densities grouped based on MOI and** T_i | Each box shows the final densities of the planktonic bacteria when the sample was allowed to develop biofilms for 0, 4, 8, and 12 h respectively. The densities are grouped based on the MOI.

samples do not significantly alter the outcomes of the planktonic state.

3.4 Discussion

The systematic exploration of population dynamics dynamics revealed several key features of the dynamics between planktonic-state bacteria and phage in mixed-state systems. We gathered that lytic phage are effective at reducing planktonic-state bacteria under most initial conditions. Some conditions with underlying biofilms lead to quasi steady-state, plateau-like outcomes when exposed to phage. These quasi steady-state densities are lower than that of the mock control and its magnitude changes with the dosage of phage exposed. Further, we observed that bacterial populations proliferate until a critical threshold before declining drastically due to phage lysis. This maximal density and its time of occurrence scales inversely with phage dosage.

These results vary significantly from that of a homogeneously mixed system. In collaboration with the Weitz group, we find that the classic ODE models do not recapitulate the observed dynamics and outcomes. Along with Marian Dominguez from Weitz group, we are exploring PDE based models as well as individual-based models for a better understanding and mechanistic insight into the observed results.

CHAPTER 4

BIOFILM DEVELOPMENTAL STAGE DURING PHAGE EXPOSURE DETERMINES DOSE-RESPONSE AND SPATIOTEMPORAL DYNAMICS

Adapted from H. Selvakumar, M. Dominguez, S. P. Diggle, J. S. Weitz, and J. E. Curtis., Developmental stage of biofilms during phage exposure determines dose-response and spatiotemporal dynamics, (In preparation).

Broader Context: Development of bacterial biofilms have been widely studied in the literature and it is known that more than three-fourths of all existing chronic infections are associated with biofilms, a microbial mode of existence that is intrinsically resistant to antibiotics and resilient against immune defenses. Recently, phages have been proposed as a promising strategy to combat antibiotic resistance and clear infections and little is known about their phage-biofilm dynamics. In this context, it is crucial to understand the advantages and limitations of phage when it comes to combating biofilms. We hypothesized that biofilms at different stages of development would play a significant role in influencing the overall dynamics in the presence of phage. Investigation of biofilms at different growth stages when exposed to a wide range of phage densities led to the identification of four distinct classes of responses with unique functional dependences on phage dosage. The phage response class of a biofilm sensitively depends on its developmental stage at the time of phage exposure. Further, mature biofilms exhibit a paradoxical response where bacterial survival levels are higher in the presence of high phage levels. Detailed spatiotemporal data suggests role of nutrient recycling in spatial niches. Nevertheless, it appears that for each class of response, high phage conditions restrain the biofilm from transitioning to its next developmental stage in the unperturbed timeline. These insights provide a simple yet powerful framework to understand phage-biofilm dynamics and provides perspective to

guide phage treatments.

4.1 Overview

The effects of bacterial infections often amplify when bacteria adhere to surfaces, form communities, and build complex structures known as biofilms with the aid of exuded polymeric substances that contributes to its viscous matrix [64, 104–107]. Biofilms offer the perfect environment for the constituent bacteria to become virulent and often acquire antibiotic resistance, turning an acute infection into a persistent chronic infection, thereby posing critical clinical challenges [57, 108]. According to a public announcement by NIH, over 80% of chronic infections in the body are associated with biofilms [109]. The complex chemical gradients within biofilms lead to both local and global stress responses that enable differentiation within sub-populations with varying susceptibilities [110, 111]. In addition to providing an environment that assists in the evolution of antibiotic resistance, biofilms shield the bacteria against host immune responses by altering their mechanical and chemical properties [50, 58, 112]. Multidrug resistance, especially resistance to last resort antibiotics such as carbapenems in some *P.aeruginosa* infections threatens human healthcare [113, 114]. With few, if any, novel antibiotics in the clinical pipeline, there is a resurgence of interest in identifying effective therapeutic alternatives [115, 116].

Phage therapy is the practice of using bacterial viruses known as bacteriophages that infect and lyse bacteria to treat infections [117–120]. In the last few years, phage therapy in the US has gone from compassionate use to its first FDA approved clinical trial [121]. In addition, phage treatment is being considered for Covid-19 patients with bacterial co-infections during clinical trials (https://clinicaltrials.gov/ct2/show/NCT04636554). Obligately lytic phages have been considered for therapeutic use due to their high killing rate [122]. Phages are highly specific with a narrow host range (protects commensal bacteria), self-amplifying, and are tolerated well by the immune system [28, 123]. Phages have been highly effective in controlling and eliminating acute infections in pre-clinical

animal models [124]. With chronic infections containing biofilm components, phages have been successful in treating wounds and lung infections in certain cases [125–127], whereas in others, they do not conclusively lead to better clinical outcomes [128, 129]. A comprehensive understanding of the effect of phages on biofilms and identification of underlying mechanisms would help evaluate their therapeutic effectiveness. Such insights have the potential to further advance phage-based personalized medicine when generalized treatments fail.

Biofilm development has been studied and described extensively in the literature [130–133]. Yet, little is known about the interactions of phage with bacterial populations in biofilms at various stages of development. P. aeruginosa biofilm development on surfaces is well-characterized by a number of studies and is known to occur in stages [134–139] associated with - initial attachment (reversible and irreversible), early biofilm assembly (microcolony development), biofilm maturation development (three dimensional structural expansion), and dispersion (autolysis and differentiation) resulting in the release of a motile sub-population. The current view of phage-biofilm dynamics derives from an assortment of various types of studies, some with outcomes of phage exposure to biofilms grown for a specific duration [140, 141], some involving the dynamics of phage exposure to planktonic bacteria to determine biofilm inhibition ability [89, 142, 143], and some with mathematical modeling and simulations to identify the major factors driving dynamics [94, 144–146]. Furthermore, the conditions of growth such as phage-bacteria pair, nutrient availability, and hydrodynamic conditions vary between these studies. To date, no integrated holistic study exploring the various conditions exists.

Our main goal is an exhaustive study of the dynamics between phage and biofilm-forming bacteria under different conditions including initial bacterial densities, phage-bacteria ratios, and biofilm maturation stages with the overall aim to assess the impact of phage on biofilm communities. We therefore monitored the impact of PEV2 lytic phage addition on P. aeruginosa biofilms at different stages of the developmental cycle under static

conditions at high spatiotemporal resolution for a large number of initial biofilm conditions and phage titer combinations. Four distinct response classes emerged, corresponding to the different biofilm developmental stages. The response classes exhibit unique functional dependences on the phage dosage. While nearly any phage dosage is sufficient to suppress biofilm formation in the first developmental stage, very little impact on biofilm outcome is evident for the dispersion stage even at high phage exposures. We also found that the early biofilm stage is increasingly suppressed by higher phage exposures, while paradoxically, the mature biofilm stage is enhanced by increasing phage exposure. Additionally, for each of the response classes, high phage exposure halts the biofilm from transitioning into the next developmental stage of the biofilm lifecycle. These insights combined with the measurements of the rich spatiotemporal dynamics of the biofilms will facilitate future mathematical modeling and experimental efforts to test mechanistic hypotheses, while at the same time provide more perspective to guide clinical studies and treatments.

4.2 Background

4.2.1 Biofilm developmental process

Detailed knowledge of the biofilm developmental process is essential in order to develop effective phage dosing strategies to treat chronic infections. Biofilms at different developmental stages have distinct characteristics which can be targeted through appropriate approaches [147]. *P.aeruginosa* biofilm development generally progresses in four stages which includes an initial attachment stage, an early biofilm stage, a mature biofilm stage, and a dispersion stage. Knowledge about the biofilm growth stages were mainly obtained through *in vitro* experimentation [139, 148].

Biofilm formation is initiated when planktonic bacteria irreversibly bind to a surface or to each other and form aggregates. Components such as flagella [149], Type IV pili, eDNA, and Psl polysaccharide have been found to influence the biofilm initiation process by modulating bacterial attachment and chemically conditioning the surface [148].

Irreversible binding is characterized by the longitudinal attachment of the bacteria to the surface as opposed to reversible binding where the bacteria loosely attach via a single pole, often rapidly spinning at this phase [150].

The early biofilm formation occurs via the contribution non-motile and motile bacterial sub-populations on the surface. The non-motile bacteria form microcolonies at the attached site through cell division. The motile sub-population move on the surface using Type IV twitching mobility [151, 152]. Subsequently, biofilm maturation occurs via microcolony expansion, bacterial migration, and production of EPS. The characteristics of a mature P.aeruginosa biofilm depends on various environmental conditions such as fluid flow [153], nutrient type and availability, quorum sensing, interaction between various sub-populations [154], and gravity [155]. In conditions such as glucose irrigated flow-chambers, *P.aeruginosa* forms mushroom-shaped microcolonies as a result of a complex interplay between the sub-populations of differential migratory abilities [156]. Whereas in other conditions, such distinct mushroom structures are absent and the biofilms are rather flat and lack distinct microcolonies.

The EPS secreted by bacterial cells within the biofilm provide structural integrity and a protective environment. The EPS is a complex mixture of exopolysaccharides, proteins, and extracellular DNA (eDNA) [14, 157]. The most abundant polysaccharides in *P.aeruginosa* biofilms are Pel, Psl, and alginate [156]. Pel and Psl mediate cell-surface and cell-cell adhesion respectively, and are essential for microcolony formation. Alginate is overproduced in chronic infections of cystic fibrosis and has a substantial role in structuring mature biofilms [52, 108, 138, 158]. Proteins in the EPS influence the biofilm structure and in turn, antimicrobial tolerance. Some of the proteinaceous matrix components are Type IV pili [159], Cup fimbriae [160], surface adhesions like CdrA [161], carbohydrate binding lectin lecB [162], and functional amyloid protein Fap [163]. Further, DNA from a bacterial sub-population contributes to the strength of the matrix [164]. Autolysis of a fraction of the biofilm population has been compared to the programmed cell death in multicellular life.

In some cases, the process is associates with the induction of genomic prophages, such as the filamentous Pf1 phage in *P.aeruginosa* [134].

On maturation, the biofilm proceeds to the dispersion stage where a motile-subpopulation within the biofilm interior is freed into the exterior. This process is analogous to metastasis in cancer, where some cells within the aggregates are released to colonize new spaces. The dissemination process is of clinical importance since the released bacteria can infect other parts of the body and cause acute infections [111, 134, 165]. Studies have also demonstrated that dispersion could occurs as a response to environmental changes in carbon availability [135, 166], oxygen starvation, nitrosative stress [167, 168], etc.

In addition, secondary messenger molecules such as c-di-GMP and cAMP are known to modulate biofilm formation and dispersion through signaling mechanisms [169]. Reduction in intracellular c-di-GMP results in biofilm dispersal and has been shown to increase resistance to antimicrobial peptides. Changes in carbon availability, iron or oxygen levels can lead to ATP-dependent response which modulates biofilm retention and dispersal. Often, the intracellular levels of such secondary messengers are individual responses to global stresses [110]. Unlike mechanical and passive dispersal which include sloughing off of biofilm cells, active dispersal is specific and highly regulated [170].

4.2.2 In vitro *phage-biofilm experimentation*

Phage susceptibity tests are often performed on planktonic samples rather than biofilms [171–173]. Recent interest in phage therapy to treat chronic infections has encouraged the field to probe biofilm susceptibility to phage. In general, there is a lack of consensus for in vitro biofilm models for susceptibility testing of antimicrobial agents [174–176]. In vitro biofilm models used for phage studies can be broadly classified into two groups including closed or static models and open or dynamic models [147]. Microtiter-plate based systems are a common form of closed or static model systems where there is no flow

of growth media or waste materials. Such conditions lead to gradual changes in nutrient levels and accumulation of signalling compounds and waste products. Flow displacement model system is common manifestation used to study open and dynamic biofilm models. Such systems allow for inflow of nutrients and removal of secreted waste products. They can also be used to exclusively retain sessile populations and eliminate planktonic fractions by adjusting the flow rate.

Biofilms and their response to antimicrobials can be tested using various examination methods [147, 175]. Staining assays such as crystal violet assay and congo red assay can be used to identify biofilm presence and in some cases, quantify the level of biomass. Bioluminescent assays and XTT reduction assays are used to quantify metabolic activity within the biofilms. Optical examination techniques include optical fluorometry, confocal microscopy (CLSM, CSDM), electron microscopy (SEM, TEM), light microscopy, and infrared and reflectance spectroscopy. Fluorescence staining of specific components coupled with confocal microscopy allows for 3D visualization of biofilms and identification of biofilm heterogeneities.

In experiments conducted with *E. coli* and T7 phages, Drescher et al. observed that the outcome of phage infection is a function of matrix structure. As the *E. coli* biofilms mature, they produce curli fibres as a component of their extracellular matrix. These fibres completely coat the surface of the bacteria rendering the cell surface receptors inaccessible to phages. In addition, these curli amyloid fibres offer collective cell protection by preventing phage transport into the biofilm [177]. Phages have been observed to infect biofilms in nutrient-limited conditions with altered phage population dynamics, for example, some studies report phage production to be proportional to the metabolic activity of the host [46, 178]. This indicates that using the phage growth parameters obtained from chemostat experiments might not be accurate for simulations involving phage-biofilm dynamics.

Pseudomonas-specific phage was first discovered in the 1950s and since then, have

been objects of interest to treat innately antibiotic-resistant Pseudomonas. The effect of various phage strains against MDR P.aeruginosa biofilms have been reviewed in [48]. Pseudomonas phage have been shown to reduce the growth rate and decrease biofilm levels after few hours of treatment, some phage types being potent against planktonic forms (phiKZ-like) and some effective against biofilms (LUZ24-like). The effectiveness of phage is dependent on the specific phage-bacteria and phage-matrix interactions, such as lysis parameters and production of depolymerases.

A recent review by Sullivan et al., calls for improved in vitro experimentation to study phage-biofilm systems [179]. They suggest distinguishing between biofilm control and biofilm removal, exploration of large parameter spaces in terms of phage dosage and treatment times, and kinetic analyses. Such detailed characterization would help better understand phage-mediated biofilm disruption and build better quantitative models.

4.2.3 Models and simulations of phage-biofilm systems

It is well known that bacterial biofilms are spatially structured, heterogeneous, and their growth depends on a wide range of factors including nutrient, oxygen, and temperature gradients. The constituent bacteria are genetically and phenotypically diverse. These self-assembled structures modulated through complex signalling systems in response to various environmental feedbacks, are of great interest to physicists [3, 180–182]. Modelling their temporal growth involves the inclusion of space. Waclaw et al., present a comprehensive review on spatially structured bacterial growth models ranging from simple models such as connected habitats and Fisher-KPP waves to continuum models and on- and off-lattice individual-based models [183].

Spatial models of phage-bacteria dynamics include PDE-based models with a focus on plaque growth [145, 184, 185] and individual-based models [186] which emphasize individual position and state of the cells. In the continuum approach, both chemical and bacterial populations are modelled as continuous fields. When considering smaller,

heterogeneous populations, individual-based models are more appropriate. They can be on- or off-lattice based, where bacterial movement is restricted to lattice sites in the former and bacteria can move in continuous space and interact via other physical mechanisms in the latter. Various spatial models often predict coexistence of phage and bacteria, due to spatial heterogeneity which allows for the creation of spatial refuges.

The elucidation of phage-biofilm dynamics is therefore a highly challenging task. In this study, we attempt to understand the bacterial dynamics that arise due to the presence of phage for a range of initial conditions. The results help shed light on effectiveness and limitations of phage therapy as a prophylactic and therapeutic against acute and chronic infections.

4.3 Results

4.3.1 Reproducible P. aeruginosa *biofilm growth in limited nutrient conditions*

We first examined typical biofilm growth with no phage exposure, and established the reproducibility of the system. P. aeruginosa were seeded with initial concentrations $c_0 = 10^6, 10^7, 10^8$ CFU/mL and allowed to form static biofilms for different intervals of time (T_i = 0,4,8,12 h), at which point the biofilms were imaged every hour for an additional 16 hours, using confocal microscopy (Figure 4.1).

For all initial seeding conditions, the biofilms mature until they reach a maximum population of ~ 4.9 x $10^4 \pm 3.6$ x 10^2 bacteria (in the given measurement volume of 120 x 120 x 20 μm^3). At this point, the living bacterial count begins to decline due to natural cell death and dispersion likely driven in part by the limited resources available under static biofilm conditions. The key aspects of the observed biofilm dynamics, including onset time, duration of rapid growth, maximum bacterial count, and time of biofilm decline are reproducible for each c_0, a necessary condition for the phage-biofilm experiments that are the focus of this study (Table C.1). Further, the onset of each developmental phase for a given biofilm depends on the initial bacterial seeding density, c_0. The colored boxes on the

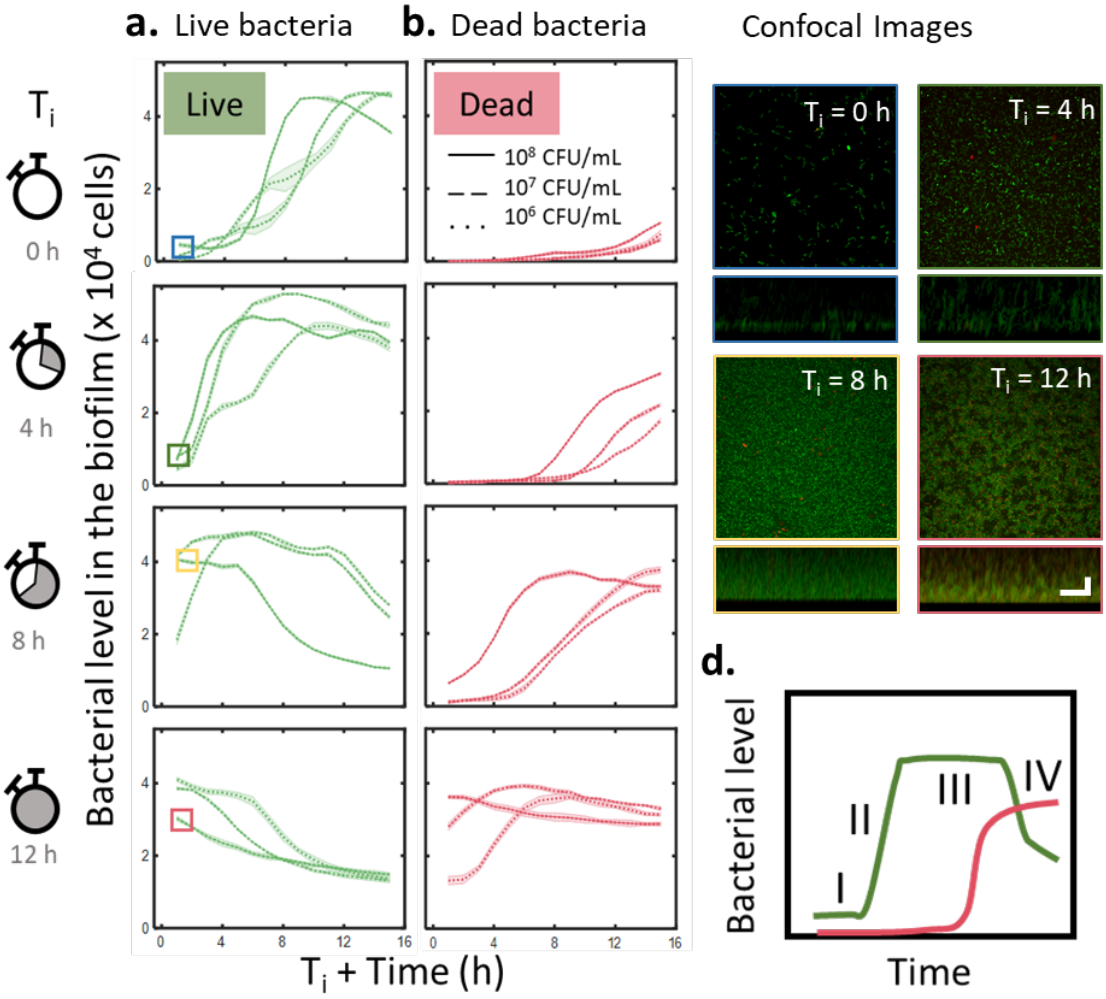

Figure 4.1: **P.aeruginosa biofilm growth after different incubation times. a., b.** | Green and red lines denote the mean number of live and dead bacteria in the mock-control biofilm (initial bacterial density $c_0 = 10^6, 10^7 and 10^8$ CFU/mL) and the shaded areas denote the standard error of the mean (n=3). The colored boxes (blue, green, yellow, red) enclosing the live bacterial levels correspond to the images in (c) outlined with the respective colors. **c** | Images of the biofilm surface and mean view of the biofilm cross-section at time T_i + 0 h and $c_0 = 10^8$ CFU/mL revealed through confocal microscopy. **d** | Schematic of the developmental curve of *P.aeruginosa* biofilm growth; green line denotes the live bacterial growth and red line denotes the dead bacterial levels in the biofilm. Biofilm growth in *P.aeruginosa* follows has four developmental stages: I. Initial attachment, II. Early biofilm, III. Mature biofilm, and IV. Dispersal stage.

bacterial growth curves in Figure 4.1a demarcate the onset of each of these developmental stages for $c_0 = 10^8$ CFU/mL, with a corresponding image from those time points displayed in Figure 4.1c.

Here, we define the criteria to identify these four developmental stages (see Figure 4.1d) in the phage-biofilm study to follow. The initial adhesion stage occurs from the seeding of the bacteria to the start of rapid bacterial growth. The early biofilm stage is the period of rapid biofilm growth. The mature biofilm stage is the period just before the peak population as the growth begins to slow through the start of the decline of the live bacterial levels in the biofilm. Last, the dispersal stage is the period in which the biofilm population decreases rapidly, with a clearly different slope from the mature stage.

4.3.2 Phage-treated biofilm dynamics and outcomes depend on biofilm developmental stage

Next we designed and implemented a phage-biofilm assay to examine the role of biofilm developmental stage and phage dosage on the dynamics and outcomes of biofilms. *P. aeruginosa* biofilms were established using three initial bacterial concentrations, $c_0 = 10^6, 10^7, 10^8$ CFU/mL, and then inoculated with phage over a range of titers from $p_0 = 10^1 - 10^9$ PFU/mL in factors of 10 PFU/mL, at four different inoculation times, T_i = 0, 4, 8, 12 h (Figure 4.2). For each sample condition, confocal stacks were obtained every hour for 16 hours. Image analysis was used to quantify the total number of bacteria in the stack volume (X x Y x Z = 120 μm x 120 μm x 20 μm). Complementary spectrophotometry measurements and crystal violet data were collected at the end of each experiment (T = T_i+16 h, Figure **??**). The large number of phage titers will provide access to quantitative assessment of biofilm dynamics versus phage treatment and facilitate quantitative modeling efforts that test mechanistic hypotheses. The combination of seeding bacterial densities, c_0, and different times of uninterrupted bacterial growth prior to phage inoculation, T_i, will provide insight into how biofilm maturity impacts the success of the phage treatment.

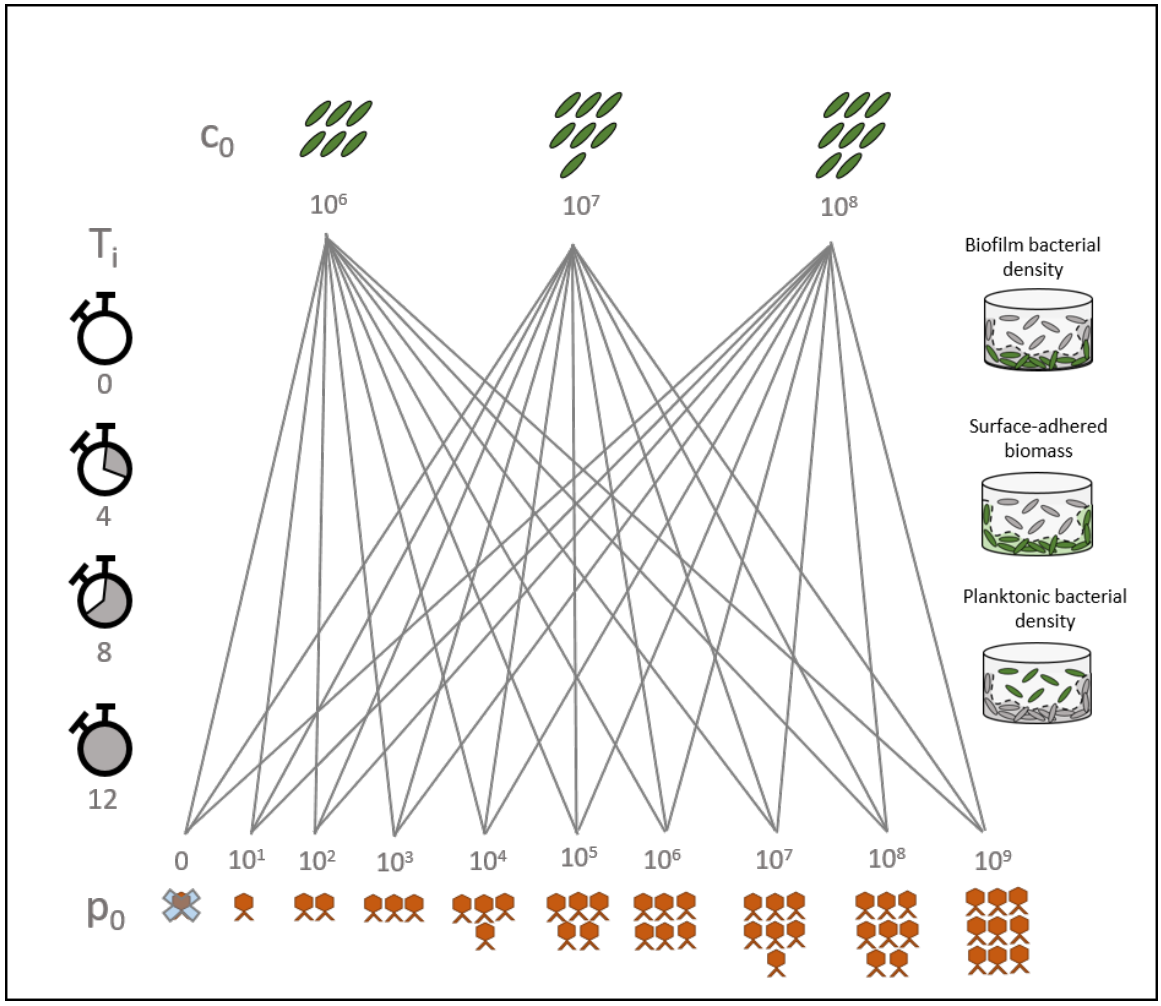

Figure 4.2: **Experimental design** | The schematic is based on the *in vitro* experimental design employed in this study to discern the effect of initial conditions on phage-treated biofilms. Green rods denote *P.aeruginosa* bacteria and orange hexagons with two tails denote PEV2 bacteriophages. Different initial densities of P.aeruginosa bacteria (c_0 = $10^6, 10^7$and 10_8 CFU/mL) are allowed to form biofilms for various lengths of time (T_i = 0, 4, 8, and 12 h) and exposed to a number of phage titers ((p_0 = 0 (mock-control), $10, 10^1, 10^2, 10^3, 10^4, 10^5, 10^6, 10^7, 10^8$ and 10_9 PFU/mL). Properties such as bacterial density in the biofilm and planktonic parts were monitored for 16 h following phage exposure. The surface-adhered biofilm mass was quantified at 16 h after phage exposure.

The resultant biofilm dynamics are reported in Figure 4.3. Four distinct response classes are evident in the population dynamics, which correlate with the developmental stage of the biofilm at the time that the phage were added (see Table 4.1). This insight is succinctly depicted by examining the final biofilm bacterial count versus phage dosage (Figure 4.4). Stark differences in the biofilm response to increasing phage titers are evident for the response classes. For biofilms in the initial attachment stage, biofilm formation is inhibited at even the lowest phage densities. When phages are added to the early biofilm stage, we observe a density-dependent biofilm clearance with increasing phage doses leading to increased elimination of bacteria. Inversely, when the phage is added to mature biofilms, the biofilm is initially reduced by the phage but then partially re-established, particularly at higher phage densities. Last, when phage is added to the dispersion stage, the biofilms exhibit dynamics similar to that of the mock control, independent of the amount of phage exposure.

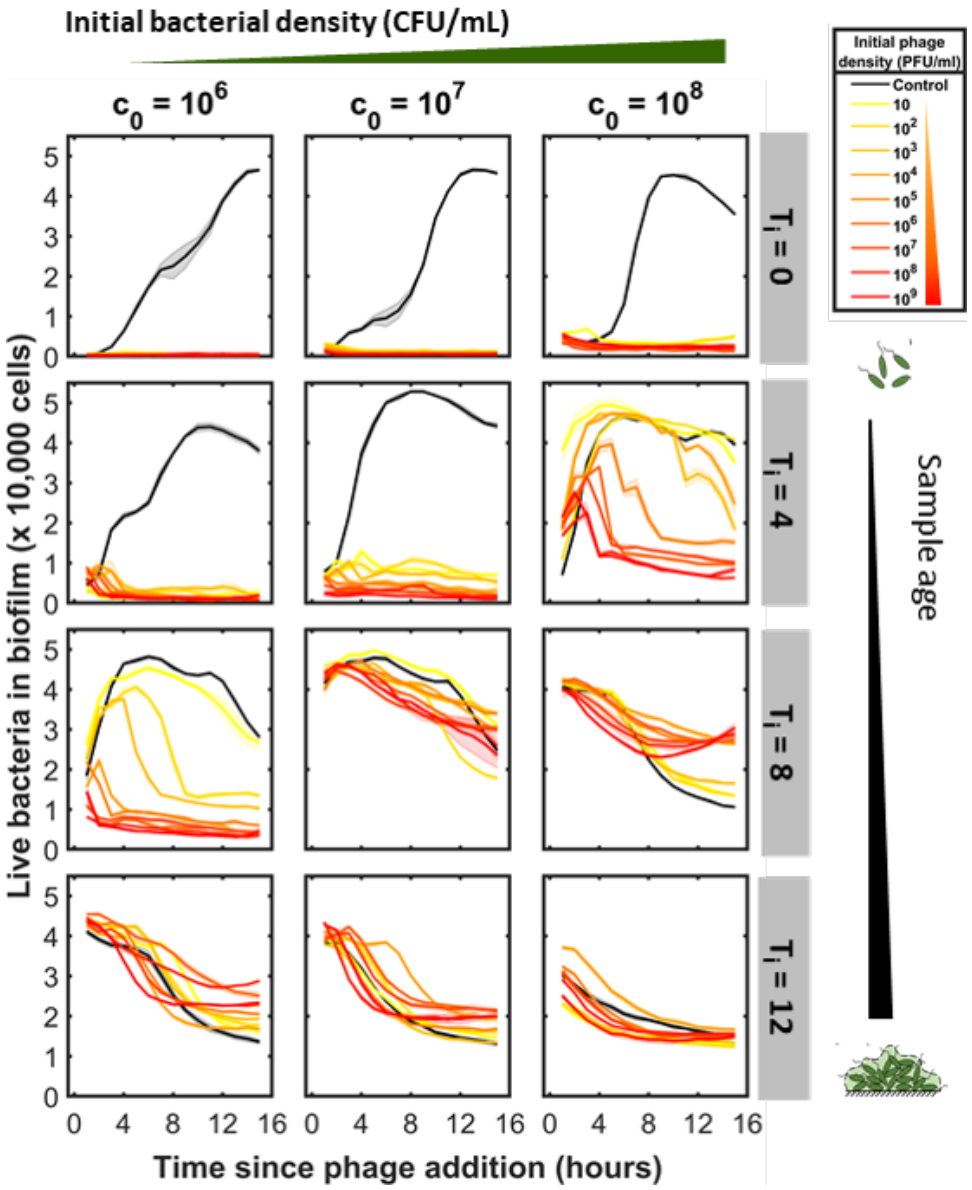

Figure 4.3: **Phage dose-response of biofilms** | The surface-adhered biofilm fractions of the samples when exposed to a range of phage densities were imaged every hour using spinning disk confocal microscopy. Phages densities positively correlate with bacterial elimination in the biofilm of younger biofilms and samples inoculated at low bacterial densities. This trend changes in mature, established biofilms; in other words, higher initial phage exposure leads to higher (or similar levels, not lower) bacterial retention in the biofilm compared to the samples exposed to fewer phages.

These four response classes are well-represented by the c_0=10^8 CFU/mL samples because these biofilms span the four developmental stages during the course of the experiments. Figure 4.5 displays the biofilm outcomes versus phage titer and exposure time for the four response classes in side views and cross sections of the biofilm at the surface. Figure 4.6 compares the spatiotemporal dynamics of living bacteria and dead bacteria (labelled with propidium iodide) for the control biofilms versus those treated with phage (p_0=10^9 PFU/mL), revealing the distinct differences in population dynamics for each class.

Table 4.1: **Biofilm phage dose-response** The response of biofilms towards different phage doses can be organized into 4 response classess. These response types are determined by the developmental stage of the biofilm at the time of phage exposure.

Response class	Response	Sample condition (h, CFU/mL)	# of conditions	Developmental stage during phage exposure
1	Biofilm growth inhibition	T_i = 0, c_0 = 10^6- 10^8; T_i = 4, c_0 = 10^6	4	I. Initial attachment
2	Biofilm elimination directly proportional to p_0	T_i = 4, c_0 = 10^7- 10^8; T_i = 8, c_0 = 10^6	3	II. Early biofilm
3	Biofilm elimination inversely dependent on p_0	T_i = 8, c_0 = 10^7- 10^8; T_i = 12, c_0 = 10^6-10^7	4	III. Mature biofilm
4	Biofilm elimination independent of p_0	T_i = 12, c_0 = 10^8	1	IV. Dispersal

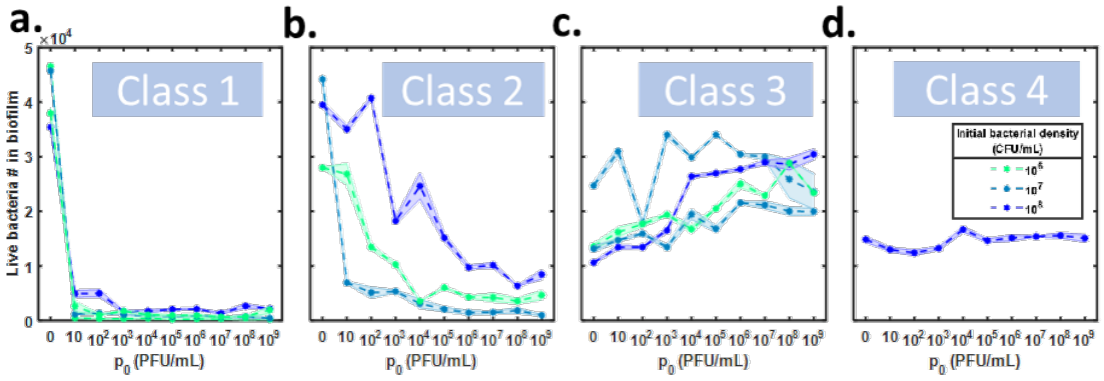

Figure 4.4: **Phage dose-response of P.aeruginosa biofilms. a,b,c,and d** | Each box corresponds to the four response classes 1, 2, 3, and 4. The dashed lines in green, teal, and blue denote the final live bacterial levels as phage titers increase for the initial seeding densities of $c_0 = 10^6, 10^7, and 10^8$ CFU/mL respectively.

4.3.3 Simultaneous inoculation and early phage exposure inhibits biofilm growth

The simultaneous inoculation of phage with bacterial culture substantially suppresses biofilm growth (T_i=0 h, Figure 4.4a, Figure 4.5a). The immediate impact of the phage is evident in the spatiotemporal dynamics of biofilm growth with and without phage addition at T_i=0, which shows the biofilm never passes beyond the first developmental stage (Figure 4.6, T_i=0 h). The living bacteria in the biofilm are reduced to 0.5% - 14.8% relative to that of the mock control at the end of the experiment at T=0+16 h. These results can be found summarized for each phage dosage in Table C.2, which records all outcomes relative to the control for the final bacterial percentage versus condition.

Biofilm samples close to the transition between developmental stage I and stage II include those treated at T_i=4 h with phage, and seeded with c_0=10^6 CFU/mL. Unlike the T_i=0 h experiments, these bacterial communities continue to grow for a short period before peaking and then decay to final values less than 10^4 bacteria. Small numbers of bacteria remain as a thin layer of remnant bacteria persists despite the highest phage treatments, approximately 5.1% of the control population at the experiments end.

For all but 5 of the 36 relevant conditions, (T_i, c_0, p_0,), the final biofilm count is reduced

by more than 94%. Together, these results suggest that *P. aeruginosa* biofilms in the early developmental stage of initial adhesion are successfully eliminated using phage treatment and that even relatively low amounts of phage are effective.

4.3.4 Early biofilms survive with diminished populations upon higher phage exposure

Next we evaluated the response of immature biofilms in the second developmental stage at the time of phage exposure (Fig 4.4b). At the time of phage inoculation, the biofilms are steadily increasing their numbers, facilitating rapid phage amplification. Unlike the stage I biofilms, the final outcome for stage II biofilms reveals a sensitive dependence on the phage inoculation density, p_0, consistent with the intuitive prediction that higher phage exposures result in reduced biofilm numbers. At all phage exposures, however, a reduced biofilm remains intact at T=T_i+16 h (Table C.2). Only the biofilm condition at the transition between developmental stage I and II at the time of treatment has near full elimination of the bacteria at highest phage exposure (2.2% remaining), similar to the class 1 response (T_i=4 h, $c_0 = 10^7$ CFU/mL). On the other hand, this biofilm condition has the phage titer dependence of response class 2. The outcomes of the other two sample conditions in this response class are less ideal, with 18-23% of the living bacteria remaining at even the highest phage titer.

Figure 4.5b provides side and top views of the typical biofilm appearance versus phage exposure for response class 2 at T=T_i+16 hr (T_i=4 h) and $c_0 = 10^8$ CFU/mL. The improved outcome with phage titer is evident, as is the diminished success of treating biofilms in developmental stage II versus stage I. The spatiotemporal dynamics of response class 2 (Figure 4.6, T_i=4 h) show that a modest biofilm is established but that the biofilm height and density shrinks over time. These data establish that stage II biofilms are substantially reduced but not fully eliminated by phage exposure and that their final biofilm population scales inversely with the phage dosage, a central feature of the class 2 response. Additionally, for the duration of the experiment, phage treatment blocks the biofilm from

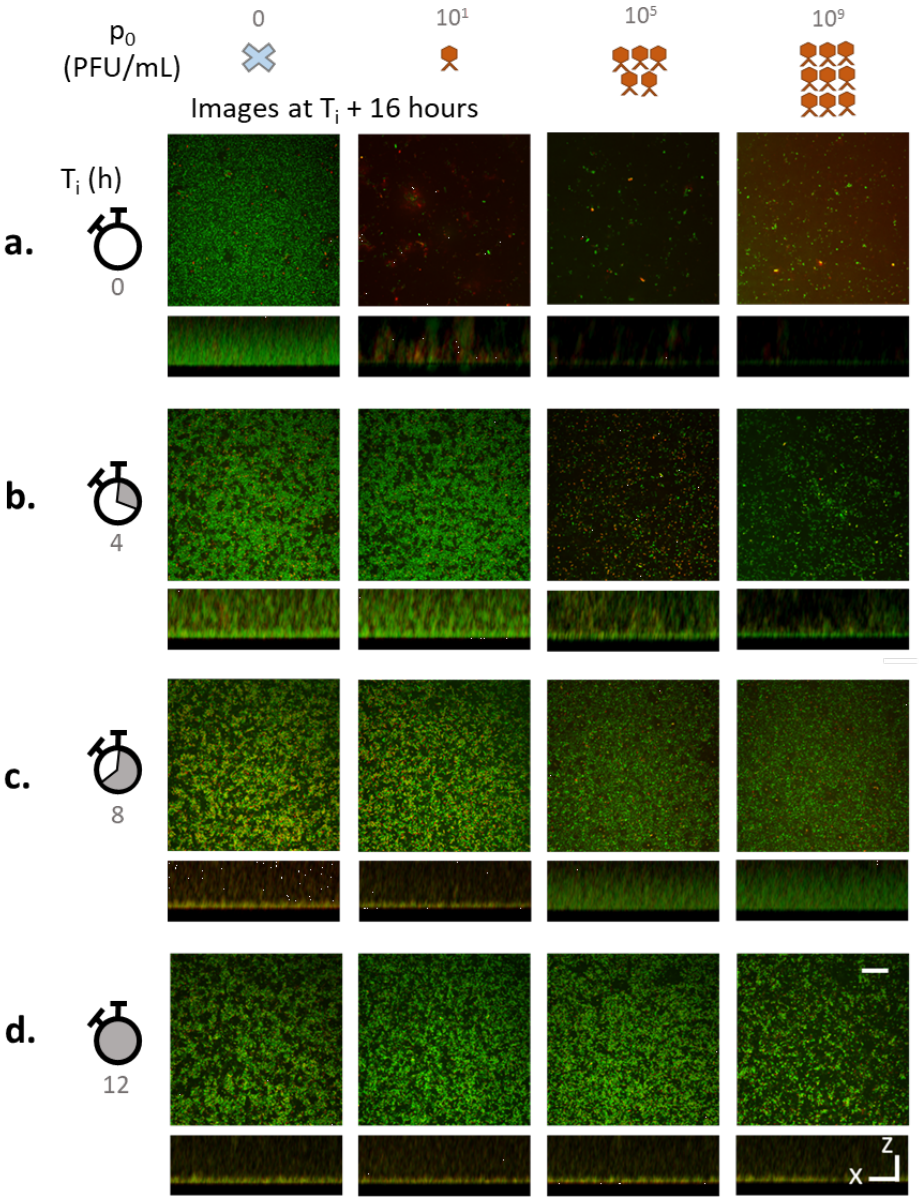

Figure 4.5: **Confocal microscopy images of biofilms after 16 hours of phage exposure** | XY views of the biofilm surface and Y-averaged XZ side views of the biofilm cross-section. Each row (a,b,c, and d) denotes the four response classes 1, 2, 3, and 4 corresponding to the biofilm developmental stages I, II, III, and IV at the time of phage exposure for the initial bacterial seeding condition of $c_0 = 10^8$ CFU/mL. The columns correspond to the mock-control and $p_0 = 10, 10^5, and 10^9$ PFU/mL phage-treated samples. X scale bars = 30 μm and Z scale bar = 5 μm for all images.

transitioning from the early biofilm to the mature biofilm developmental stage.

4.3.5 High phage exposure paradoxically enhances mature biofilms

The response of stage III mature biofilms upon phage inoculation yields a surprising outcome. Phage treatment substantially enhances the final living population of mature biofilms. Even more paradoxically, the maximum phage exposure leads to the highest final bacterial counts (Figure 4.4c). This phage dependence is markedly the opposite of that observed for biofilms treated at stage II, as is apparent by comparing the biofilm outcomes after 16 hours of phage treatment for stage II and III in Figures 4.5b, c. This particular phage dependence is consistent for three of the four treatment conditions associated with the mature biofilm stage. The enhanced final living bacterial count ranges from 52 to 187% more than the control values for the $p_0 = 10^9$ PFU/mL treatment (Table C.2). The one outlying condition again, lies on the edge of the transition between early biofilm and mature biofilm development. That samples phage dose dependence reflects that balance, showing a noisy but relatively flat dependence with the two dependences apparently cancelling out.

Increasing the phage dosing of stage III biofilms results in thicker, more uniform bacterial communities by the end of the experiment. The final high phage titer-treated samples consist of a relatively voidless homogenous biofilms, as seen in images of a typical cross section and a x-y slice taken at the substrate (Figure 4.5c). This suggests that the biofilm has been arrested from entering the dispersal stage (IV) for the duration of the experiment. In contrast, the mock control associated with response class 3 (Figure 4.5c, column 1) is a thin remnant biofilm with numerous voids, consistent with the onset of cell dispersal in P. aeruginosa [110, 134].

The dynamics of this process are captured in Figures 4.3 and 4.6. For those conditions associated with the response class 3, the total living bacterial count first decreases in time but eventually begins to recover until it overtakes values associated with the control. This dynamic is especially evident when examining the spatiotemporal profile of the biofilm. At

the start of phage treatment, the biofilm is near its peak thickness and population (c_0=10^8 CFU/mL, T_i=8 h). The added phages drive a rapid reduction of the biofilm height and density, compared to the natural decay seen in the mock control. However, after 10 hours pass, the biofilm begins to recover its lost height and population, in contrast to the control, which by that time has entered the dispersive developmental stage.

These data establish that stage III biofilms have a response to phage treatment inverse to that of Stage II biofilms. Increasing phage dosing enhances rather than reduces the final biofilm population. We hypothesize that this effect, as discussed below, likely arises from the recycling of nutrients from lysed bacteria at a critical time when restricted nutrient conditions normally lead to the onset of stage IV, and death and dispersal of the biofilm.

4.3.6 Phage-treated biofilms in dispersion stage perform similar to mock control

Phage treatment of biofilms in the fourth developmental stage of dispersion generates remarkably little reduction in the living bacterial count. The outcome is similar to the control biofilm, and increasing the phage dosage makes no large difference (Figure 4.4d, Figure 4.5d). The final biofilm count ranges from a $\sim$12% reduction at the lowest phage condition to a $\sim$5% increase at the higher phage treatments. Similar to the control biofilm at this late time point, a heterogeneous, few micron thick layer of bacteria remains intact at the surface as shown in Figure 4.5d.

The spatiotemporal profile of the live and dead bacteria (Figure 4.6, T_i=12 h) reveals that the stage IV biofilm has high levels of dead bacteria and possibly eDNA near the surface, since propidium iodide stains both. Crystal violet data taken at the end point is consistent with this observation, showing that the OD signal measured for the control versus phage treated biofilms is very similar, unlike the other response classes which showed more sensitivity to the presence of phage, especially classes 1 and 2 (Figure C.2). The crystal violet data suggests that a high level of remnant EPS might play a role in the observed protective benefits against phage treatment independent of the dosage, or reduced metabolic

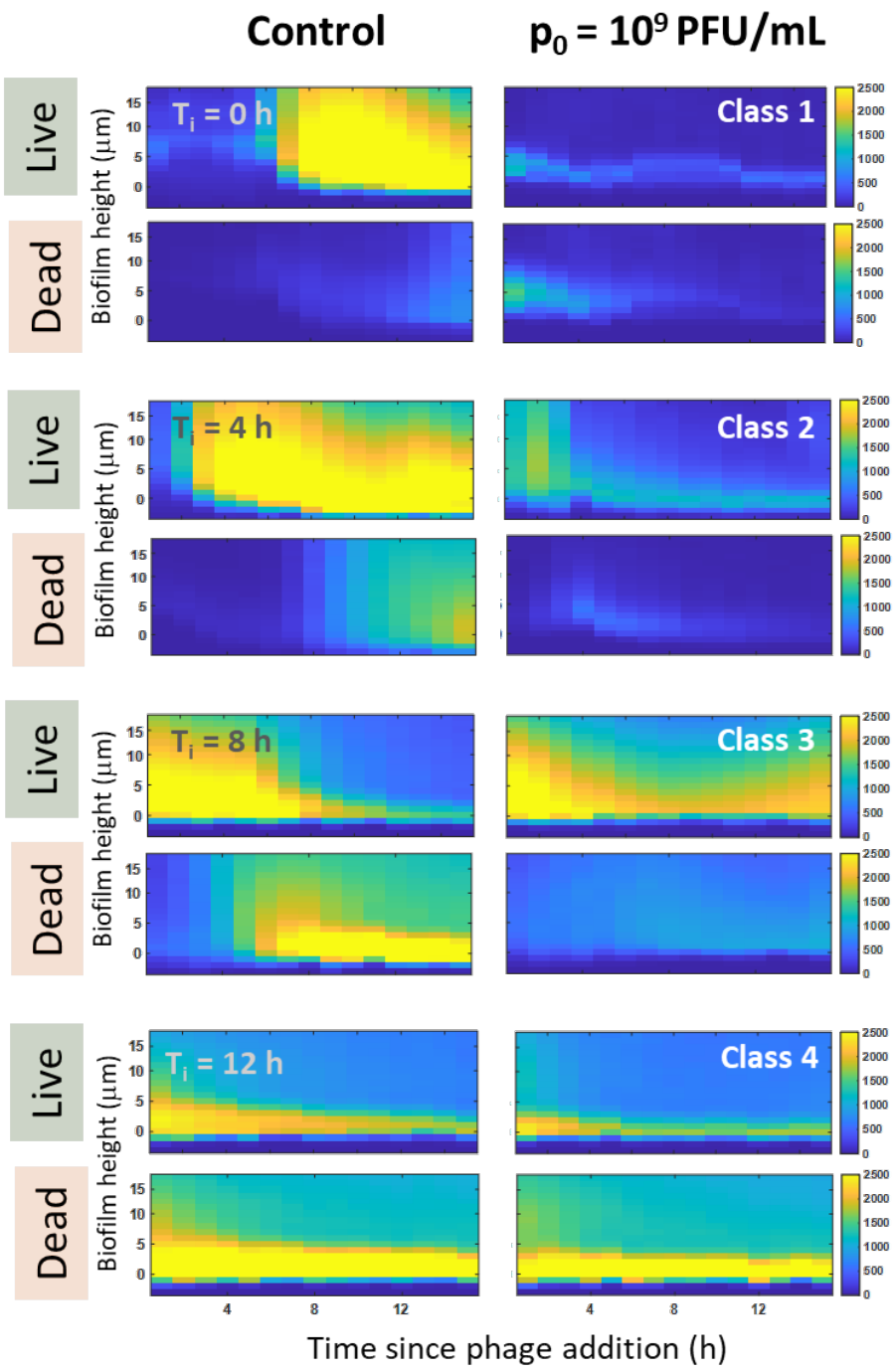

Figure 4.6: **Spatiotemporal profile of bacterial levels within biofilms in the absence and presence of phage reveals key impact of phage** |Heatmap indicates the live and dead bacterial levels at different heights within the biofilm (initial bacterial seeding condition of $c_0 = 10^8$ CFU/mL) for a duration of 16 hours from phage exposure. The spatiotemporal dynamics of the mock-control for different T_is corresponding to the four developmental stages at time of phage exposure is shown on the left column and the dynamics of phage-treated samples at high phage exposure ($p_0 = 10^9$ PFU/mL) is shown on the right column.

activity as a result of nutrient depletion or other stressors may block any serious impact from phage activity [110, 187–189].

Contrary to the biofilm bacterial levels and biomass levels, the planktonic fraction of the samples decreases in a dose-dependent fashion to phage at all four developmental stages (Figure **??**). This suggests that although phages are effective against planktonic bacteria, certain factors in a biofilm reduce their impact, where the particular mechanism varies with developmental stage.

4.4 Discussion

Recently, there has been a renewed interest in phage therapy as a promising antibacterial strategy. Continued presence of pathogenic bacteria could lead to chronic infections where the bacteria are embedded within a matrix and are attached to soft tissues or hard surfaces such as medical implants [57, 105, 106, 108, 190]. Further, the surge in multidrug resistance among bacterial strains poses a grave threat to human healthcare [104, 191]. Therefore, gaining a comprehensive understanding of phage-biofilm dynamics will enable the assessment of the therapeutic potential of phage against bacterial infections. In this study, we explored the dynamical impact of exposing *P. aeruginosa* biofilms at different developmental stages to a wide range of phage densities.

This experimental study establishes that the biofilm response to phage treatment depends sensitively on the developmental stage of the biofilm. We broadly organize the phage dose-based impact on biofilms into four response classes. In the first response class, phage treatment successfully prevents biofilm formation when the biofilm is at its earliest stage of initial adhesion. In the second response class, the final number of living bacteria in the biofilm depends on phage treatment in a dose-dependent fashion, where more phage eliminates more of the biofilm. The biofilms that exhibit this response were in the developmental phase of early biofilm formation at the time of phage addition. The rapidly growing biofilm is largely but not entirely reduced by the phage treatment. The

third class of response presents a reversed dependence on phage titers, where high phage levels enhance the amount of live bacteria in biofilms compared to the untreated samples. In the last response class, we find that biofilms in their final dispersion stage of development appear to be quite robust against phage treatment at any dosage. A thin biofilm persists, apparently immune to phage attack, maintaining bacterial populations that are similar to that of the mock control.

One of the more surprising results of the study was the observation that when mature biofilms are exposed to phages above a threshold density, they tend to regrow after an initial reduction. We hypothesize that the biofilm regrowth could be driven by two potential mechanisms 1) recruitment of bacteria in the planktonic fraction to strengthen the dwindling biofilm, and/or 2) enhanced bacterial growth due to lysis-driven local nutrient regeneration in the biofilm microenvironment. Since these biofilms are in the mature developmental stage transitioning to the dispersion stage, we expect high levels of nutrient and oxygen stress in the biofilm microenvironment. This is consistent with the onset of cell death captured in the spatiotemporal dynamics of the mock control in Figure 4.6 (T_i=8 h). Lysis of metabolically active bacteria in the upper regions of the biofilm could transiently remove these stressors through the release of nutrients from the lysed cells. Further, the diffuse spatiotemporal signals in the corresponding propidium iodide data suggests that the biofilm reduction is due to phage-driven lysis rather than other means (such as death, dispersion, erosion, sloughing, etc), thereby supporting the second hypothesis. Although such nutrient recycling through viral shunt has been recorded in marine environments [165, 192, 193], to our knowledge it has not been discussed in the context of laboratory based phage-biofilm systems.

Phage-driven control of dispersion is of particular interest in light of recent studies that report dispersal-induced septicemia in mice [135]. Native dispersion following the mature biofilm stage is a highly orchestrated event in *P. aeruginosa* biofilms [111], where a motile-subpopulation is freed into the exterior leaving behind characteristic void-like structures.

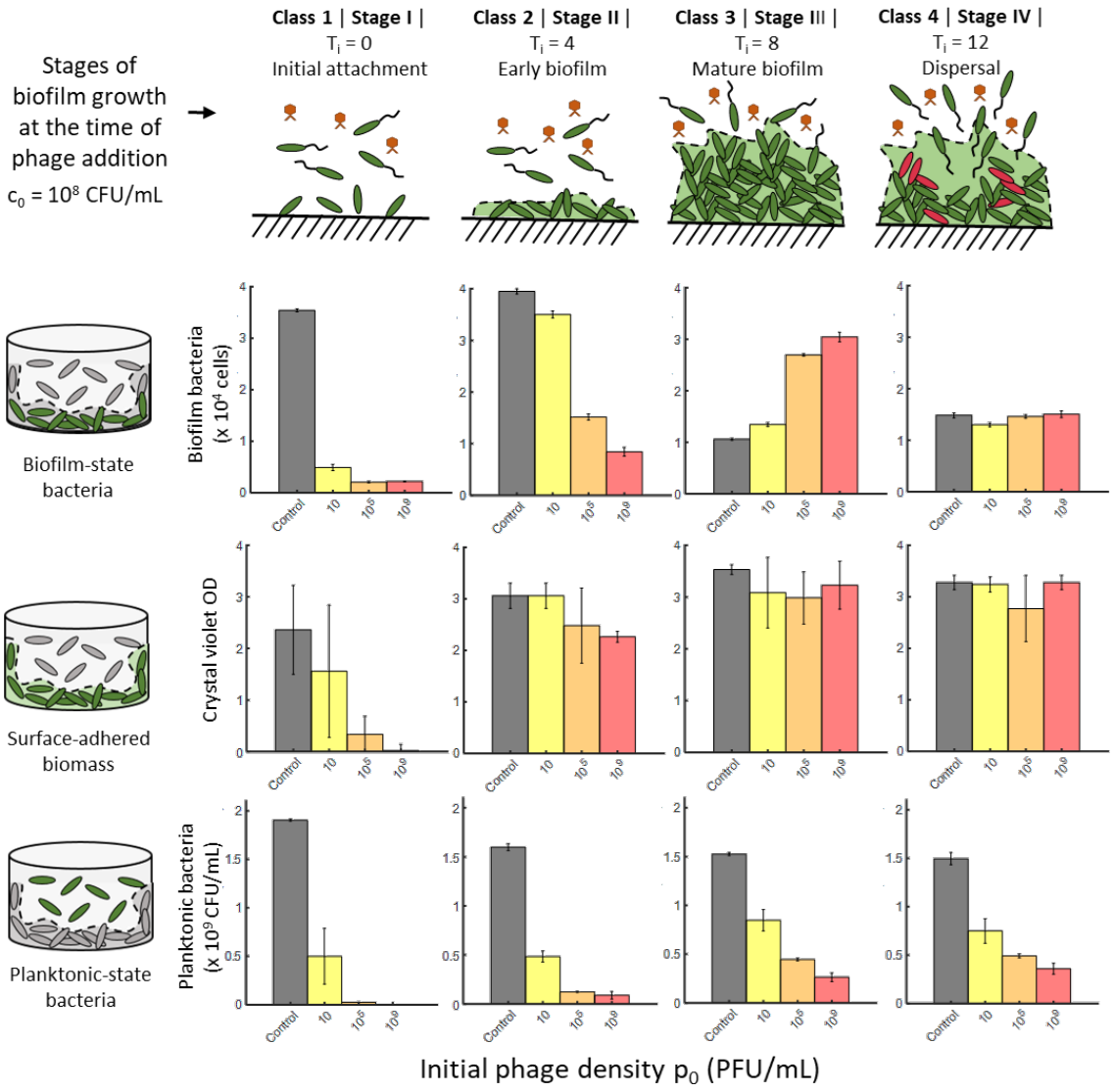

Figure 4.7: **Susceptibility of P.aeruginosa biofilms depends on the biofilm developmental stage** | The four response classes I, II, III, and IV correlate with the four developmental stages of the biofilm: I. Initial attachment, II. Early biofilm, III. Mature biofilm, and IV. Dispersal stage. Illustrated here with the example of $c_0 = 10^8$ CFU/mL.

This stage is further associated with increased cell death due to local anaerobic conditions within the biofilm [48, 111, 167, 194], consistent with our observations in the mock-control biofilms. In the third response class, the lack of retained propidium iodide signal in the spatiotemporal profile (Figure 4.6, T_i=8 h) and the absence of characteristic voids (Figure 4.5c, p_0=10^9 PFU/mL), suggests the inhibition of cell death and dispersion at similar times upon exposure of external introduction of lytic phages. Since, biofilms at the dispersion stage disseminate relatively virulent bacteria and shield the remaining bacteria to a high degree, our observation on the suppression of biofilm transition to the dispersion stage by phage and other recent reports on phage inhibition of bacterial migrants [143] suggest the potential use of phage to restrict the virulence of existing infections and prevent the initiation of biofilms in other regions.

The insights offered by grouping biofilm dynamics and outcomes into response classes helps to synthesize the scattered results from biofilm-phage studies in the literature. Our findings associated with response class 1 are consistent with previous reports of inhibition of biofilm formation by phage [85, 86, 90]. Similarly, the dose-dependent bacterial elimination in response class 2 corroborates studies of early stage *in vivo P. aeruginosa* infections [195, 196] and report of a dose-dependent reduction of biomass in a recent *in vitro* study with *A. baumanii* biofilms [86]. We observe, however, that biomass estimations using crystal violet assays alone may present pitfalls, as seen by comparing crystal violet results with quantitative microscopy, especially for aged biofilms (Figure **??** compare rows 1 and 2). In addition, biofilm enhancement on phage treatment similar to the Class 3 response has in fact been reported in a few studies [177, 197]. Our work here goes further to show that this paradoxical enrichment of the biofilm in resource-limited conditions is likely due to nutrient recycling in biofilm microenvironments and suggests that prolonging the mature biofilm stage with phage can delay dispersion of the biofilm. Taken together, this study clarifies the importance of assessing the biofilm developmental stage and phage dosage in determining the dynamics and outcome of the treatment, and may put a wide

range of studies using limited and varied conditions into context.

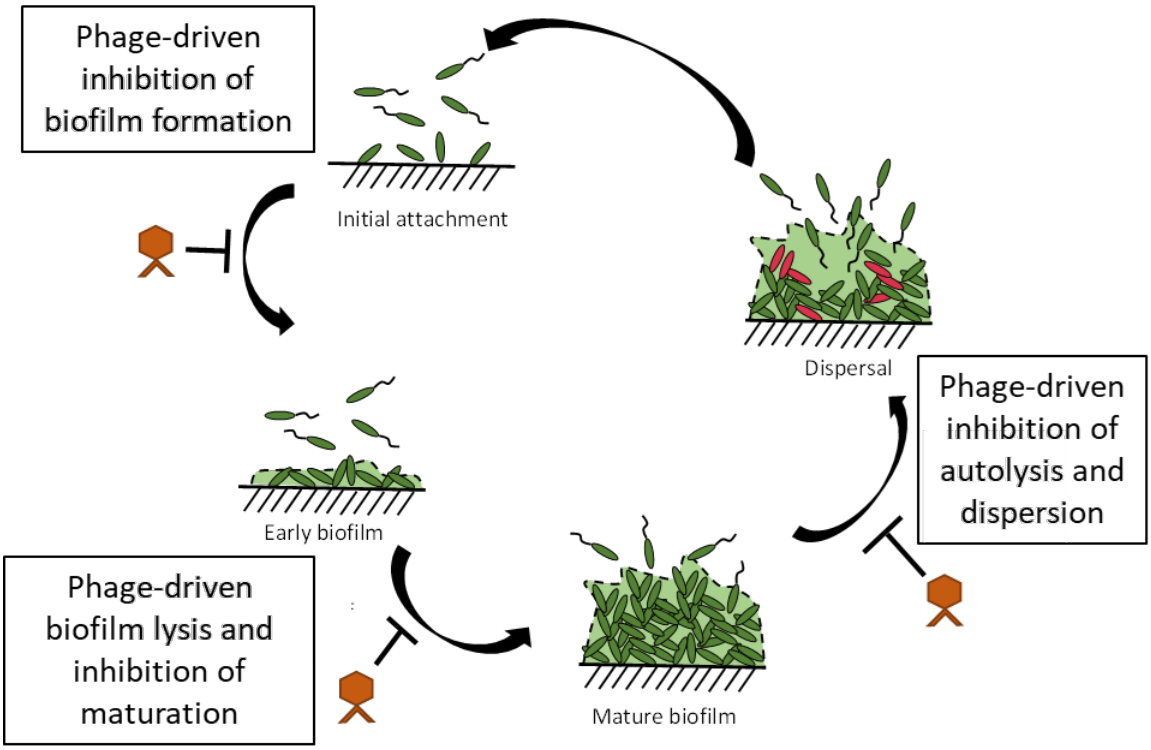

Figure 4.8: **Impact of phage exposure on during various developmental stages of the biofilm** | Schematic illustrating the restraining effect of high phage titers on biofilms. Phages seem to inhibit the natural progression of biofilm development.

4.5 Conclusion

Collectively, our results suggest that high phage doses restrain the developmental progression of biofilms at the observed timescales. When added during the early stages of biofilm formation, namely initial attachment, phage inhibit the formation of biofilm. Thus, phage show high promise as a prophylactic against developing chronic infections. Their ability to remove or lyse bacteria in the early biofilm suggests that they would be effective as biofilm eradication agents under certain conditions. Further, phage delay or inhibit mature biofilms from progressing into the next developmental stage of dispersion, when added above a threshold density. Although phage do not eliminate the biofilm sub-population in these conditions, they reduce the planktonic sub-populations significantly and inhibit the induction of native cell death and biofilm dispersal. Hence, phage could potentially be used as a therapeutic agent to localize the infection and restrict the systemic spread. Yet, the local regrowth of the biofilm could pose other challenges. This situation could potentially be thwarted in combination with other phages, antibiotics, enzymes, iron-chelators, etc. Since the biofilm response to any form of treatment is highly sensitive to the developmental stage at the time of intervention, careful assessment of infection state is crucial to the determination and success of the therapeutic approach.

CHAPTER 5

OUTLOOK

Through the studies reported in this thesis, our understanding of phage-biofilm dynamics has improved substantially. In the first part of this thesis, we presented the experimental protocols that played a key role in performing these studies (Chapter 2). It includes procedures for handling the three different classes of samples bacteria, virus, and immune cells. Further, it establishes protocols for high-throughput experimentation of biofilm systems, especially for understanding the spatiotemporal impact of various phage treatments. The next part delves into the dynamics of planktonic bacterial fraction on exposure to phage (Chapter 3). This study led to the identification of various interesting dynamical features. Some of these features can be explained by mathematical models (being developed in collaboration with Weitz group, Georgia Tech) whereas some are yet to be understood. Nevertheless, the rich dataset facilitates the testing of dynamical models and offers mechanistic insights. Finally, in the last part of this thesis, we mapped the spatiotemporal dynamics of *P. aeruginosa* biofilm systems when exposed to PEV2 phage (Chapter 4). Such detailed mapping of the dynamics for a large parameter space led to the generation of high-quality data and helped identify critical factors driving the observed dynamics. We identified distinct patterns of biofilm response with phage dosing. Further, we showed that the biofilm developmental stage at the time of phage exposure is a critical factor that dictates the phage dose-response of a given biofilm. Additionally, our data suggests that phages stop the developmental clock of biofilms from moving forward, in other words, phages appear to restrain biofilm development. These results have the potential for far-reaching implications in clinical settings and biocontrol applications.

While these studies fill the data gap in the literature and provide interesting perspectives about phage-bacteria and phage-biofilm interactions and dynamics, they also raise many

important questions for further investigation such as – Can the phage dose-response class be extended to other phage-bacteria systems? What is the role of phenotypic and genotypic resistance in driving the dynamics? How do phages affect the polymeric matrix of the biofilm structurally and functionally? How do phage populations vary spatiotemporally in these systems? What are the clinical implications and the outcomes be improved using combination therapies? What are the mechanisms driving immunophage synergy? In the following sections, we discuss some aspects of these open-ended questions and consider ways to address them.

5.1 Extending the response class framework

The framework of phage dose-response classes developed in Chapter 4 serves as an concise model for understanding the impact of PEV2 phage on *P. aeruginosa* biofilms. It is a simple model that groups the biofilm response to phage dosing and helps recognize the role of biofilm developmental stage in modulating outcomes. This framework is powerful tool that allows for the prediction of biofilm outcome on exposure to any phage dosage. Itll be important for future studies to assess if this framework applies to treatment with other phages on *P. aeruginosa* biofilms. Given the data from crystal violet assay, we know that PEV2 phages do not effectively remove the biofilm matrix. It would be interesting to probe the biofilm dynamics in the presence of the phage that degrades the biofilm polymeric matrix. Additionally, similar experiments on other bacterial strains and would shed light on generalizability of this framework across microbial strains and species.

Further, it would be interesting to probe the impact of environmental conditions on phage-biofilm dynamics. Differences in factors such as temperature and nutrient media composition would alter metabolic properties of the constituent bacteria. Such changes in turn would influence factors such as phage diffusivity, adsorption, latent period, and burst size. This would lead to changes in dynamics and resultant outcomes. The applicability of the response-class framework under these perturbations is an interesting open question.

Future studies probing these factors would lead to mechanistic insights.

The emergence of bacterial resistance against phage is an aspect that is yet to be probed in this study. In Chapter 3, we recognized that some planktonic-state bacteria developed resistance in a stochastic fashion and increased in numbers. This resistance could stem from phenotypic or genotypic factors. It is still not clear whether such resistant populations exist in the biofilm fraction of these samples. If so, how do they impact the overall dynamics? Do they alter the dynamics significantly? Resistance evaluation would be crucial towards understanding the underlying interactions.

5.2 Phage effect on biofilm matrix and structure

The biofilm matrix, also known as extracellular polymeric substance, is composed of polysaccharides, nucleic acids, and proteins. Various matrix components are synthesized at different stages of biofilm development. The matrix in turn modulates cell-cell and cell-matrix interactions. The role of biofilm matrix in supporting the biofilm architecture and providing protective properties is an active area of exploration. Exoploysaccharides such as Psl, Pel, and alginate contribute to biofilm formation and extracellular DNA (eDNA) helps connect individual cells within *P. aeruginosa* biofilms. Further, biofilms selectively degrade matrix components, often during the dispersion stage to release motile bacteria. The addition of phages leads to changes in the microenvironmnets of the biofilm matrix. Vidakovic et al., [177] have shown that envelopment of biofilm bacteria by curli fibers leads to protection against phages. Study of phage-induced changes in biofilm matrix through the labeling of matrix components would be necessary. For this purpose, dyes such as Calcofluor White (non-specific fluorochrome that binds to cellulose and chitin), SYPRO Ruby Matrix stain (labels most classes of proteins, including glycoproteins, phosphoproteins, lipoproteins, calcium binding proteins, fibrillar proteins), and nucleic acid stains like SYTO9 and propidium iodide can be used. Further, a pH-sensitive ratiometric fluorescent probe called CSNARF4 could be used to characterize the resulting

changes in biofilm pH due to phage activity. The results from such experiments would help assess the broader impact of phages on biofilms.

Another approach for improved biophysical characterization of phage-biofilm systems would be to tailor biofilm-phage interfaces and characterize the spatiotemporal impact of phage using direct visualization at the microscopic level. Elucidation of intricate aspects of the dynamics helps toward improved understanding of the complex interaction between the two microbes. Biofilm growth in spatially confined regions leads to the formation of dense bacterial layers. Such systems have proved useful to study mechanisms of signaling between bacterial sub-populations [8]. High density quasi two-dimensional bacterial layers with elevated levels of bacterial connectivity offers the ideal conditions to visualize the propagation of changes due to external stimuli at the edge of the layer. Such experimental setups would enable the visualization of bacterial lysis patterns formed due to phage exposure at a defined interface. In order to achieve this, we conceptualized and implemented a tuneable experimental platform to achieve various interface configurations between phage and bacterial populations. To create initially separated system of phage and biofilm, we designed and constructed a fluidic device that would allow for microscopic investigation of bacterial lysis as phage propagates through the biofilm. The main principle involves tailoring phage-biofilm interfaces by constraining the biofilm and phage to regions under the agar pads and the spaces between them, respectively (Figure 5.1b).

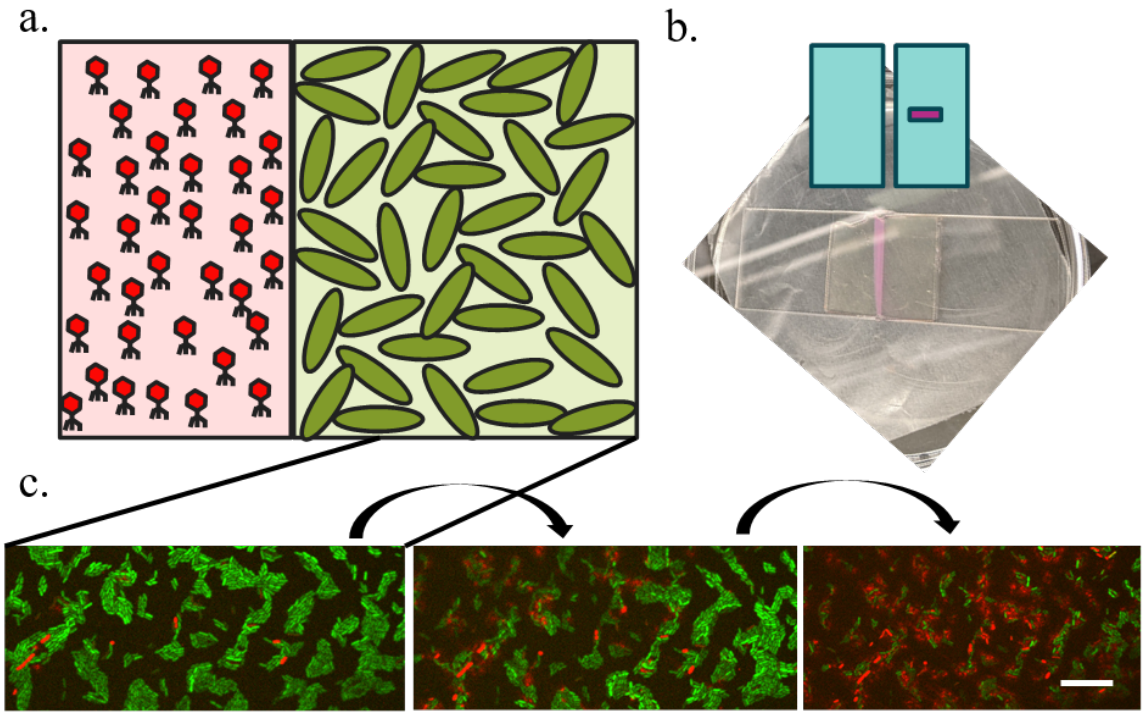

Figure 5.1: **Concept to realization of biofilm lysis by phage with well-defined initial spatial separation** | a. Schematic of spatially separated phage-bacteria populations in a new experimental setup to study the spatiotemporal propagation of phage through bacterial layers/biofilms; b. Prototype of a novel microfluidic device design to realize the spatial arrangement of the two species system; c. Confocal microscopy images of the bacterial layer 1mm away from the phage channel. Phage propagate from left to right in this setup. Green denotes live bacteria and red denotes dead bacteria stained with propidium iodide left: 2 hours after phage were added in the channel, middle: 2 hours 40 minutes after phage were added in the channel, and right: 3 hours 40 minutes after phage were added in the channel. Scale bar: 15 μm.

Further optimization of this device to maintain humidity levels would enable observations for longer durations. Using bacterial strains that produce EPS of different compositions and studying the impact of phage under such dense conditions would be interesting problem to study from a polymer physics and soft matter perspective.

5.3 Understanding the spatiotemporal dynamics of phage

In these experiments, we track the changes in bacterial populations in the planktonic and biofilm state and indirectly infer insights about the spatiotemporal impact of phage. Traditional methods for mapping phage dynamics involve multiple replicates and abortion of the experiment for a few samples (number of replicates) to obtain the phage titer at that piont in time. This is a time, resource, and labor intensive process and cannot be scaled easily. Further, it does not reveal any information about the spatial propagation of phage through biofilms.

Fluorescent labeling of phages allows tracking of infected host bacterium through confocal fluorescence microscopy. While engineering phages with a fluorescent protein expressing construct is a much more involved approach, fluorescent labeling or tagging of phages is relatively a simpler method to view initial phage-bacteria interactions. Prior studies have employed this this method to understand the mechanisms of phage infection of biofilms [177, 198]. Such fluorescent labelling or tagging of phage would help characterize the spatiotemporal invasion of phage and the response of biofilms towards it.

5.4 Better clinical perspectives

The effectiveness of phage as a prophylactic and therapeutic agent depends on the developmental stage of the biofilm and the interaction mechanism of the phage-bacteria pair. This has been demonstrated in Chapter 4 through the response-class framework and its connection with biofilm developmental stage. In clinical settings, the characteristics of the biofilm infection is often unknown. Better characterization prior to phage treatment would in principle provide the opportunity to optimize the state of the biofilm for maximal phage response. Treatment of biofilms with antibiotics and other antimicrobials in addition to phage exposure could improve outcomes as well [199]. Avilability of iron is known to play a significant role in biofilm development and virulence [200], hence adding iron-chelators

to the mix would help tune the physiological state of bacteria in biofilms. Further,the order of the combination treatments could have a significant role in determining outcome and needs to studied. Our improved understanding of phage impact on biofilms at different growth stages can now be used to design experiments to test combination approaches and identify synergistic regimes.

Phage cocktails for treatment of infections and inhibition of phage-resistance has been explored in previous studies [201]. A natural extension of this work would be to test the framework for polymicrobial biofilms and phage cocktails. Additionally, in the cystic fibrosis lung, *P. aeruginosa* resides in a nutritional environment that is distinct from that of the LB media. Using synthetic medium that closely mimics the composition of human CF sputum (rich in macromolecules such as mucin, DNA, lipids would help provide a relevant in vitro growth environment for studying chronic P. aeruginosa infections.

The bacteriophage PEV2 used in this study leverages the B-Band of the LPS as a receptor for adsorption. Clinical isolates of *P. aeruginosa* often lack this receptor unit. Phage engineering of PEV2 to broaden receptor range would be an effective strategy for handling clinical samples. Such synthetic biology approaches have the potential to transform therapeutic approaches with phages. These advances in bioengineering would facilitate personalized treatments using phage when other traditional approaches fail.

5.5 Towards immunophage therapy

The success of phage as therapeutic agents ultimately depends on their joint interaction with the pathogenic bacterial population and the immune system of the host. This requires the integration of phage-bacteria dynamics with immunological principles. Recently, Roach et al.[28], demonstrated that phage and innate immune response in tandem could eliminate bacterial populations in an animal model, when neither approach in isolation could do so. This led to the identification of the mechanism termed immunophage synergy that was instrumental in resolving acute *P. aeruginosa* infection in mice. They developed an in silico

model to explain the *in vivo* synergy, with modifications to a prior non-linear dynamical model that explicitly considered the density-dependent effects of immune response. The *in vivo* model included modifications such as incorporation of 1) sub-linear lysis rate (compared to linear lysis-rate) and 2) phage-resistant sub-populations.

Studies have identified neutrophils as an essential component of innate immunity against bacterial infections. The presence or absence of neutrophils could be a crucial factor for the determination of recovery or fatality of the host. This was illustrated through the success and failure of phage therapy for *P.aeruginosa* infections in neutrophil-competent and neutropenic mice, respectively [25]. It was further corroborated by the highly reduced efficacy of phage therapy in neutrophil depleted mice [28]. In the absence of neutrophils or innate immune activation, phage-resistant strains get selected and proliferate leading to host mortality.

Immunophage synergy has been demonstrated to be effective in clearing acute infections. Yet, the success of the approach for successful elimination of chronic infections remains a mystery. Would the synergy effect continue to occur in spatially heterogeneous landscape of biofilm infections? If so, under what spatiotemporal and density-based initial conditions? How would the emergent properties of biofilm populations, such as, extracellular polymeric matrix, density-dependent quorum sensing signalling, modulation of virulence factors, impact the efficacy of phage therapy?

Preliminary investigations of neutrophil-biofilm interactions suggest that while neutrophils readily form neutrophil extracellular traps (NETs) in response to planktonic bacteria, their formation is spatiotemporally confined to the upper regions and early times when exposed to biofilms. Many factors contribute to NET release and suppression such as Type 3 Secretion System, quorum sensing mechanisms, and bacterial motility [202, 203]. Such factors change dynamically based on the microenvironment. NET formation has both beneficial and deleterious effects on the host. Recent studies of biofilm infection in ocular keratitis of mice has shown the crucial role of NETs in compartmentalization of bacteria

[203]. Although NET formation appears to be an undesired effect resulting in vision loss, it prevents bacteria from crossing the blood-brain barrier and fatally disseminating into the brain. Detailed characterization of neutrophil-biofilm systems could lead to further insights about the temporal window and rate of NET release in biofilms. Observation of other interesting effects such as disintegration of neutrophils, presence of live bacteria within neutrophils, and slower penetration rates of neutrophils through biofilms formed by quorum sensing mutants, all of which warrants further systematic investigation.

In conclusion, phage-immune synergy has been proposed a potential mechanism that leads to the observed success of phage therapy. The central concept is that as long as phages drive down the bacterial populations to levels that the immune system of the host can handle, the infection can be eliminated synergistically. We hope that knowledge from detailed exploration of the neutrophil-biofilm dynamics in combination with the insights obtained from the study of phage-biofilm dynamics in this thesis would help foster a comprehensive understanding of immunophage synergy.

5.6 Summary

The work on systematic exploration of phage-biofilm dynamics presented in this thesis opens up a wide spectrum of future research at the intersection of biophysics, soft condensed matter, mathematical biology, biopharmacodynamics, and bioengineering. We hope this outlook can serve as a map for future graduate students who would like to actively explore phage-biofilm systems. Further, we hope that the insights from this thesis fuel more research that enable a better understanding of immunophage synergy and other combination therapeutic approaches.

Appendices

APPENDIX A

SUPPLEMENTARY MATERIALS FOR CHAPTER 2

A.1 Pseudo-code to explain the image processing workflow

% Accessing the image and extracting relevant features

for (loop over parameter 1, c0)

for (loop over parameter 2, p0)

for (loop over parameter 3, replicate)

for (loop over parameter 4, timepoint)

for (loop over parameter 5, plane)

% obtain the image from the appropriate folder using custom written function

% S denoted image from the SYTO9 channel

S = `fn_get_image`(b_0, p_0, replicate, timepoint, channel, plane);

% binarize the image using the corresponding optimal binarization routine for that channel

`S_bn` = `fn_binarize_adapt`(S, channel);

% Add the pixels of the binarized image to obtain the area occupied by the objects of interest

`area_syto9` = sum(`S_bn`, [1 2]);

%obtain the image from the appropriate folder using custom written function

% P denoted image from the propidium iodide channel

P = `fn_get_image`(b_0, p_0, replicate, timepoint, channel, plane);

```
                    %binarize the image using the corresponding optimal binarization
                    routine for that channel
                    P_bn = fn_binarize_adapt(P, channel);
                    % Add the pixels of the binarized image to obtain the area occupied
                    by the objects of interest
                    area_pi = sum(P_bn, [1 2]);

                    % Obtain the overlap between the two channels
                    O_bn = S_bn.*P_bn;
                    area_overlap = sum(O_bn,[1 2]);

                    %Compile all area data
                    pixel_areas(b_cond,p,r,t,plane,syto9) = area_syto9;
                    pixel_areas(b_cond,p,r,t,plane,pi) = area_pi;
                    pixel_areas(b_cond,p,r,t,plane,overlap) = area_overlap;
                    end
                end
                sprintf('ti%d_p%d_r%d_t%d_done',b(b_cond),p,r,t)
            end
        end
end

    % calculate the area occupied by live and dead bacteria in each image
pixel_areas_live = area_syto9 - area_pi;
pixel_areas_dead = area_pi;

    %% function for binarizing images using adaptive thresholding
```

```
function binary_image = binarize_adapt(image, channel)
%% certain situations the following operation leads to better outputs. It wasnt used for the data presented in this thesis.
% if channel == 1
% image = rescale(image, 0, 65535);
% end
% convert the pixels of the image into unsigned intergers with values from 0 to 65535. It works since the data we obtained are 16-bit images
image = uint16(image);
%Generate the threshold using adaptthresh  first parameter is the image, second one is the sensitivity factor which needs to be tuned for each channel, the third parameter is the statistic that is applied in the local neighborhood  mean gave optimal results and is good tradeoff between accuracy and processing time
T = adaptthresh(image,0.4,'Statistic','mean'); % Sensitivity factor % Statistic
%imbinarize applies the obtained threshold to the image and generates a binarized image
BW = imbinarize(image,T);
%create the structuring element using strel function
se = strel('disk', 2); %choice of strel size
%morphologically close the image using the obtained structuring element
BW = imclose(BW, se);
%Remove any object smaller than the size specified as the second parameter of the bwareaopen function
BW = bwareaopen(BW, 12); % choice of bwareaopen size
binary_image = BW;
```

APPENDIX B

SUPPLEMENTARY MATERIALS FOR CHAPTER 3

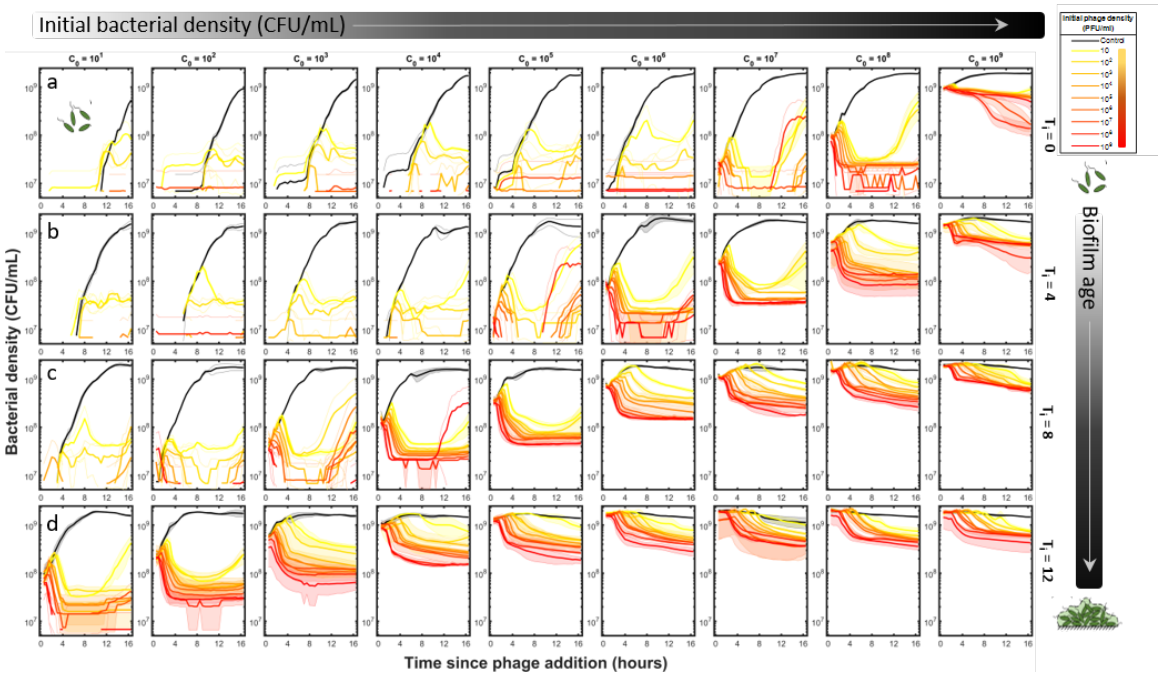

Figure B.1: **Plots of phage-bacteria dynamics in the planktonic sections** | We observe the effect of adding phages to bacteria at different stages of biofilm formation and/or maturity and investigate the dynamics as a function of initial bacterial density, initial phage density, and biofilm age. We show the bacterial density as a function of time since phage addition on a logarithmic scale. Each column shows the responses of samples initiated with the same bacterial density to different levels of phage, while the rows indicate increasing biofilm age and growth maturity (a) T_i =0 h : well-mixed bacteria and phage at the time of phage addition, (b) T_i =4 h, (c) T_i =8 h, and (d) T_i =12 h respectively. In the well-mixed samples with no time for biofilm formation in the 96 well plates prior to phage addition, phages are quite effective at driving the bacterial densities well below detection thresholds except when initiated at high bacterial densities and a few exceptions where we observe stochastic reemergence. When the time prior to biofilm formation is longer, the bacteria often survives at lower levels determined by the initial phage densities.

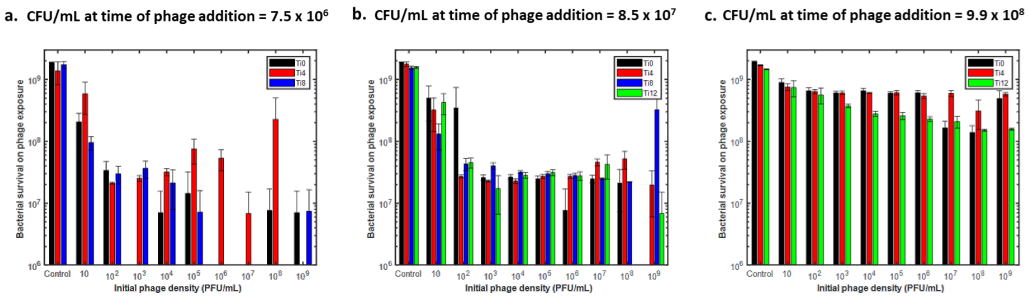

Figure B.2: **Direct comparison of similar starting conditions** (p_0/c_i) **for different sample ages.** Here, we see that the effect of MOI is diminished. In fact, these plots show that sample age has little impact on the final outcome of the planktonic bacterial population.

APPENDIX C

SUPPLEMENTARY MATERIALS FOR CHAPTER 4

Table C.1: Characterization of mock-control biofilm growth

Features / c0 (in CFU/mL)	10^6	10^7	10^8
Biofilm onset time (h)	5—8	4—6	3—5
Rapid growth duration (h)	8—14	6—12	5—8
Max bac count (# +/- SEM)	4.8×10^4 +/- 3.5×10^2	5.3×10^4 +/- 2.0×10^2	4.6×10^4 +/- 5.2×10^2
Onset time of biofilm decline (h)	18—24	14-20	12—16

Table C.2: Percentage difference in average surviving bacterial populations within the biofilm between phage-treated samples and mock-control

Response Class	T_i (h)	c_0 (CFU/mL)	p_0 (PFU/mL)								
			10	10^2	10^3	10^4	10^5	10^6	10^7	10^8	10^9
1	0	10^6	-99.0	-99.3	-99.3	-99.1	-99.5	-99.4	-99.4	-99.0	-99.5
	0	10^7	-97.4	-97.0	-97.7	-98.1	-98.4	-98.3	-98.6	-98.4	-99.1
	0	10^8	-86.2	-85.9	-95.3	-95.2	-94.2	-94.1	-96.2	-92.5	-93.9
	4	10^6	-93.2	-97.3	-95.4	-97.3	-97.5	-97.6	-98.2	-98.2	-94.9
2	4	10^7	-84.3	-88.4	-87.9	-93.0	-95.3	-96.7	-96.6	-95.8	-97.8
	4	10^8	-11.3	3.1	-53.8	-37.7	-61.6	-75.4	-74.3	-84.0	-78.7
	8	10^6	-4.3	-52.0	-63.4	-87.4	-78.4	-84.8	-84.9	-87.2	-83.4
3	8	10^7	25.3	-27.9	37.6	20.9	37.6	23.2	21.2	4.7	-4.6
	8	10^8	26.7	26.8	55.9	148.6	154.3	161.2	173.2	170.1	187.0
	12	10^6	19.1	30.3	42.7	23.4	51.1	84.3	68.4	112.2	72.3
	12	10^7	12.0	21.2	2.3	48.0	27.7	64.2	60.9	52.5	51.8
4	12	10^8	-12.4	-16.5	-10.7	12.3	-1.5	1.9	3.7	4.9	1.5

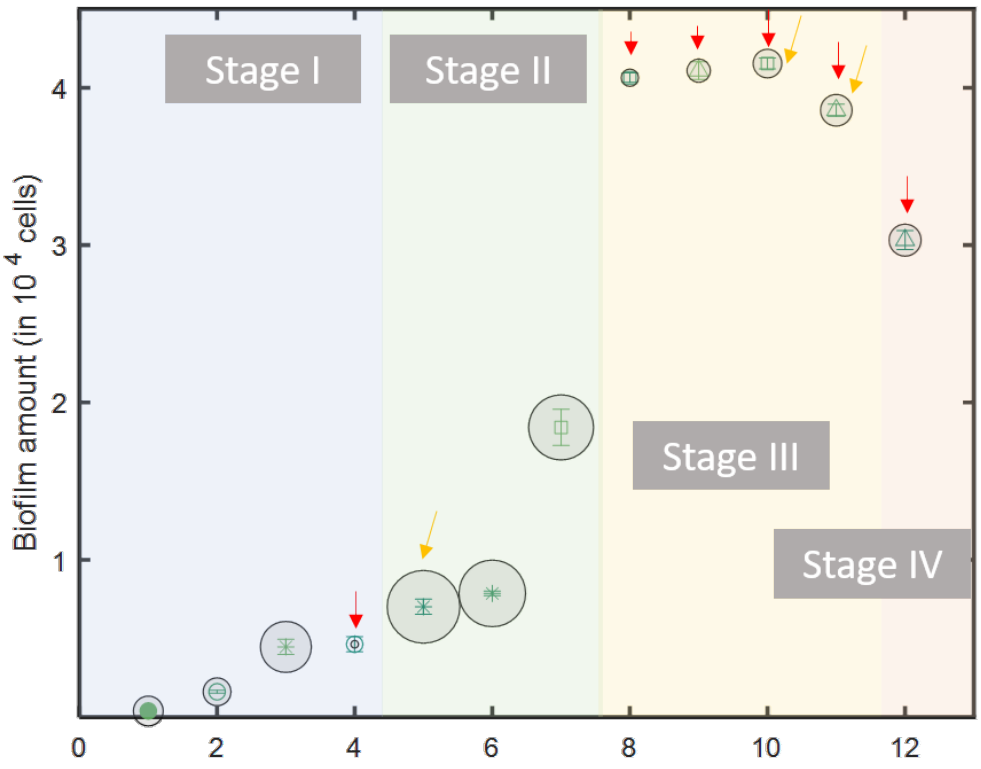

Figure C.1: **Developmental stage of *P.aeruginosa* biofilms at the time of phage exposure** | Each colored section denotes the developmental stages 1, 2, 3, and 4.

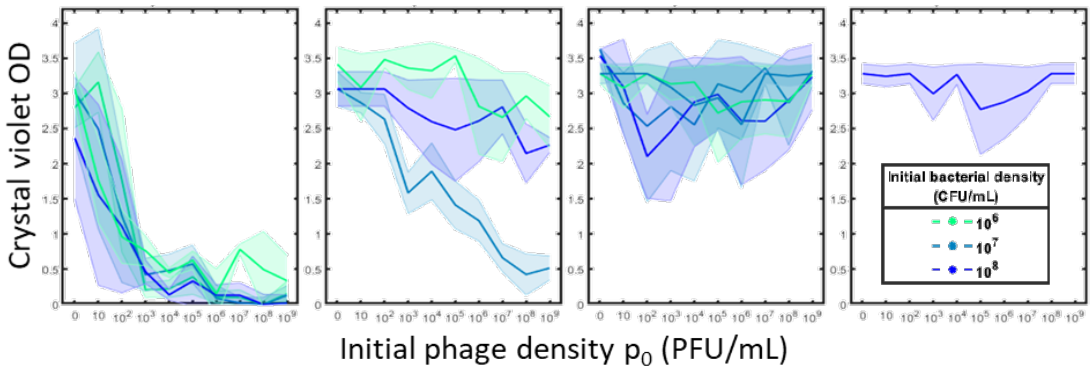

Figure C.2: **Crystal violet assay** | Crystal violet assay results grouped according to the phage dose-response of the biofilms. The crystal violet optical density was obtained at 530 nm for 16 h phage-treated biofilms.

For Response Class 1, crystal violet data taken at the end of these experiments T=T_i+16 hr, show a dose-dependent response with phage exposure. For the two lowest phage conditions, $p_0 = 10^1, 10^2$ PFU/mL, crystal violet signal was reduced but remained above 1 OD (with one exception). The T_i = 4h experiments yields an OD slightly higher than values for simultaneous inoculation. In samples belonging to Response Class 2, crystal violet measurements are qualitatively consistent with these results. Early biofilms with no phage exposure have high final OD values of 3.0 and 3.4 (T_i = 4, 8 h). The OD values tend to decrease with increasing phage densities, in agreement with the confocal data. The final values associated with the largest phage dose (10^9 PFU / mL) are much higher than those associated with stage one biofilms, standing at (0.5 vs 3.0 OD) and 2.3 vs 3.0 OD and 2.7 vs 3.4 OD for the two (three) conditions. Interestingly, the crystal violet data are not reflective of the proportional decrease of the bacteria in the biofilm. While the confocal data illustrates that they are reduced by a factor of $\sim$4 at 10^9 PFU/mL, the crystal violet decrease far less presumably because of remnant EPS.

The crystal violet data of Response Class 3 is at odds with live bacterial levels in the biofilm for these conditions. Although the mock control shows the biofilm has only 10^4

living bacteria, four times less than most other controls reported thus far, the CV value is larger than in any other scenario (3.5 OD). This is likely due to the history of the biofilm, which peaked and then decayed, leaving the debris and extra polymeric substance (EPS) still detected by the CV measurement despite substantial bacterial reduction. Similarly, the trends in the CV value with phage treatment does not perfectly follow the paradoxical trend reported by direct confocal microscopy. Nevertheless, the OD for $p_0 = 10^9$ PFU/mL which has the best outcome in the confocal data of all conditions, including the control, still has a value of 3.2, lower than the 3.5 OD of the control. For Response Class 4, the crystal violet levels of the mock-control and phage-treated biofilms remain at similar values.

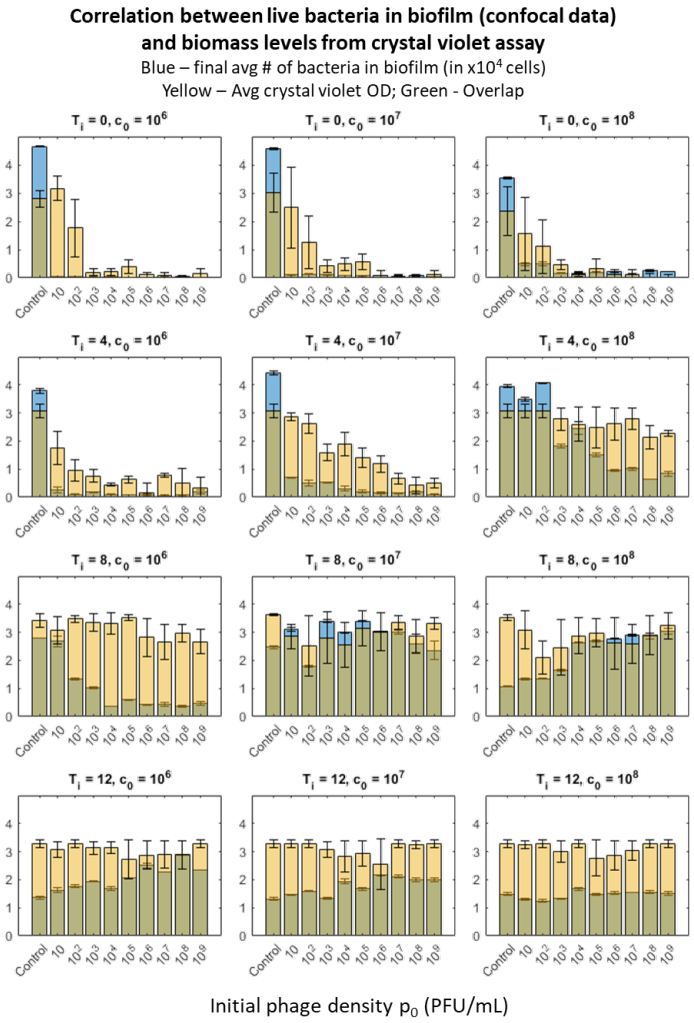

Figure C.3: **Correlation between live bacteria in biofilm (confocal data) and biomass levels from crystal violet assay.** Bar plots of the live bacteria within biofilms and optical density results from crystal violet assay versus phage doses are plotted to show the similarities and differences. The quantities were recorded after 16 hours of phage exposure. The coloumns correspond to different seeding bacterial densities ($c_0 = 10^6, 10^7$, and 10^8 CFU/mL) and rows correspond to different times at which phages were added (T_i = 0,4,8,12 h).

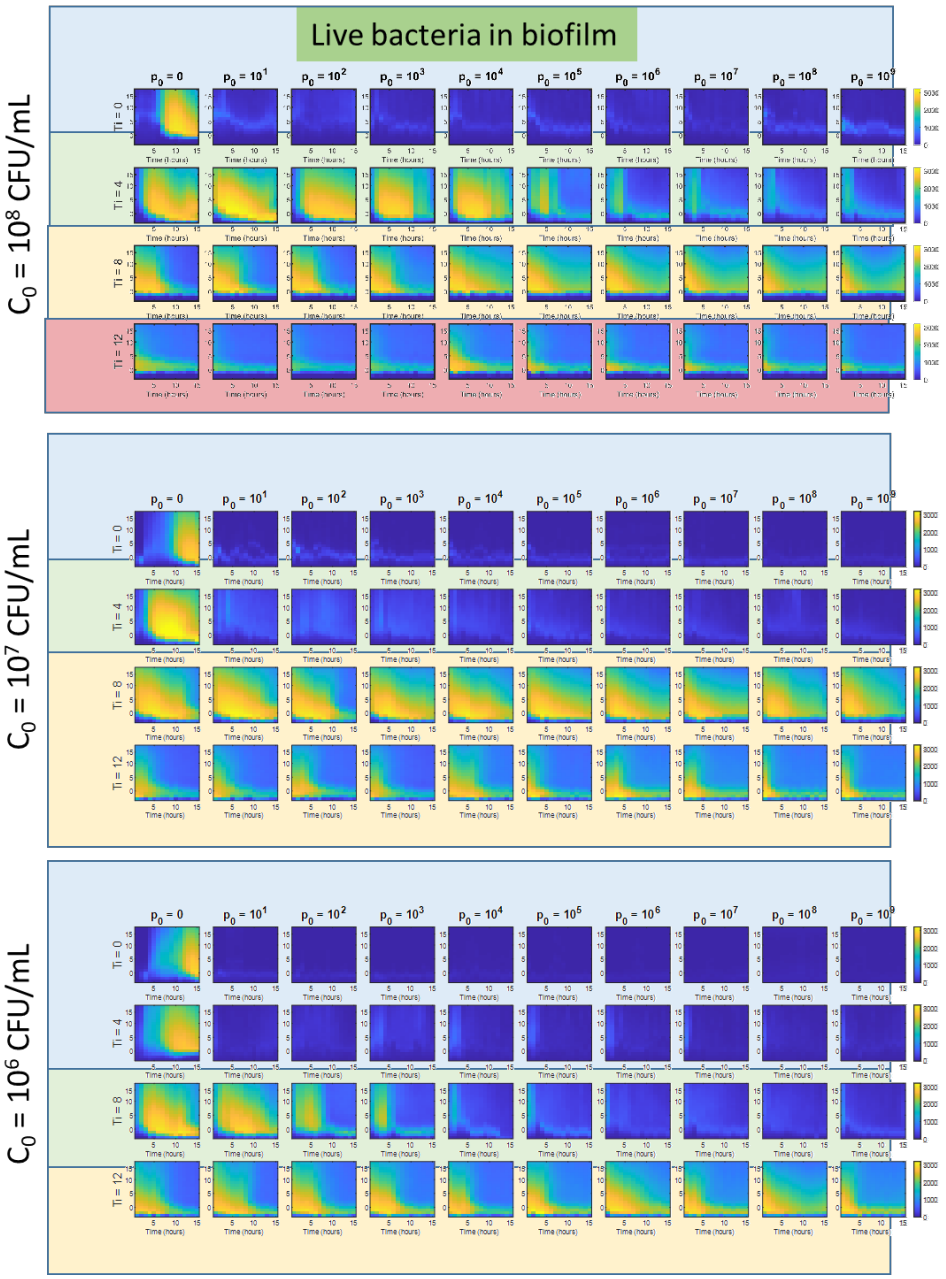

Figure C.4: **Spatiotemporal profile of live bacterial levels within biofilms in the absence and presence of phage** | Heatmap indicates the live bacterial levels at different heights within the biofilm for a duration of 16 hours from phage exposure. The spatiotemporal dynamics of the samples belonging to different Response Classes are indicated by the color in the background. Blue, green, yellow, and red correspond to Class 1, 2, 3, and 4 respectively.

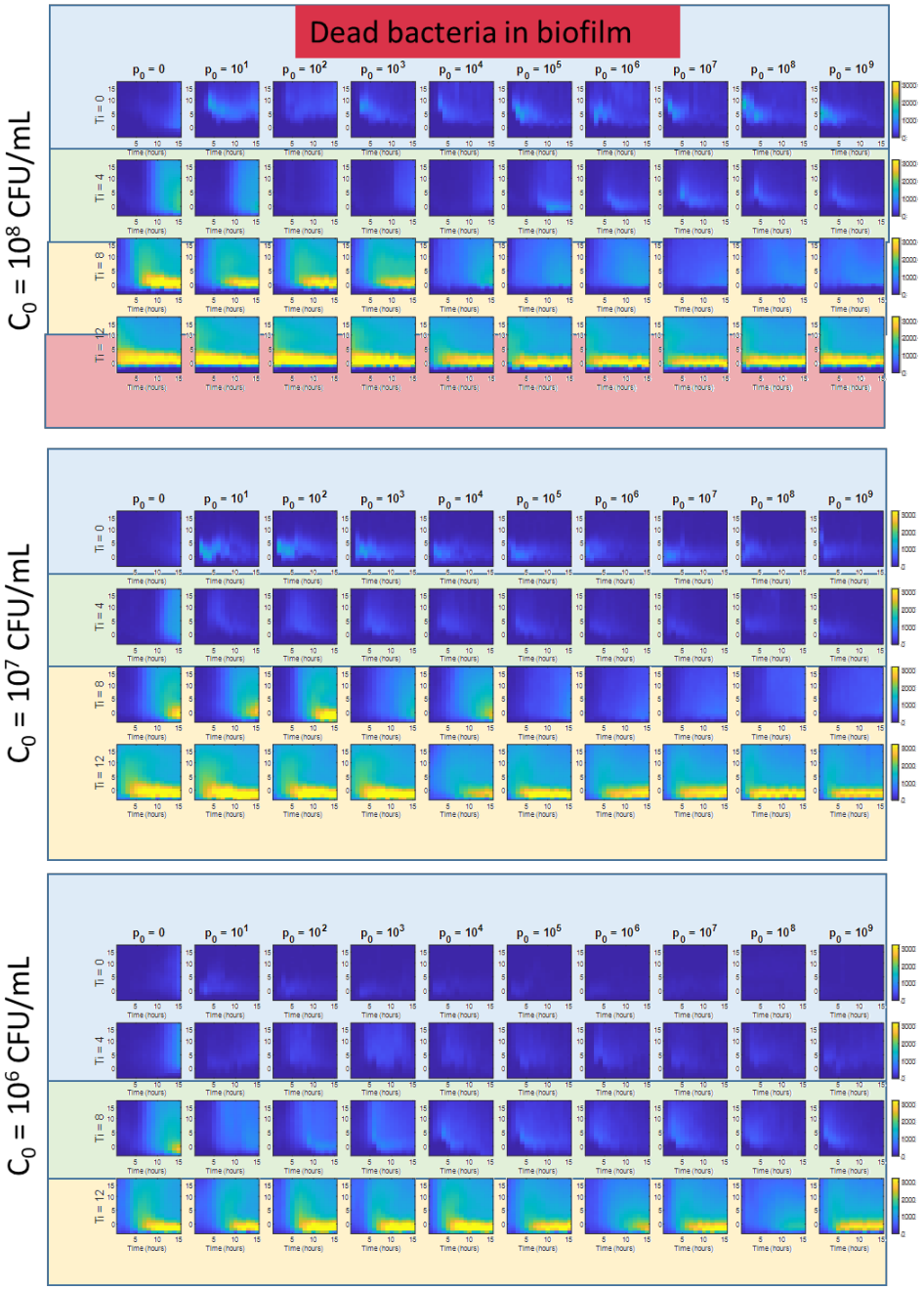

Figure C.5: **Spatiotemporal profile of dead bacterial levels within biofilms in the absence and presence of phage** | Heatmap indicates the dead bacterial levels at different heights within the biofilm for a duration of 16 hours from phage exposure. The spatiotemporal dynamics of the samples belonging to different Response Classes are indicated by the color in the background. Blue, green, yellow, and red correspond to Class 1, 2, 3, and 4 respectively.

REFERENCES

1. Costerton, J. W., Lewandowski, Z., Caldwell, D. E., Korber, D. R. & Lappin-Scott, H. M. Microbial biofilms. *Annual review of microbiology* **49,** 711–745 (1995).

2. Costerton, J. W., Stewart, P. S. & Greenberg, E. P. Bacterial biofilms: a common cause of persistent infections. *Science* **284,** 1318–1322 (1999).

3. Mazza, M. G. The physics of biofilmsan introduction. *Journal of Physics D: Applied Physics* **49,** 203001 (2016).

4. Bassler, B. L. How bacteria talk to each other: regulation of gene expression by quorum sensing. *Current opinion in microbiology* **2,** 582–587 (1999).

5. Bassler, B. L. Small talk: cell-to-cell communication in bacteria. *Cell* **109,** 421–424 (2002).

6. Miller, M. B. & Bassler, B. L. Quorum sensing in bacteria. *Annual Reviews in Microbiology* **55,** 165–199 (2001).

7. Trovato, A. *et al.* Quorum vs. diffusion sensing: a quantitative analysis of the relevance of absorbing or reflecting boundaries. *FEMS microbiology letters* **352,** 198–203 (2014).

8. Suel, G. Electrical Signaling in Biofilms. *Biophysical Journal* **114,** 28a (2018).

9. Bellows, C. & Smith, A. In Vitro Study of Biofilm Growth on Biologic Prosthetics. *Polish Journal of Microbiology* **63,** 409–414 (2014).

10. Jamal, M. *et al.* Bacterial biofilm and associated infections. *Journal of the Chinese Medical Association* **81,** 7–11 (2018).

11. Shafran, N. *et al.* Secondary bacterial infection in COVID-19 patients is a stronger predictor for death compared to influenza patients. *Scientific reports* **11,** 1–8 (2021).

12. Rawson, T. M. *et al.* Bacterial and fungal coinfection in individuals with coronavirus: a rapid review to support COVID-19 antimicrobial prescribing. *Clinical Infectious Diseases* **71,** 2459–2468 (2020).

13. Nadell, C. D., Drescher, K., Wingreen, N. S. & Bassler, B. L. Extracellular matrix structure governs invasion resistance in bacterial biofilms. *Isme Journal* **9,** 1700–1709 (2015).

14. Percival, S. L., Malic, S., Cruz, H. & Williams, D. W. Introduction to Biofilms. *Biofilms and Veterinary Medicine* **6,** 41–68 (2011).

15. Donlan, R. M. Preventing biofilms of clinically relevant organisms using bacteriophage. *Trends in microbiology* **17,** 66–72 (2009).

16. Keen, E. C. Phage therapy: concept to cure. *Frontiers in Microbiology* **3** (2012).

17. Godany, A., Bukovska, G., Farkasovska, J. & I, M. Phage therapy: alternative approach to antibiotics. *Biologia* **58,** 313–320 (2003).

18. Kutter, E. *et al.* Phage Therapy in Clinical Practice: Treatment of Human Infections. *Current Pharmaceutical Biotechnology* **11,** 69–86 (2010).

19. Kutter, E. M., Kuhl, S. J. & Abedon, S. T. Re-establishing a place for phage therapy in western medicine. *Future Microbiology* **10,** 685–688 (2015).

20. Abedon, S. T. Bacteriophages as Drugs: The Pharmacology of Phage Therapy. *Phage Therapy: Current Research and Applications,* 69–100 (2014).

21. Dixon, B. New dawn for phage therapy. *Lancet Infectious Diseases* **4,** 186–186 (2004).

22. Dublanchet, A. Felix d'Herelle (1873-1949) Before antibiotics, phage therapy. *Biofutur,* 60–62 (2013).

23. Rohde, C., Wittmann, J. & Kutter, E. Bacteriophages: A therapy concept against multi-drug–resistant bacteria. *Surgical infections* **19,** 737–744 (2018).

24. Weitz, J. S. *Quantitative viral ecology: dynamics of viruses and their microbial hosts* ISBN: 1400873967 (Princeton University Press, 2016).

25. Tiwari, B. R., Kim, S., Rahman, M. & Kim, J. Antibacterial efficacy of lytic Pseudomonas bacteriophage in normal and neutropenic mice models. *Journal of Microbiology* **49,** 994–999 (2011).

26. Levin, B. R. & Bull, J. J. Population and evolutionary dynamics of phage therapy. *Nature Reviews Microbiology* **2,** 166–173 (2004).

27. Leung, C. Y. J. & Weitz, J. S. Modeling the synergistic elimination of bacteria by phage and the innate immune system. *Journal of theoretical biology* **429,** 241–252 (2017).

28. Roach, D. R. *et al.* Synergy between the host immune system and bacteriophage is essential for successful phage therapy against an acute respiratory pathogen. *Cell host microbe* **22,** 38–47. e4 (2017).

29. Luria, S. E. & Delbrck, M. Mutations of bacteria from virus sensitivity to virus resistance. *Genetics* **28,** 491 (1943).

30. Msken, M., Di Fiore, S., Rmling, U. & Hussler, S. A 96-well-platebased optical method for the quantitative and qualitative evaluation of Pseudomonas aeruginosa biofilm formation and its application to susceptibility testing. *Nature protocols* **5,** 1460 (2010).

31. Bull, J., Millstein, J, Orcutt, J & Wichman, H. Evolutionary feedback mediated through population density, illustrated with viruses in chemostats. *The American Naturalist* **167,** E39–E51 (2006).

32. Bohannan, B. J. & Lenski, R. E. Effect of resource enrichment on a chemostat community of bacteria and bacteriophage. *Ecology* **78,** 2303–2315 (1997).

33. Lowery, N. V., McNally, L., Ratcliff, W. C. & Brown, S. P. Division of labor, bet hedging, and the evolution of mixed biofilm investment strategies. *MBio* **8,** e00672–17 (2017).

34. Shariati, A *et al.* Insertional inactivation of oprD in carbapenem-resistant Pseudomonas aeruginosa strains isolated from burn patients in Tehran, Iran. *New microbes and new infections* **21,** 75–80 (2018).

35. Mah, T.-F. *et al.* A genetic basis for Pseudomonas aeruginosa biofilm antibiotic resistance. *Nature* **426,** 306–310 (2003).

36. Remold, S. K. *et al.* Differential habitat use and niche partitioning by Pseudomonas species in human homes. *Microbial ecology* **62,** 505 (2011).

37. Wagner, V. E., Filiatrault, M. J., Picardo, K. F. & Iglewski, B. H. Pseudomonas aeruginosa virulence and pathogenesis issues. *Pseudomonas genomics and molecular biology,* 129–158 (2008).

38. Breidenstein, E. B., de la Fuente-Nez, C. & Hancock, R. E. Pseudomonas aeruginosa: all roads lead to resistance. *Trends in microbiology* **19,** 419–426 (2011).

39. Cornelis, P. *Pseudomonas: genomics and molecular biology* ISBN: 1904455190 (Horizon Scientific Press, 2008).

40. Fajardo, A. *et al.* The neglected intrinsic resistome of bacterial pathogens. *PloS one* **3,** e1619 (2008).

41. Ceyssens, P.-J. *et al.* Molecular and physiological analysis of three Pseudomonas aeruginosa phages belonging to the N4-like viruses. *Virology* **405,** 26–30 (2010).

42. Ceyssens, P.-J. & Lavigne, R. Bacteriophages of Pseudomonas. *Future microbiology* **5,** 1041–1055 (2010).

43. Debarbieux, L. Experimental phage therapy in the beginning of the 21st century. *Medecine Et Maladies Infectieuses* **38,** 421–425 (2008).

44. Kutter, E. Phage therapy: bactericiphages as natural, self-replicating and self-limiting antibiotic, a historical perspective. *Journal of Pharmacy and Pharmacology* **56,** S103–S103 (2004).

45. October 2011: This Month in JoVE. *Jove-Journal of Visualized Experiments* (2011).

46. Azeredo, J. & Sutherland, I. W. The use of phages for the removal of infectious biofilms. *Current Pharmaceutical Biotechnology* **9,** 261–266 (2008).

47. Chan, B. K. & Abedon, S. T. Bacteriophages and their Enzymes in Biofilm Control. *Current Pharmaceutical Design* **21,** 85–99 (2015).

48. Chegini, Z. *et al.* Bacteriophage therapy against Pseudomonas aeruginosa biofilms: a review. *Annals of Clinical Microbiology and Antimicrobials* **19,** 1–17 (2020).

49. Bjarnsholt, T. The role of bacterial biofilms in chronic infections. *Apmis* **121,** 1–58 (2013).

50. Bjarnsholt, T. *et al.* The in vivo biofilm. *Trends in Microbiology* **21,** 466–474 (2013).

51. Alhede, M., Bjarnsholt, T., Givskov, M. & Alhede, M. Pseudomonas aeruginosa Biofilms: Mechanisms of Immune Evasion. *Advances in Applied Microbiology, Vol 86* **86,** 1–40 (2014).

52. Bjarnsholt, T. *et al.* Pseudomonas aeruginosa Biofilms in the Respiratory Tract of Cystic Fibrosis Patients. *Pediatric Pulmonology* **44,** 547–558 (2009).

53. Bjarnsholt, T. *et al.* Why chronic wounds will not heal: a novel hypothesis. *Wound Repair and Regeneration* **16,** 2–10 (2008).

54. Donlan, R. M. Biofilm formation: a clinically relevant microbiological process. *Clinical Infectious Diseases* **33,** 1387–1392 (2001).

55. Donlan, R. M. & Costerton, J. W. Biofilms: Survival mechanisms of clinically relevant microorganisms. *Clinical Microbiology Reviews* **15,** 167–+ (2002).

56. Drenkard, E. & Ausubel, F. M. Pseudomonas biofilm formation and antibiotic resistance are linked to phenotypic variation. *Nature* **416,** 740–743 (2002).

57. Hoiby, N. *et al.* The clinical impact of bacterial biofilms. *International Journal of Oral Science* **3,** 55–65 (2011).

58. Jensen, P. O., Givskov, M., Bjarnsholt, T. & Moser, C. The immune system vs. Pseudomonas aeruginosa biofilms. *Fems Immunology and Medical Microbiology* **59,** 292–305 (2010).

59. Chanishvili, N. Phage Therapy-History from Twort and d'Herelle Through Soviet Experience to Current Approaches. *Advances in Virus Research, Vol 83: Bacteriophages, Pt B* **83,** 3–40 (2012).

60. d'Herelle, M. Sur un microbe invisible antagoniste des bacilles dysentriques. *Acta Kravsi* (1961).

61. Twort, F. W. An investigation on the nature of ultra-microscopic viruses. *Acta Kravsi* (1961).

62. Keen, E. C. A century of phage research: bacteriophages and the shaping of modern biology. *Bioessays* **37,** 6–9 (2015).

63. Salmond, G. P. & Fineran, P. C. A century of the phage: past, present and future. *Nature Reviews Microbiology* **13,** 777–786 (2015).

64. Marcinkiewicz, J., Strus, M. & Pasich, E. Antibiotic resistance: a "dark side" of biofilm-associated chronic infections. *Polskie Archiwum Medycyny Wewnetrznej-Polish Archives of Internal Medicine* **123,** 309–313 (2013).

65. Mulyukin, A. L. *et al.* Surviving forms in antibiotic-treated Pseudomonas aeruginosa. *Microbiology* **84,** 751–763 (2015).

66. Dublanchet, A. & Patey, O. The phage therapy: Past and future (new facts and procedure[s] for a rehabilitation). *Immuno-Analyse Biologie Specialisee* **26,** 165–175 (2011).

67. Inal, J. M. Phage therapy: a reappraisal of bacteriophages as antibiotics. *Archivum Immunologiae Et Therapiae Experimentalis* **51,** 237–244 (2003).

68. Maura, D. & Debarbieux, L. Bacteriophages as twenty-first century antibacterial tools for food and medicine. *Applied Microbiology and Biotechnology* **90,** 851–859 (2011).

69. Rossitto, M., Fiscarelli, E. V. & Rosati, P. Challenges and Promises for Planning Future Clinical Research Into Bacteriophage Therapy Against Pseudomonas aeruginosa in Cystic Fibrosis. An Argumentative Review. *Frontiers in Microbiology* **9** (2018).

70. Thiel, K. Old dogma, new tricks - 21st century phage therapy. *Nature Biotechnology* **22,** 31–36 (2004).

71. Hraiech, S., Brgeon, F. & Rolain, J.-M. Bacteriophage-based therapy in cystic fibrosis-associated Pseudomonas aeruginosa infections: rationale and current status. *Drug design, development and therapy* **9,** 3653 (2015).

72. Verma, V., Harjai, K. & Chhibber, S. Structural changes induced by a lytic bacteriophage make ciprofloxacin effective against older biofilm of Klebsiella pneumoniae. *Biofouling* **26,** 729–737 (2010).

73. Lewis, K. Persister cells, dormancy and infectious disease. *Nature Reviews Microbiology* **5,** 48–56 (2007).

74. Abedon, S. T. Deconstructing chemostats towards greater phage-modeling precision. *Contemporary trends in bacteriophage research. Nova Science Publishers, Hauppauge, New York,* 249–283 (2009).

75. Lenski, R. E. & Levin, B. R. Constraints on the coevolution of bacteria and virulent phage: a model, some experiments, and predictions for natural communities. *The American Naturalist* **125,** 585–602 (1985).

76. Chao, L., Levin, B. R. & Stewart, F. M. A complex community in a simple habitat: an experimental study with bacteria and phage. *Ecology* **58,** 369–378 (1977).

77. Xie, Y., Wahab, L. & Gill, J. J. Development and validation of a microtiter plate-based assay for determination of bacteriophage host range and virulence. *Viruses* **10,** 189 (2018).

78. Cerca, N., Oliveira, R. & Azeredo, J. Susceptibility of Staphylococcus epidermidis planktonic cells and biofilms to the lytic action of staphylococcus bacteriophage K. *Letters in applied microbiology* **45,** 313–317 (2007).

79. Orengo, A & Tchen, T. Studies on the rate of synthesis of phage-induced enzymes in relation to the multiplicity of infection. *Biochemical and biophysical research communications* **6,** 261–263 (1961).

80. Abedon, S. T. Phage therapy dosing: The problem (s) with multiplicity of infection (MOI). *Bacteriophage* **6,** e1220348 (2016).

81. Shabram, P. & Aguilar-Cordova, E. Multiplicity of infection/multiplicity of confusion. *Molecular therapy* **2,** 420–421 (2000).

82. Knezevic, P. & Petrovic, O. A colorimetric microtiter plate method for assessment of phage effect on Pseudomonas aeruginosa biofilm. *Journal of Microbiological Methods* **74,** 114–118 (2008).

83. Rajnovic, D., Muoz-Berbel, X. & Mas, J. Fast phage detection and quantification: An optical density-based approach. *PloS one* **14,** e0216292 (2019).

84. Rajnovic, D., Muoz-Berbel, X. & Mas, J. Fast phage detection and quantification: An optical density-based approach. *PloS one* **14,** e0216292 (2019).

85. Tkhilaishvili, T. *et al.* Real-time assessment of bacteriophage T3-derived antimicrobial activity against planktonic and biofilm-embedded Escherichia coli by isothermal microcalorimetry. *Research in microbiology* **169,** 515–521 (2018).

86. Wintachai, P., Naknaen, A., Pomwised, R., Voravuthikunchai, S. P. & Smith, D. R. Isolation and characterization of Siphoviridae phage infecting extensively drug-resistant Acinetobacter baumannii and evaluation of therapeutic efficacy in vitro and in vivo. *Journal of medical microbiology* **68,** 1096–1108 (2019).

87. Thawal, N. D., Yele, A. B., Sahu, P. K. & Chopade, B. A. Effect of a novel podophage AB7-IBB2 on Acinetobacter baumannii biofilm. *Current microbiology* **65,** 66–72 (2012).

88. Pei, R. & Lamas-Samanamud, G. R. Inhibition of biofilm formation by T7 bacteriophages producing quorum-quenching enzymes. *Applied and environmental microbiology* **80,** 5340–5348 (2014).

89. Knezevic, P *et al.* Phages of Pseudomonas aeruginosa: response to environmental factors and in vitro ability to inhibit bacterial growth and biofilm formation. *Journal of applied microbiology* **111,** 245–254 (2011).

90. Guo, Y., Chen, P., Lin, Z. & Wang, T. Characterization of two Pseudomonas aeruginosa viruses vB_PaeM_SCUT-S1 and vB_PaeM_SCUT-S2. *Viruses* **11,** 318 (2019).

91. Campbell, A. Life in Science: Alan Campbell. *Bacteriophage* **2,** 137–138 (2012).

92. Weitz, J. S. & Dushoff, J. Alternative stable states in host–phage dynamics. *Theoretical Ecology* **1,** 13–19 (2008).

93. Bull, J. J. *et al.* Phage-Bacterial Dynamics with Spatial Structure: Self Organization around Phage Sinks Can Promote Increased Cell Densities. *Antibiotics-Basel* **7** (2018).

94. Eriksen, R. S., Mitarai, N. & Sneppen, K. Sustainability of spatially distributed bacteria-phage systems. *Scientific reports* **10,** 1–12 (2020).

95. Murray, J. D. *Mathematical biology II: spatial models and biomedical applications* (Springer New York, 2001).

96. Taylor, B. P., Penington, C. J. & Weitz, J. S. Emergence of increased frequency and severity of multiple infections by viruses due to spatial clustering of hosts. *Physical biology* **13,** 066014 (2017).

97. Stern, A. & Sorek, R. The phage-host arms race: shaping the evolution of microbes. *Bioessays* **33,** 43–51 (2011).

98. Lenski, R. E. & Levin, B. R. Constraints on the coevolution of bacteria and virulent phage: a model, some experiments, and predictions for natural communities. *The American Naturalist* **125,** 585–602 (1985).

99. Payne, R. J. & Jansen, V. A. Evidence for a phage proliferation threshold? *Journal of virology* **76,** 13123–13124 (2002).

100. Cairns, B. J., Timms, A. R., Jansen, V. A., Connerton, I. F. & Payne, R. J. Quantitative models of in vitro bacteriophage–host dynamics and their application to phage therapy. *PLoS Pathogens* **5,** e1000253 (2009).

101. Xie, Y., Wahab, L. & Gill, J. J. Development and validation of a microtiter plate-based assay for determination of bacteriophage host range and virulence. *Viruses* **10,** 189 (2018).

102. Bull, J. J., Vegge, C. S., Schmerer, M., Chaudhry, W. N. & Levin, B. R. Phenotypic resistance and the dynamics of bacterial escape from phage control. *PloS one* **9,** e94690 (2014).

103. Hampton, H. G., Watson, B. N. & Fineran, P. C. The arms race between bacteria and their phage foes. *Nature* **577,** 327–336 (2020).

104. Høiby, N., Bjarnsholt, T., Givskov, M., Molin, S. & Ciofu, O. Antibiotic resistance of bacterial biofilms. *International journal of antimicrobial agents* **35,** 322–332 (2010).

105. Sanclement, J. A., Webster, P., Thomas, J. & Ramadan, H. H. Bacterial biofilms in surgical specimens of patients with chronic rhinosinusitis. *Laryngoscope* **115,** 578–582 (2005).

106. Burmolle, M. *et al.* Biofilms in chronic infections - a matter of opportunity - monospecies biofilms in multispecies infections. *Fems Immunology and Medical Microbiology* **59,** 324–336 (2010).

107. Cooper, R., Bjarnsholt, T & Alhede, M. Biofilms in wounds: a review of present knowledge. *Journal of wound care* **23,** 570–582 (2014).

108. Bjarnsholt, T. & Givskov, M. Ecology of Biofilms in Chronic Wounds. *Advances in Wound Care, Vol 1* **1,** 287–292 (2010).

109. Of Health, N. I. *et al.* NIH guide: research on microbial biofilms. *URL https://grants. nih. gov/grants/guide/pa-files/PA-03-047. html* (2002).

110. Rode, D. K., Singh, P. K. & Drescher, K. Multicellular and unicellular responses of microbial biofilms to stress. *Biological Chemistry* **401,** 1365–1374 (2020).

111. Rumbaugh, K. P. & Sauer, K. Biofilm dispersion. *Nature Reviews Microbiology* **18,** 571–586 (2020).

112. Watters, C., Fleming, D., Bishop, D. & Rumbaugh, K. P. Host Responses to Biofilm. *Host-Microbe Interactions* **142,** 193–239 (2016).

113. Meletis, G, Exindari, M, Vavatsi, N, Sofianou, D & Diza, E. Mechanisms responsible for the emergence of carbapenem resistance in Pseudomonas aeruginosa. *Hippokratia* **16,** 303 (2012).

114. Walters, M. S. *et al.* Carbapenem-resistant Pseudomonas aeruginosa at US emerging infections program sites, 2015. *Emerging infectious diseases* **25,** 1281 (2019).

115. Czaplewski, L. *et al.* Alternatives to antibioticsa pipeline portfolio review. *The Lancet infectious diseases* **16,** 239–251 (2016).

116. Ghosh, C., Sarkar, P., Issa, R. & Haldar, J. Alternatives to conventional antibiotics in the era of antimicrobial resistance. *Trends in microbiology* **27,** 323–338 (2019).

117. Burrowes, B., Harper, D. R., Anderson, J., McConville, M. & Enright, M. C. Bacteriophage therapy: potential uses in the control of antibiotic-resistant pathogens. *Expert review of anti-infective therapy* **9,** 775–785 (2011).

118. Kutter, E. *et al. Clinical phage therapy* (Caister Academic Press, Norfolk, UK, 2014).

119. Lin, D. M., Koskella, B. & Lin, H. C. Phage therapy: An alternative to antibiotics in the age of multi-drug resistance. *World journal of gastrointestinal pharmacology and therapeutics* **8,** 162 (2017).

120. Górski, A., Targońska, M., Borysowski, J. & Weber-Dabrowska, B. The potential of phage therapy in bacterial infections of the eye. *Ophthalmologica* **223,** 162–165 (2009).

121. Voelker, R. FDA approves bacteriophage trial. *Jama* **321,** 638–638 (2019).

122. Guttman, B., Raya, R. & Kutter, E. Basic phage biology. *Bacteriophages: Biology and applications* **4** (2005).

123. Chatterjee, A. & Duerkop, B. A. Beyond bacteria: bacteriophage-eukaryotic host interactions reveal emerging paradigms of health and disease. *Frontiers in microbiology* **9,** 1394 (2018).

124. Debarbieux, L. *et al.* Bacteriophages can treat and prevent Pseudomonas aeruginosa lung infections. *The Journal of infectious diseases* **201,** 1096–1104 (2010).

125. Abedon, S. T. in *Biofilm, Pilonidal Cysts and Sinuses* 121–158 (Springer, 2018).

126. Pinto, A. M., Cerqueira, M. A., Baobre-Lpes, M., Pastrana, L. M. & Sillankorva, S. Bacteriophages for chronic wound treatment: From traditional to novel delivery systems. *Viruses* **12,** 235 (2020).

127. Abedon, S. T. Use of phage therapy to treat long-standing, persistent, or chronic bacterial infections. *Advanced drug delivery reviews* **145,** 18–39 (2019).

128. Rhoads, D. *et al.* Bacteriophage therapy of venous leg ulcers in humans: results of a phase I safety trial. *Journal of wound care* **18,** 237–243 (2009).

129. Sarker, S. A. *et al.* Oral phage therapy of acute bacterial diarrhea with two coliphage preparations: a randomized trial in children from Bangladesh. *EBioMedicine* **4,** 124–137 (2016).

130. Goodwin, D. G. *et al.* Biofilm development on carbon nanotube/polymer nanocomposites. *Environmental Science: Nano* **3,** 545–558 (2016).

131. Drescher, K. *et al.* Architectural transitions in Vibrio cholerae biofilms at single-cell resolution. *Proceedings of the National Academy of Sciences of the United States of America* **113,** E2066–E2072 (2016).

132. Hammer, B. K. & Bassler, B. L. Quorum sensing controls biofilm formation in Vibrio cholerae. *Molecular microbiology* **50,** 101–104 (2003).

133. Yan, J., Sharo, A. G., Stone, H. A., Wingreen, N. S. & Bassler, B. L. Vibrio cholerae biofilm growth program and architecture revealed by single-cell live imaging. *Proceedings of the National Academy of Sciences* **113,** E5337–E5343 (2016).

134. Webb, J. S. *et al.* Cell death in Pseudomonas aeruginosa biofilm development. *Journal of Bacteriology* **185,** 4585–4592 (2003).

135. Sauer, K *et al.* Characterization of nutrient-induced dispersion in Pseudomonas aeruginosa PAO1 biofilm. *Journal of bacteriology* **186,** 7312–7326 (2004).

136. Saraswathi, P. & Beuerman, R. W. Corneal biofilms: from planktonic to microcolony formation in an experimental keratitis infection with Pseudomonas aeruginosa. *The ocular surface* **13,** 331–345 (2015).

137. Thi, M. T. T., Wibowo, D. & Rehm, B. H. Pseudomonas aeruginosa biofilms. *International Journal of Molecular Sciences* **21,** 8671 (2020).

138. Hoiby, N., Ciofu, O. & Bjarnsholt, T. Pseudomonas aeruginosa biofilms in cystic fibrosis. *Future Microbiology* **5,** 1663–1674 (2010).

139. Sauer, K., Camper, A. K., Ehrlich, G. D., Costerton, J. W. & Davies, D. G. Pseudomonas aeruginosa displays multiple phenotypes during development as a biofilm. *Journal of bacteriology* **184,** 1140–1154 (2002).

140. Guo, M. *et al.* A novel antimicrobial endolysin, LysPA26, against Pseudomonas aeruginosa. *Frontiers in microbiology* **8,** 293 (2017).

141. Jamal, M. *et al.* Isolation and characterization of a bacteriophage and its utilization against multi-drug resistant Pseudomonas aeruginosa-2995. *Life sciences* **190,** 21–28 (2017).

142. Chhibber, S., Nag, D. & Bansal, S. Inhibiting biofilm formation by Klebsiella pneumoniae B5055 using an iron antagonizing molecule and a bacteriophage. *BMC microbiology* **13,** 1–8 (2013).

143. Darch, S. E. *et al.* Phage Inhibit Pathogen Dissemination by Targeting Bacterial Migrants in a Chronic Infection Model. *Mbio* **8** (2017).

144. Heilmann, S., Sneppen, K. & Krishna, S. Coexistence of phage and bacteria on the boundary of self-organized refuges. *Proceedings of the National Academy of Sciences* **109,** 12828–12833 (2012).

145. Eriksen, R. S., Svenningsen, S. L., Sneppen, K. & Mitarai, N. A growing microcolony can survive and support persistent propagation of virulent phages. *Proceedings of the National Academy of Sciences* **115,** 337–342 (2018).

146. Simmons, M., Drescher, K., Nadell, C. D. & Bucci, V. Phage mobility is a core determinant of phagebacteria coexistence in biofilms. *The ISME journal* **12,** 531 (2017).

147. Roy, R., Tiwari, M., Donelli, G. & Tiwari, V. Strategies for combating bacterial biofilms: A focus on anti-biofilm agents and their mechanisms of action. *Virulence* **9,** 522–554 (2018).

148. Rybtke, M., Hultqvist, L. D., Givskov, M. & Tolker-Nielsen, T. Pseudomonas aeruginosa biofilm infections: community structure, antimicrobial tolerance and immune response. *Journal of molecular biology* **427,** 3628–3645 (2015).

149. Belas, R. Biofilms, flagella, and mechanosensing of surfaces by bacteria. *Trends in microbiology* **22,** 517–527 (2014).

150. Petrova, O. E. & Sauer, K. Sticky situations: key components that control bacterial surface attachment. *Journal of bacteriology* **194,** 2413–2425 (2012).

151. Klausen, M. *et al.* Biofilm formation by Pseudomonas aeruginosa wild type, flagella and type IV pili mutants. *Molecular Microbiology* **48,** 1511–1524 (2003).

152. Klausen, M., AaesJrgensen, A., Molin, S. & TolkerNielsen, T. Involvement of bacterial migration in the development of complex multicellular structures in Pseudomonas aeruginosa biofilms. *Molecular microbiology* **50,** 61–68 (2003).

153. Persat, A. *et al.* The Mechanical World of Bacteria. *Cell* **161,** 988–997 (2015).

154. Parsek, M. R. & Tolker-Nielsen, T. Pattern formation in Pseudomonas aeruginosa biofilms. *Current opinion in microbiology* **11,** 560–566 (2008).

155. Kim, W. *et al.* Spaceflight promotes biofilm formation by Pseudomonas aeruginosa. *PloS one* **8,** e62437 (2013).

156. Harmsen, M., Yang, L., Pamp, S. J. & Tolker-Nielsen, T. An update on Pseudomonas aeruginosa biofilm formation, tolerance, and dispersal. *FEMS Immunology Medical Microbiology* **59,** 253–268 (2010).

157. Flemming, H.-C. & Wingender, J. The biofilm matrix. *Nature reviews microbiology* **8,** 623–633 (2010).

158. Pedersen, S. S., Kharazmi, A., Espersen, F. & Hiby, N. Pseudomonas aeruginosa alginate in cystic fibrosis sputum and the inflammatory response. *Infection and immunity* **58,** 3363–3368 (1990).

159. Yang, L., Nilsson, M., Gjermansen, M., Givskov, M. & TolkerNielsen, T. Pyoverdine and PQS mediated subpopulation interactions involved in Pseudomonas aeruginosa biofilm formation. *Molecular microbiology* **74,** 1380–1392 (2009).

160. Vallet, I. *et al.* Biofilm formation in Pseudomonas aeruginosa: Fimbrial cup gene clusters are controlled by the transcriptional regulator MvaT. *Journal of Bacteriology* **186,** 2880–2890 (2004).

161. Borlee, B. R. *et al.* Pseudomonas aeruginosa uses a cyclicdiGMPregulated adhesin to reinforce the biofilm extracellular matrix. *Molecular microbiology* **75,** 827–842 (2010).

162. Tielker, D. *et al.* Pseudomonas aeruginosa lectin LecB is located in the outer membrane and is involved in biofilm formation. *Microbiology* **151,** 1313–1323 (2005).

163. Dueholm, M. S. *et al.* Expression of Fap amyloids in P seudomonas aeruginosa, P. fluorescens, and P. putida results in aggregation and increased biofilm formation. *Microbiologyopen* **2,** 365–382 (2013).

164. AllesenHolm, M. *et al.* A characterization of DNA release in Pseudomonas aeruginosa cultures and biofilms. *Molecular microbiology* **59,** 1114–1128 (2006).

165. Kirov, S. M. *et al.* Biofilm differentiation and dispersal in mucoid Pseudomonas aeruginosa isolates from patients with cystic fibrosis. *Microbiology-Sgm* **153,** 3264–3274 (2007).

166. Gjermansen, M., Ragas, P., Sternberg, C., Molin, S. & TolkerNielsen, T. Characterization of starvationinduced dispersion in Pseudomonas putida biofilms. *Environmental microbiology* **7,** 894–904 (2005).

167. Ma, L. M. *et al.* Assembly and Development of the Pseudomonas aeruginosa Biofilm Matrix. *Plos Pathogens* **5** (2009).

168. Li, Y., Heine, S., Entian, M., Sauer, K. & Frankenberg-Dinkel, N. NO-induced biofilm dispersion in Pseudomonas aeruginosa is mediated by an MHYT domain-coupled phosphodiesterase. *Journal of bacteriology* **195,** 3531–3542 (2013).

169. Armbruster, C. R. & Parsek, M. R. New insight into the early stages of biofilm formation. *Proceedings of the National Academy of Sciences* **115,** 4317–4319 (2018).

170. Petrova, O. E. & Sauer, K. Escaping the biofilm in more than one way: desorption, detachment or dispersion. *Current opinion in microbiology* **30,** 67–78 (2016).

171. Perlemoine, P. *et al.* Phage susceptibility testing and infectious titer determination through wide-field lensless monitoring of phage plaque growth. *PloS one* **16,** e0248917 (2021).

172. Negu, A. C. *et al.* Experimental approach for bacteriophage susceptibility testing of planktonic and sessile bacterial populationsStudy protocol. *Germs* **4,** 92 (2014).

173. He, Y., Fan, E., Wang, M., Lu, S. & Fu, Z. Antimicrobial susceptibility testing by using virulent phages to evaluate bacterial viability. *Analytical Methods* **10,** 1799–1804 (2018).

174. Macia, M., Rojo-Molinero, E & Oliver, A. Antimicrobial susceptibility testing in biofilm-growing bacteria. *Clinical Microbiology and Infection* **20,** 981–990 (2014).

175. Bahamondez-Canas, T. F., Heersema, L. A. & Smyth, H. D. Current status of in vitro models and assays for susceptibility testing for wound biofilm infections. *Biomedicines* **7,** 34 (2019).

176. Buhmann, M. T., Stiefel, P., Maniura-Weber, K. & Ren, Q. In vitro biofilm models for device-related infections. *Trends in biotechnology* **34,** 945–948 (2016).

177. Vidakovic, L., Singh, P. K., Hartmann, R., Nadell, C. D. & Drescher, K. Dynamic biofilm architecture confers individual and collective mechanisms of viral protection. *Nature microbiology* **3,** 26 (2018).

178. Corbin, B. D., McLean, R. J. C. & Aron, G. M. Bacteriophage T4 multiplication in a glucose-limited Escherichia coli biofilm. *Canadian Journal of Microbiology* **47,** 680–684 (2001).

179. Abedon, S. T., Danis-Wlodarczyk, K. M., Wozniak, D. J. & Sullivan, M. B. Improving Phage-Biofilm In Vitro Experimentation. *Viruses* **13,** 1175 (2021).

180. Wilking, J. N., Angelini, T. E., Seminara, A., Brenner, M. P. & Weitz, D. A. Biofilms as complex fluids. *Mrs Bulletin* **36,** 385–391 (2011).

181. Stewart, P. S. Biophysics of biofilm infection. *Pathogens and Disease* **70,** 212–218 (2014).

182. Lecuyer, S., Stocker, R. & Rusconi, R. Focus on the physics of biofilms. *New Journal of Physics* **17** (2015).

183. Allen, R. J. & Waclaw, B. Bacterial growth: A statistical physicists guide. *Reports on Progress in Physics* **82,** 016601 (2018).

184. You, L. & Yin, J. Amplification and spread of viruses in a growing plaque. *Journal of theoretical biology* **200,** 365–373 (1999).

185. Yin, J. & McCaskill, J. Replication of viruses in a growing plaque: a reaction-diffusion model. *Biophysical journal* **61,** 1540–1549 (1992).

186. Hellweger, F. L., Clegg, R. J., Clark, J. R., Plugge, C. M. & Kreft, J.-U. Advancing microbial sciences by individual-based modelling. *Nature Reviews Microbiology* **14,** 461–471 (2016).

187. Vidakovic, L., Singh, P. K., Hartmann, R., Nadell, C. D. & Drescher, K. Dynamic biofilm architecture confers individual and collective mechanisms of viral protection. *Nature microbiology* **3,** 26 (2018).

188. Abedon, S. T. Bacteriophage exploitation of bacterial biofilms: phage preference for less mature targets? *FEMS microbiology letters* **363,** fnv246 (2016).

189. Ferriol-González, C. & Domingo-Calap, P. Phages for biofilm removal. *Antibiotics* **9,** 268 (2020).

190. Trostrup, H., Thomsen, K., Calum, H., Hoiby, N. & Moser, C. Animal models of chronic wound care: the application of biofilms in clinical research. *Chronic Wound Care Management and Research* **3,** 123–132 (2016).

191. Hoiby, N. *et al.* Pseudomonas aeruginosa Biofilms in the Lungs of Cystic Fibrosis Patients. *Biofilm Infections,* 167–184 (2011).

192. Fleming, D. & Rumbaugh, K. The consequences of biofilm dispersal on the host. *Scientific reports* **8,** 1–7 (2018).

193. Chua, S. L. *et al.* Dispersed cells represent a distinct stage in the transition from bacterial biofilm to planktonic lifestyles. *Nature communications* **5,** 1–12 (2014).

194. Rice, S. A. *et al.* The biofilm life cycle and virulence of Pseudomonas aeruginosa are dependent on a filamentous prophage. *The ISME journal* **3,** 271–282 (2009).

195. Morello, E. *et al.* Pulmonary bacteriophage therapy on Pseudomonas aeruginosa cystic fibrosis strains: first steps towards treatment and prevention. *PloS one* **6,** e16963 (2011).

196. Matsuzaki, S. *et al.* Experimental protection of mice against lethal Staphylococcus aureus infection by novel bacteriophage ϕMR11. *The Journal of infectious diseases* **187,** 613–624 (2003).

197. Hosseinidoust, Z., Tufenkji, N. & van de Ven, T. G. Formation of biofilms under phage predation: considerations concerning a biofilm increase. *Biofouling* **29,** 457–468 (2013).

198. Bond, M. C., Vidakovic, L., Singh, P. K., Drescher, K. & Nadell, C. D. Matrix-trapped viruses can prevent invasion of bacterial biofilms by colonizing cells. *Elife* **10,** e65355 (2021).

199. Chaudhry, W. N. *et al.* Synergy and Order Effects of Antibiotics and Phages in Killing Pseudomonas aeruginosa Biofilms. *Plos One* **12** (2017).

200. Chua, S. L. *et al.* Dispersed cells represent a distinct stage in the transition from bacterial biofilm to planktonic lifestyles. *Nature communications* **5,** 1–12 (2014).

201. Yang, Y. *et al.* Development of a bacteriophage cocktail to constrain the emergence of phage-resistant Pseudomonas aeruginosa. *Frontiers in microbiology* **11,** 327 (2020).

202. Hauser, A. R. The type III secretion system of Pseudomonas aeruginosa: infection by injection. *Nature Reviews Microbiology* **7,** 654–665 (2009).

203. Thanabalasuriar, A. *et al.* Neutrophil extracellular traps confine Pseudomonas aeruginosa ocular biofilms and restrict brain invasion. *Cell host & microbe* **25,** 526–536 (2019).

VITA

Hemaa Selvakumar was born in Rasipuram, Tamilnadu, India. She received her Bachelors degree in Physics from the Indian Institute of Science, Bangalore, India in 2015. She was awarded the National Young Scientist (KVPY) fellowship by the Indian government during her undergraduate studies. After experimenting with various sub-fields in physics, such as particle physics, semiconductor physics, and nanobiophysics, she pursued her doctoral degree in Physics at Georgia Tech. During this time, she received the Management of Technology certification from the Scheller College of Business at Georgia Tech. She was also awarded the *Graduate Student Excellence Award for Leadership and Service* in 2020. Her research interests are highly interdisciplinary in nature and she has worked in collaboration with diverse faculties from Georgia Tech and Emory University.